Pontifícia Universidade Católica
do Rio de Janeiro

Felipe Neves Piancó

Distribution grid planning with lines investment and topology reconfiguration for wildfire resilience under Decision-Dependent Uncertainty

Dissertação de Mestrado

Dissertation presented to the Programa de Pós–graduação em Engenharia de Produção of PUC-Rio in partial fulfillment of the requirements for the degree of Mestre em Engenharia de Produção.

Advisor : Prof. Bruno Fânzeres dos Santos
Co-advisor: Dr. Alexandre Moreira da Silva

Rio de Janeiro
February 2024

Pontifícia Universidade Católica
do Rio de Janeiro

Felipe Neves Piancó

Distribution grid planning with lines investment and topology reconfiguration for wildfire resilience under Decision-Dependent Uncertainty

Dissertation presented to the Programa de Pós–graduação em Engenharia de Produção of PUC-Rio in partial fulfillment of the requirements for the degree of Mestre em Engenharia de Produção. Approved by the Examination Committee:

Prof. Bruno Fânzeres dos Santos
Advisor
Departamento de Engenharia Industrial – PUC-Rio

Dr. Alexandre Moreira da Silva
Co-advisor
Lawrence Berkeley National Laboratory

Prof. Rafael Martinelli Pinto
Departamento de Engenharia Industrial – PUC-Rio

Prof. André Luís Marques Marcato
UFJF

Prof. Albert Cordeiro Geber de Melo
UERJ

Rio de Janeiro, February 7th, 2024

Felipe Neves Piancó

Graduated in electrical engineering from Rio de Janeiro State University (Uerj). Affiliate at the Lawrence Berkeley National Laboratory (LBNL).

Bibliographic data

Piancó, Felipe Neves

Distribution grid planning with lines investment and topology reconfiguration for wildfire resilience under Decision-Dependent Uncertainty / Felipe Neves Piancó; advisor: Bruno Fânzeres dos Santos; co-advisor: Alexandre Moreira da Silva. – 2024.

95 f: il. color. ; 30 cm

Dissertação (mestrado) - Pontifícia Universidade Católica do Rio de Janeiro, Departamento de Engenharia Industrial, 2024.

Inclui bibliografia

1. Engenharia Industrial – Teses. 2. Sistemas de distribuição. 3. Configuração da topologia de rede. 4. Resiliência a incêndios florestais. 5. Otimização sob incerteza. 6. Incerteza endógena. I. Santos, Bruno Fânzeres dos. II. Silva, Alexandre Moreira da. III. Pontifícia Universidade Católica do Rio de Janeiro. Departamento de Engenharia Industrial. IV. Título.

CDD: 658.5

Acknowledgments

I dedicate this work to my parents, Marcia and Wanderlei, for their unconditional support my entire life. To my sister Carol and all my family for always being there and encouraging me. And to my girlfriend, Maria, for her partnership and love.

During my Master's program, the friendship and intellectual support of my friends at PUC-Rio and LAMPS proved invaluable. I especially want to thank Bruna, João, Carlos, André, Luiza, Marina, Carol, and Professors Davi and Street.

My journey wouldn't have been the same without the incredible people I met at Berkeley Lab. Patricia, Willian, Amanda, Rafael, Lenard, Luis, Youba, Robin, Albane, Anamika, Agathe, Felix, Mauricio, and Daniel, your kindness and support helped me navigate this challenging experience. I also extend my sincerest thanks to my closest friends for their support: Gustavo, Rodrigo, Enrico, Afonso, Hans, Igor, Leo, André, Daniel, Luciana, Eric, Anna, Phillipe, and Bruna.

Finally, my deepest gratitude goes to my advisor Bruno Fanzeres, and my co-advisor Alexandre Moreira, for their guidance and inspiration. I am also grateful to my dissertation committee members, professors Rafael Martinelli, André Marcato, and Albert Cordeiro, for their insightful feedback and help in different stages of my education. I thank Professor Ruiwei Jiang, Professor Chaoyue Zhao, and Miguel Heleno for their significant contributions to this research. I would also like to express my appreciation to Professor Carlos Aparecido for his wisdom and friendship, and to every professor and professional who has provided mentorship and support throughout my career.

This study was financed in part by the Coordenação de Aperfeiçoamento de Pessoal de Nível Superior - Brasil (CAPES) - Finance Code 001.

The Fundação de Amparo à Pesquisa do Estado do Rio de Janeiro (FAPERJ) and the Lawrence Berkeley National Laboratory (LBNL) partially financed this research.

Abstract

Piancó, Felipe Neves; Santos, Bruno Fânzeres dos (Advisor); Silva, Alexandre Moreira da (Co-Advisor). **Distribution grid planning with lines investment and topology reconfiguration for wildfire resilience under Decision-Dependent Uncertainty**. Rio de Janeiro, 2024. 95p. Dissertação de Mestrado – Departamento de Engenharia Industrial, Pontifícia Universidade Católica do Rio de Janeiro.

Wildfires can be a source of vulnerability for power systems operations. These events can especially affect the operation of distribution systems. They can interrupt energy supply, increase costs, and decrease grid resilience. Numerous approaches can be executed to prevent them. In this dissertation, it is considered the relationship between operative actions and the probability of wildfire disruption. This type of study has not been properly evaluated in technical and scientific literature. By not recognizing this aspect, the operation of power systems may be impaired. Properly modeling this dependency could lower wildfire disruption and loss of load. Considering this, a two-stage distributionally robust optimization problem with decision-dependent uncertainty is developed to consider distribution system multiperiod operation. The first stage determines the optimal switching actions and line investments, and the second stage evaluates the worst-case expected operation cost. It is designed a decision-dependent uncertainty framework where the line failure probabilities are a function (dependent) of its power flow levels. An iterative method is proposed to solve this model and an out-of-sample analysis is developed to validate it through different case studies. Results showed that, by neglecting the uncertainty dependency on operative decisions, there could be a higher expected loss of load and a higher operational cost. By considering this new approach when operating power lines, the grid's resilience could be improved and wildfire consequences can be mitigated with less costly actions.

Keywords

Distribution systems; Topology Reconfiguration; Wildfire Resilience; Optimization Under Uncertainty; Decision-Dependent Uncertainty.

Resumo

Piancó, Felipe Neves; Santos, Bruno Fânzeres dos; Silva, Alexandre Moreira da. **Planejamento de Sistemas de Distribuição com Investimento em Linhas e Reconfiguração de Topologia para Resiliência a Incêndios Florestais sob Incerteza-Dependente de Decisão**. Rio de Janeiro, 2024. 95p. Dissertação de Mestrado – Departamento de Engenharia Industrial, Pontifícia Universidade Católica do Rio de Janeiro.

Os incêndios florestais podem ser uma fonte de vulnerabilidade para sistemas de potência. Esses eventos podem afetar especialmente a operação de sistemas de distribuição, interrompendo o fornecimento de energia, aumentando os custos, e diminuindo a confiabilidade. Nesta dissertação, é considerada a relação entre as decisões operativas e a probabilidade de falha nas linhas sob o contexto de queimadas. Este tipo de estudo ainda não foi devidamente avaliado pelo meio acadêmico. Ao não reconhecer este aspecto, o funcionamento dos sistemas de potência pode estar sendo prejudicado. A modelagem adequada dessa dependência poderia reduzir a incidência de queimadas e perda de carga. Considerando este aspecto, um problema de otimização distributivamente robusto de dois estágios com incerteza endógena foi desenvolvido para considerar a operação multiperíodo de sistemas de distribuição. O primeiro estágio determina a topologia da rede e os investimentos nas linhas, e o segundo estágio avalia o custo operacional esperado no pior caso. Nessa estrutura, a incerteza é modelada de forma dependente das decisões do modelo, onde as probabilidades de falha da linha são em função do fluxo de potência das próprias linhas. Um método iterativo é proposto para resolver este modelo e uma análise fora da amostra é desenvolvida para validação através de diferentes estudos. Os resultados mostraram que, ao negligenciar a dependência da incerteza, uma maior perda de carga e um maior custo operacional são esperados. Ao considerar esta nova abordagem, a confiabilidade da rede pode ser melhorada e as consequências dos incêndios podem ser mitigadas com ações mais econômicas.

Palavras-chave

Sistemas de distribuição; Configuração da topologia de rede; Resiliência a incêndios florestais; Otimização sob incerteza; Incerteza endógena.

Table of contents

List of figures

List of tables

List of algorithms

List of Abreviations

AC – Alternating Current

CAISO – California Independent System Operator

CPUC – California Public Utilities Commission

CVaR – Conditional Value at Risk

DDU – Decision-Dependent Uncertainty

DER – Distributed Energy Resource

DFS – Depth-First Search algorithm

DRO – Distributionally Robust Optimization

EPSS – Enhanced Powerline Safety Settings program

LB – Lower-bound

MER – Mobile Emergency Resource

MILP – Mixed-Integer Linear Programming

MINLP – Mixed-Integer Non Linear Programming

PG&E – Pacific Gas and Electric Company

PSPS – Public Safety Power Shutoff program

SCE – Southern California Edison

SDG&E – San Diego Gas & Electric

UB – Upper-bound

[. . .] The Badger People saw Hummingbird coming and said, "Cover the fire! Cover the fire!" They hid their fire and covered it over with a deerskin. But the deerskin had a hole in it, where an arrow had gone through, and Hummingbird reached in with his long, narrow beak. He took out a hot ember and carried it away – but before he could put it safely into his armpit, it flamed, turning his throat a brilliant red.

Linda Yamane, *How Hummingbird Got Fire: A Rumsien Ohlone Story.*

1
Introduction

1.1
Motivation

Given a perspective of a more erratic weather due to climate changes, being able to predict extreme conditions and how to handle them has been a very important aspect in the operation and planning of the electricity sector. In the context of wildfires, different accidents have drawn the attention of the community into this subject. The damage caused by these events might cost an enormous capital to society. When human lives are involved, the costs can be irreparable.

The state of California/USA, for instance, has undergone a growth in wildfire accidents [2]. Between 2000 and 2016, local utilities had to pay more than $700 million in damage for transmission and distribution systems [3]. In 2018, one of the most threatening wildfires in the state's history was caused by power lines, leading to 85 human deaths. The state was considered in 2021 the worst state in the USA in terms of quantity and extension of wildfires [4]. Recent cases in Brazil, Australia, Chile, Greece, and the United Kingdom warn the importance of the topic worldwide [1, 5].

Although the interaction between power systems and vegetation is not the major cause of wildfires, the consequences can be catastrophic and should not be ignored [6]. The failure of power system components, or the contact of power lines with other lines and external objects can produce arcs or molten particles that can ignite a fire [7]. Combined with climate factors such as extreme wind conditions, dry weather, and temperature, the interaction between power lines and vegetation can be intensified, promoting fire propagation and a large incident [8]. In this context, in the state of California, according to aggregated data from 2022 CPUC Fire Incident reports from the three major utility companies of the state, incidents with distribution systems accounted for more than 90% of the reported cases [9, 10, 11].

To prevent this kind of event, novel operative policies are important to establish efficient power system operations amidst wildfire-prone climate conditions. Actions such as vegetation clearing, equipment inspection and maintenance, line undergrounding, and line shut-off are some of the most common actions taken by utility companies [1]. These actions demand considerable efforts from the companies, and some of them would require areas without

electricity supply and huge investments.

Planning strategies that consider the relationship between operative decisions and the probability of wildfire disruption have not been properly evaluated by technical and scientific literature. From a modeling perspective, in general, uncertainties in power system operations are typically exogenously induced into the decision-making process. In this framework, uncertainty sources are solely associated with external factors and are not endogenously affected by operational actions. However, in many realistic cases, such as under wildfire-prone climate conditions, the operation of electric grids is also associated with the origin of fire ignitions, which significantly increase line failure probabilities. Due to this double role of power grids, the nature of the uncertainty is thus more complex to characterize (dependent not only on meteorological conditions – exogenous factors, but also on the grid operation decisions – endogenous factors), challenging the standard exogenously-induced approach.

In order to design resilience-oriented strategies in high fire-threat areas, utility operators must be aware of the impact of their operational decisions on the likelihood of wildfire initiation and reduction in reliability levels. The model we propose in this dissertation can help in this matter.

1.2 Contributions and objectives

In this research, we propose a methodology for a distribution system operation capable of endogenously taking into account the impact of line power flow in fault probabilities. We design a decision-dependent uncertainty (DDU) framework where the line failure probabilities are a function (dependent) of its power flow levels. In this context, we consider that during extreme weather conditions in certain parts of the grid (e.g., high wind and dry weather), switching actions can be made to reconfigure the grid's topology to reduce the power flow of the lines inside these wildfire-prone areas. The model also acknowledges line investment options that can increase the grid's flexibility for topology reconfiguration, and hardening action investments to decrease the dependency of the failure probability on the line power flow.

Structurally, the proposed methodology falls into the class of a two-stage, three-level, distributionally robust optimization problem (DRO) with DDU. In the first-stage, the model optimally decides for a single-period operation, line investments, and network topology. This is made by minimizing the investment actions and the worst-case expected cost of post-contingency multiperiod operation. Thus, in the second-stage, the post-contingency operation is addressed,

where the probabilities are adjusted according to the first-stage information of the single-period operation and the investments made. The model is summarized in Fig. 1.1.

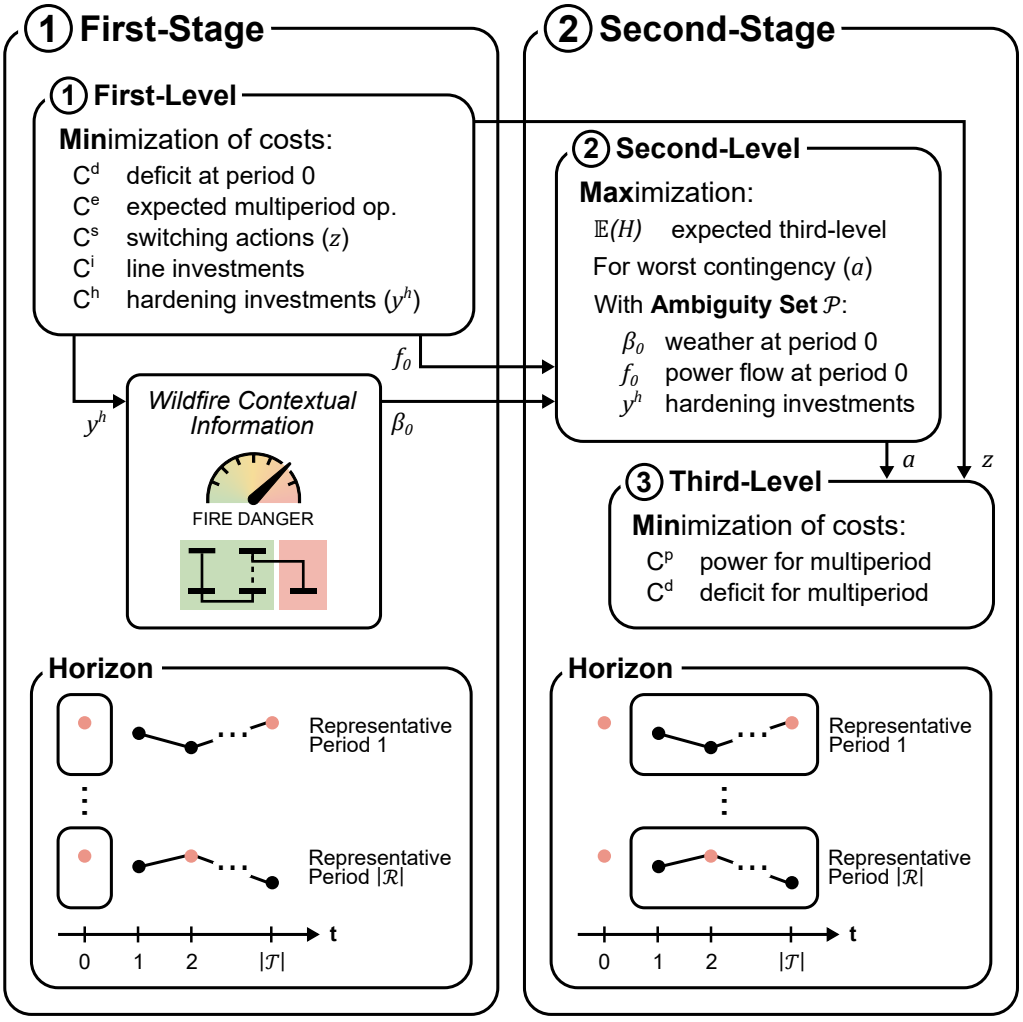

Figure 1.1: Proposed methodology of the three-level model with two stages. The final model is a min-max-min problem.

The first product of this research was reported in [12], where a single-period operation model was developed without any investment options. In this dissertation, we upgrade the model towards including line investment options for a multiperiod operation. We also construct the problem to accommodate more than one representative day, where different weather conditions and load profiles can be considered. To summarize, the contributions of this dissertation are:

1. To formulate a distribution grid planning and operation optimization problem as a two-stage DRO model to increase wildfire resilience.

2. To formulate the uncertainty framework of line failure dependent on the weather conditions and the decisions made by the model (topology).

3. To present a decomposition-based solution methodology capable of solving the proposed three-level problem.

4. To illustrate different aspects of the model with case studies evaluating the topology decisions, parameters sensitivity, costs, loss of load, and reliability.

1.3 Dissertation organization

The rest of this dissertation is structured as follows: Chapter 2 better contextualizes the problem, first showing the relationship between wildfire and power systems, then showing different resilience actions that can be taken. After that, a methodological review is presented, showcasing some works that have addressed this issue, specially considering topology reconfiguration and decision-dependent uncertainty evaluation; Chapter 3 shows the problem formulation we propose, where each level of the three-level model is explained; Chapter 4 shows the development of the methodology to solve this model, where we present the construction of the Master problem, the Subproblem, the cutting-planes, and the algorithm for the decomposition technique used; Chapter 5 shows three illustrative case studies to present to the reader different features and discussions about the proposed model. The first case study shows a 54 bus system with one representative day and no investment option, the second case a 138 bus system with one representative day and no investment option, and last, the third case with a 54 bus system planning for 3 representative days and different investment options; Chapter 6 addresses the conclusions; Appendices A and B present the complete formulation of the final Master problem and Subproblem, respectively; and Appendix C presents the nomenclature of every symbol used for sets, indexes, parameters, variables, and functions.

2
Contextualization

2.1
Wildfires and power systems

The potential for wildfires has arisen worldwide, with the interaction of humans on wild lands and extreme weather conditions as leading causes for this context [1]. The consequences of the interaction between wildfires and power systems are intensified considering the expansion of the power system and the high dependency of modern society on electricity. These events can damage different structures and directly affect the operation. The sudden growth of temperature near the lines can reduce the transmission capacity temporarily [5]. The combination of heat and smoke from wildfires can increase the probability of short circuits as this combination can change the properties of the air gap [5]. Wildfires not only have the strength to impact power systems, but the operation of these systems, in conjunction with environmental conditions, can start wildfires.

Power system's induced wildfires can be started mainly by two forms: when external objects (e.g., tree parts) come in contact with the power line (Fig. 2.1a); or when the line itself comes in contact with nearby vegetation, equipment, or other lines (Fig. 2.1b) [13]. In either case, the sequence of two events is necessary: a line fault followed by the ignition of nearby vegetation [14]. The ignition process occurs when the power flowing in the conductor finds an alternative path to the ground, closing a circuit. This action can directly start a fire when close to vegetation, by creating an arc (Fig. 2.1b), or indirectly through molten metal particles, burning embers, or burning fluids (Fig. 2.1a). In this context, high line flows and line overloading can increase the probability of line faults. Overload lines can increase the line's thermal stress and the occurrence of electric arcs [14], and the duration and intensity of these arcs are directly related to ignition probability [15].

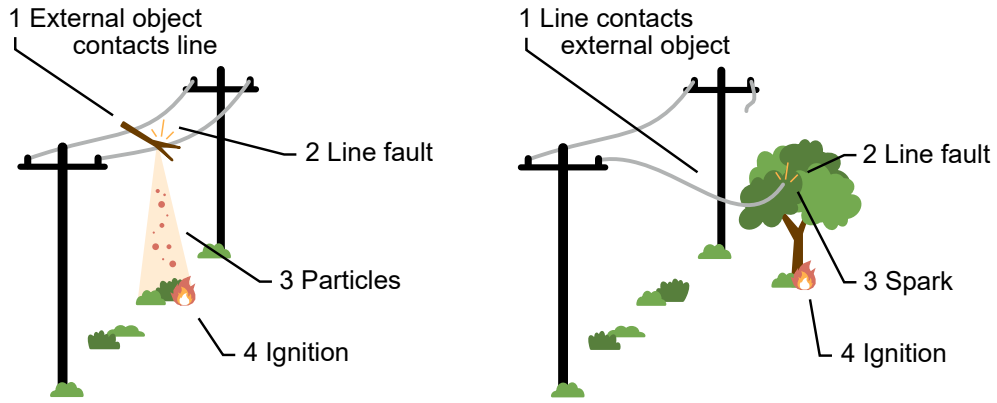

(a) Example 1 (b) Example 2

Figure 2.1: Two examples of a wildfire started by power systems. Adapted from [1].

Although events induced by power systems are not the leading cause of wildfires, their relationship with extreme weather conditions makes this type of wildfire more severe [13]. Wind is the leading weather condition, but humidity and temperature can also intensify its effect [13]. As extreme weather can comprise vast areas, it can lead to multiple line faults and multiple ignitions. Not only that, certain weather conditions can create a mechanism of rapid fire growth and ember showers, leading to multiple large fires and consequently catastrophic losses [7].

In 2009, the chain of wildfires known as “Black Saturday” occurred in Victoria state in Australia. Considered one of the worst wildfires of this century, the event destroyed more than 400,000 ha and caused 173 human deaths [16]. According to authorities, the event was partially caused by the failure of electricity equipment [16]. In 2011, the most destructive wildland-urban interface wildfire in the state of Texas in the United States lasted 55 days, known as “Bastrop fire”, leading to the death of 2 people, hundreds of home losses, and a huge financial impact on the community [17]. The event started when a tree fell over a power line creating an electric arc and igniting the vegetation [18]. Post investigations also found a different ignition point where branches debris created an ignition source when reaching power lines [18]. In 2017, Chile experienced a firestorm of more than 500,000 ha [5]. Investigations point out that some of the multiple ignitions that caused the major event were caused by different power system components malfunctioning. In the following year, in 2018, a fire event spread all over the Attica region in Greece [1]. In this event, 102 people were killed, and it was found that the first ignition

point of the major wildfire was probably also started by malfunction of power components [19].

More recently, in 2023, a wildfire on Maui Island in Hawaii, United States, renewed the world's awareness over this topic. The catastrophe led to at least 106 deaths and caused more than 5 billion dollars of damage [20]. The causes for the event are still not clear, as investigations are ongoing, but one of the possibilities being discussed is that the fire might have started from the contact of power lines and vegetation in a high wind environment [20]. This possibility gains traction considering a fire caused by power lines that were reported and contained earlier than the major fire. The local utility company affirms however that there is no relationship between the first and the second events and states that all lines from the area were de-energized when the second fire occurred [21]. Due to the destructive nature of these events, investigations can take months or even years, and the real cause might not be properly identified and reported. Because of this, it can be hard to condemn the real responsibility and plan for future actions. In the United States, the state of California stands out in this matter for the multiple wildfire cases throughout the year and a strong public opinion on the topic.

In 2018, the deadliest wildfire in California history led to the death of 85 people [22]. In this wildfire, the sequence of events began with an electrical arc between a transmission line and a tower structure. This arc led to an increase in the temperature of the steel structure, creating molten metal particles that fell over the ground. These high-temperature metal particles ignited the dry brush in the area. At a different site, it was discovered that the contact of a pine tree with a distribution line also led to a different source of ignition, starting a minor wildfire [23]. More recently, in 2021, one of the biggest wildfires in state history, the "Dixie fire", took place in an area bigger than 300,000 ha [24]. The contact of a falling tree and a distribution line created an arc that ignited the vegetation surrounding the area. Without proper protection actions, the line remained energized, which contributed to the severity of the incident [25]. Other wildfires such as Tubbs, Witch, Woolsey, and Thomas happened in the state in the past 20 years and their source were all linked with the interaction between electrical systems and vegetation [26]. In fact, out of the 20 most destructive wildfires in California, at least 9 were caused by this interaction between power equipment and the environment [27].

2.2 Wildfire resilience

In the planning and operation of power systems, ensuring the grid's reliability is essential. In this context, the National Renewable Energy Laboratory (NREL) uses the concept of the "three R's of power system reliability": resource adequacy, operational reliability, and resilience [28]. While there can be different definitions for each of these concepts, for NREL, resource adequacy is the ability of the grid to provide electricity uninterruptedly, and operational reliability is the capacity of the system to withstand variability, ramping constraints, and flexible loads [28]. The concept of resilience can be even more difficult to define and can overlap with the two previous definitions [28]. According to [29], one of the definitions used by North American Electric Reliability Corporation (NERC) includes the capability of a system to anticipate, adapt, and recover from disruptive events. The concept is usually related to high-impact events with a low probability of occurrence [30]. Under the context of extreme weather events, different actions can be taken to increase situational awareness and provide an adequate response to such events [31]. To properly enhance the grid's observability, controllability, and operation flexibility, two types of measure can be made: hardening decisions, taking part in a planning stage, that could include vegetation management and Distributed Energy Resources (DERs) allocation; and "smart" decisions that can include more cost-effective strategies developed in the context of operation [30, 32].

Under a wildfire context, a 3-line of defense framework is proposed in [33]. First, wildfire prevention is addressed by developing different strategies such as wildfire prediction, fire-inducing faults detection, wildfire detection, equipment maintenance and inspection, power lines hardening, and vegetation management. After this, wildfire risk mitigation and proactive response actions are taken, such as power lines de-energization, suppression tactics, wildfire monitoring and tracking, and grid operations management. In the end, recovery preparedness is approached through actions such as energy contingency plans, recovery logistics, disaster risk financing, and community engagement.

To increase the grid's resilience in the context of wildfire, power systems actors develop different responses, considering each grid's unique characteristics (see Table 2.1 for a summary of actions). In Latin America, Chile has experienced in the last years a growth in wildfire accidents, a context that has led to different impacts [5]. The Chilean reaction to the subject was made mostly after the 2017 firestorm event. For 19 days, about 681 ignition points were recorded, affecting 24 transmission lines, and causing about 50 line shortages. Chilean authorities' response during the event was to reduce power flow

in some areas, avoiding major load shedding. The usage of already installed DERs also helped to ensure electricity supply to areas aisled by line shortages. After the incident, the country developed platforms that can provide data for decision-making processes, such as energy facilities location, climate variables, and historical wildfire data. New security standards for transmission network planning were also promoted.

Table 2.1: Power system's wildfire resilience actions

Action type	**Examples**	**Reference**
Asset management	Visual asset inspection	[2]
	Corrosion monitoring	[34]
	Equipment inspection with drones	[35]
Education	Community planning	[1]
	Public information campaigns	[5]
Equipment hardening	Conductor covering	[2]
	Line undergrounding	[36]
	Insulator upgrades	[34]
	Wood to concrete poles	[34]
Fault management	Early fault detection	[2]
	Fault current limiter	[36]
	Automatic circuit reclosers	[34]
Fuel management	Controlled burning	[1]
	Fire retardant application	[34]
	Vegetation management	[34]
Grid planning	Switching devices installment	[35]
Grid operation	Proactive de-energization	[37]
	Microgrid formation	[38]
	DER utilization	[38]
	Mobile power sources	[5]
	Network topology control	[5]
Regulation	Fire ban	[34]
Weather awareness	Situation awareness tools	[5]
	Forecasting programs	[35]

The past years in Brazil also revealed the same experience in Chile: growth of wildfire accidents and growth of intensity [5]. In the country, wildfire and atmospheric discharges were combined the cause of more than 50% of line outages in 2020. The outages due to these two causes usually have complementary patterns. While discharges took place mainly in rainy seasons (December-April), wildfire outages took place mainly in dry season (May-November). The fact that wildfires were more abundant in dry seasons and that they were dispersed through the Midwest and Northeast regions provides an additional concern in the system operation perspective. The reason for this

concern is that in those months, a higher production of hydropower plants in the Midwest, and higher production of wind power plants in the Northeast, supply energy for the Southeast region, where the most populous cities are, with higher electricity consumption. As a consequence of those dry seasons, wildfires have erupted through Brazil's interior, leading to many events with line outages. From the operator's perspective, preventive and corrective control programs were implemented. In the planning transmission expansion, wildfire disruption probability is being considered. Regulatory actions were imposed, mainly regarding vegetation clearance below transmission lines and public awareness programs.

In Australia, although transmission lines are usually far from vegetation, smoke, and meteorological conditions can disturb operation. Distribution lines, on the other hand, are typically closer to the ground and to "bush" areas, which tends to enhance the risk of line disruption caused by wildfires. Besides typical preventive and response strategies, it is being discussed how the concept of microgrids allied with the usage of DERs can mitigate further impacts of line disruptions in the country. The operations of some areas aisled from the main grid could ensure the power supply to customers, especially to essential services [34].

In fact, microgrids potential to increase wildfire resilience where perceived in other places [38]. In the United States, the development of microgrids is usually promoted for resilience purposes, especially in the face of extreme weather events such as tornadoes and wildfires. In the Blue Lake Rancheria tribe, a microgrid was developed with a different objective, but after recent wildfire events in California, resilience became its main purpose. With a system composed of a photovoltaic plant, a battery bank, and a backup generator, the microgrid can act as a supplier to emergency customers in the case of grid islanding. In Greece, a wildfire incident in 2007 was partially responded by employing microgrids, mainly through the usage of mobile diesel generators. The relevance of these equipment was also proven in the events that took place in the country in 2021, especially in the Attica, Euboea, and Olympia regions. In Canada, local government provinces develop different incentive programs for microgrids operation, in particular considering indigenous communities. Japan is also promoting microgrid programs, considering extreme events such as earthquakes.

In the United States, California's prolonged periods of drought and high temperatures promote scenarios of extreme weather conditions. After major wildfire events during 2017 and 2018, the topic increased public awareness, which helped model authorities' response [2]. In the South, San Diego Gas &

Electric (SDG&E) company has done numerous initiatives in this matter [35]. Situational awareness and forecasting programs were developed, such as wildfire risk modeling programs, weather station integration, and fault indicators circuits. It was created a specialized department within the corporation to handle climate subjects. Initiatives in the grid design included conductors covering, equipment modernization, protection programs implementation, and microgrid development. The utility company Southern California Edison (SCE) also developed special operational protocols, vegetation clearance, and conductors hardening [2]. The operator has strengthened transmission lines by covering its conductors with different technologies. Artificial intelligence and machine learning algorithms have helped the company to identify equipment defects using a picture database obtained with aerial inspections. The implementation of microgrids has also been studied to enhance the grid resilience. Similar actions were taken by Pacific Gas and Electric Company (PG&E), the major utility company of the state [36]. The company is one of the state's utilities that uses the program Public Safety Power Shutoff (PSPS), where under high wind weather, the company actively turns off the power of high-threat areas to prevent wildfire disruption by power lines. As a consequence, this program can cause power outages for customers for long periods [37]. A more recent initiative, the Enhanced Powerline Safety Settings (EPSS) program, is helping the reduction of the PSPS necessity, decreasing customers' impact. In this program, line protection devices' responses are enhanced to de-energize line segments faster. This helps reduce the amount of time the line is in contact with external objects, decreasing the energy released, thus reducing potential sources of wildfire ignition. The company is also deploying a program to underground 10,000-mile of distribution lines under high wildfire-risk areas.

2.3 Methodological review

Many works have handled power system's planning and operation considering extreme events. At the transmission level, for instance, the work developed in [39] proposes a two-stage stochastic Mixed-Integer Non-Linear Programming (MINLP) model to define investment strategies of transmission and generation expansion to improve resilience, considering a range of earthquake events. The methodology in [40] combines optimization and simulation techniques to determine a portfolio of investments such as new lines, transformers, and substation hardening. In this case, the dependency of failure rate of a equipment and hardening decisions are not fully addressed. The occurrence of seismic hazards is also considered in [41], where is introduced different damage

states to acknowledge the fact that equipment can be impacted in different ways. A battery sitting and sizing model is then developed to increase resilience at the distribution level. In [42] the authors designed a 3-level system of optimization models to coordinate line hardening solutions and operational measures to protect the distribution grid against natural disasters and human-made attacks. Topology reconfiguration is considered as a defensive tool in the operation stage, and line hardening in the planning stage.

Wildfires alone have also motivated works in the area. In [43], the authors analyzed the problem for the expansion planning area regarding transmission lines. The novelty of the work is to account for wildfires that are ignited by transmission lines, where different intensities of fire-threat zones are considered. With that, the expansion problem is modeled as a Mixed-Integer Linear Programming (MILP) problem, where the wildfire risk is represented by the unavailability of lines within fire-threat zones. Considering the case where utility companies conduct public safety power shut-offs (PSPS) to prevent wildfire ignitions, authors in [44] develop a risk-aware planning problem. With the help of a machine learning model, they are able to quantify the risk of wildfire ignition with high accuracy by integrating weather conditions into the risk mitigation process.

A model to predict wildfire is constructed in [45] and discusses how it could help transmission line operation decisions prior to the wildfire happens. The work presented in [46] proposes a probabilistic redispatch strategy using a Markov decision process to model system state transitions and take decisions considering uncertainties of failure, load, and wildfires' spatial-temporal properties. With this model, they are able to reduce load curtailments and operational costs in the occurrence of wildfires. Authors acknowledge the high uncertainty nature of wildfires and the fact that they can propagate and impact different components of the grid.

Other works investigate the subject considering distribution level. In [47], uncertainties such as solar radiation and wind properties are considered exogenously in a stochastic model to incorporate the progression of the wildfire. The impact of these events is considered not only under the line's temperature but also in its ability to remain operative. By acknowledging that, the distribution system can be better operated with minimized load shedding. In [48], the rise of lines' temperatures is modeled given the occurrence of small to medium wildfires nearby. By considering this, decisions can be made to mitigate load outages, for instance, by committing distributed resources. Authors in [49] presented the relationship between wildfire and power line operation by considering that wildfires can change dramatically the weather

near transmission lines, and therefore it can change the ampacity of each line. A risk-averse IGPD (information-gap decision theory) method is developed to solve the problem, considering uncertainties such as wind and solar generation, load, and ampacity of the lines, being able to increase the operational resiliency of the system.

2.3.1 Topology reconfiguration

Different researchers have provided ways to increase grid resilience under extreme events using network reconfiguration. Authors in [50] propose a dynamical reconfiguration of the distribution system to form islanded microgrids that can keep providing load to certain areas in the event of natural disasters. These microgrids are supported by the usage of distributed generation in real-time operation and can also help in the grid restoration stage. In [51], it is proposed a radiality constraint methodology to fully take advantage of distribution network flexibility. Combined with distribution system automation, microgrids, and distributed generation, network configuration is shown as a measure to alleviate the risks under the occurrence of extreme events.

Authors in [52] combine a transmission expansion problem and an optimal transmission switching problem to increase the resilience of the network under typhoon-related events. The final problem is a three-level model, where the upper level minimizes the transmission expansion investment, the middle level maximizes the worst-case expected load-shedding, and the lower level minimizes the worst-case cost considering economic dispatch and optimal transmission switching. In [53], the problem of grid design is considered also in the transmission system, with measures to improve resilience under extreme weather in general. The authors model a two-stage problem, where in the first stage upgrades investments are decided and in the second stage the network performance is tested under different scenarios. The upgrade actions include the construction of new lines, the addition of switches (to improve operational flexibility), the addition of FACTS devices and transformers, hardening actions for existing lines, and the implementation of distributed generators.

In the distribution expansion problem, authors model a two-stage stochastic program in [54]. The model captures communication networks and different measures to harden the system under disaster scenarios. The first stage decides the system upgrade investments such as hardening power lines and communication links, installing new lines, making new communication pathways, installing remotely controlled switches, and placing of distributed generators. Then, the second stage can decide how to reconfigure the grid

and use the new elements to attend demand in each disaster scenario considered. By acknowledging the relationship between the distribution grid and the communication system, grid resilience can be improved with hardening and modernization investments.

The expansion problem is discussed especially under the wildfire context in [55]. The expansion model includes three different decisions: addition of new lines, modification of existing lines, and installation of DERs. With these decisions, the model aims to mitigate the wildfire risk while considering the consequences of PSPS. The modification of existing lines is modeled as any hardening measures the planner can take to decrease the vulnerability of the line to wildfire-prone environments. In real life, these measures can be a wide range of actions, such as reconductoring, undergrounding, line repositioning, anchoring, wood pole replacement, and many others. The installation of DERs is modeled as a measure to decrease the demand in its source, thus alleviating load shedding if needed. The model then accounts for the risk of wildfire by integrating different factors that affect the ignition risk, such as wind speed, vegetation, and humidity. Although it is not their main concern, in one of the case studies developed by the authors, it is highlighted the side benefit of adding a new line to the system. By taking this action, the grid can count to more possible topologies (as they consider that every line in the system can be switched on and off). Results show that by adding new lines and allowing them to perform switching actions, the overall costs of the expansion are reduced, as the wildfire risk is decreased, with lower investments on DER and line hardening deployment.

Recent works have provided this perspective also under the operation context. In [32], authors focus on the operation actions that can be made to increase resilience response, both in a preventive stage and as an emergency response. An integrated resilience response framework is developed, acknowledging operation strategies of generation redispatch, line switching, and load shedding. The line switching strategies include actions to turn on or turn off specific lines, both as a preventive action and as an emergency action during the occurrence of the event. In [56], authors develop a stochastic recovery framework to improve resilience in a post-hurricane scenario. In this case, switching actions provide ways to better restore critical loads. The best configuration chosen also helps to determine islanded areas of the grid that will need mobile emergency resources (MERs) in the post-hurricane event. Other works, such as [57], also consider islanding strategies through reconfiguration of distribution systems. The method obtains the optimized topology before the event occurs and addresses the reconfiguration after the occurrence of multiple faults caused

by the extreme event.

In these works, it is not considered the possibility of grid reconfiguration decisions to impact the uncertainty dynamics.

2.3.2 Decision-dependent uncertainty

A few works considered decision-dependent uncertainties in the context of extreme events for power systems. This type of framework models the endogenous nature that the uncertainty set might have, i.e., when the uncertainty set is dependent on a decision variable or a set of decision variables within the problem. For illustrative purposes, this type of problem can be seen in the following two-stage DRO general formulation as shown in [58]:

$$\underset{\boldsymbol{x}\in\mathcal{X}}{\text{Minimize}} \ \Big\{ f(\boldsymbol{x}) + \underset{\mathcal{Q}\in\mathcal{P}(\boldsymbol{x})}{\text{Maximize}} \ \Big\{ \mathbb{E}_{\mathcal{Q}}[H(\boldsymbol{x},\boldsymbol{\xi})] \Big\} \Big\}, \tag{2-1}$$

where $\boldsymbol{x}$ is the decision variable vector, and $\boldsymbol{\xi}$ the uncertain parameter vector that follows the probability distribution $\mathcal{Q}$. The first part of the objective function, $f(\boldsymbol{x})$, has no uncertain parameters and models the first-stage of this decision-making process. The second part of the objective function is defined following the ambiguity set $\mathcal{P}$. This maximization problem calculates the worst expected value of function H. The ambiguity set is used to model the uncertainty in the probability distributions of parameters, and in this case, is dependent on the first stage decision variables $\boldsymbol{x}$. This set is contained in $\mathcal{M}^{+}$ (set of all probability distributions) and can be defined in different ways following different purposes (see, e.g., Section 6 of [59]). The function H can be defined as:

$$H(\boldsymbol{x},\boldsymbol{\xi}) = \underset{\boldsymbol{y}}{\text{Minimize}} \ \Big\{ g(\boldsymbol{x},\boldsymbol{y},\boldsymbol{\xi}) \Big\} \tag{2-2}$$

subject to:

$$\psi_i(\boldsymbol{x},\boldsymbol{y},\boldsymbol{\xi}) \leq 0 \quad \forall i = 1,\cdots,m, \tag{2-3}$$

where $g(\cdot)$ and $\psi_i(\cdot)$ are bounded and continuous functions, and $\boldsymbol{y}$ is the decision variable vector of the second-stage. Different works considered this type of formulation with variations, aiming to tackle different problems.

In [60] a two-stage model is developed. In the first stage, hardening decisions and the deployment of DERs and switches are considered. In the second stage, operation costs are evaluated considering load curtailment costs and damage repair when the occurrence of extreme weather events. In this model, the damage caused by wind-induced events on lines is considered to be

dependent on the hardening decisions previously made.

In [61] the authors propose a decision-dependent stochastic model for the operation and maintenance of transmission lines considering the occurrence of sandstorms, and consequent line failures. The uncertainty is made endogenously considering the relationship between line failure and maintenance decisions in post-sandstorm scenarios. The first stage models the unit commitment and maintenance decisions, and the second stage models the operation scenario-wise, accounting for generator power output, wind power spillage, and load-shedding.

Authors in [62] propose a framework to enhance resilience against typhoons. Typhoon path and wind field are simulated using Monte Carlo sampling to model line impact. Decision-dependency is constructed to reflect the relationship between line enhancement measures and the probability of failure of the line given a typhoon event. A two-stage stochastic mixed-integer programming is developed and solved via sample average approximation (SAA) algorithm.

The work developed in [63] considers an investment model to protect the system against earthquakes. The two-stage stochastic optimization model decides in the first stage for the grid's investments and operation in a pre-contingency case, and in the second stage dispatch corrective actions in a post-contingency case based on different scenarios. The uncertainty is modeled in a decision-dependent approach as the investments of the transmission system can change outage probabilities, and the challenge of dealing with this type of model is addressed with a DRO framework. It is considered two types of investments: hardening substations to withstand seismic events; and the creation of new lines to allow other paths for the power flow in the event of an outage.

Also considering earthquake scenarios, authors in [64] develop a planning model to increase resilience. In this case, the investment portfolio considers hardening actions for distribution lines and investments in mobile generators and mobile storage systems. The decision to harden the lines affects directly the probability of a line to be damaged in the face of an earthquake, thus considering an endogenous uncertainty. The bi-level structure developed minimizes first the investments and the expected interruption cost, and second the post-disaster operation.

Most of the works presented here consider that investment decisions, to harden the system's components, affect outage uncertainty. However, all of them fail to directly consider an endogenous uncertainty framework under a wildfire context. As far as we are concerned, no other work other than [12]

optimizes investments in distribution grids while properly considering decision-dependent uncertainty related to power lines potentially initiating fires.

3
Problem formulation

The model we propose can optimally decide for line investments and topology configuration given a set of representative days while considering potential wildfire-prone circumstances. In the two-stage problem we develop, the first stage decides for the investments and the grid topology, while in the second stage, the operation of the whole period is robustly accounted for. To address this, we develop a three-level problem. The first-level minimizes the costs of deficit and surplus at "period 0", the worst expected cost of the multiperiod operation, the costs of the switching actions, and the costs of line and hardening investments. In this case, "period 0" can be chosen as a prior operating point, or as the worst period in the operation in terms of wildfire-prone environment. The operation of this single period will determine the ambiguity set used in the second-level (this set models the uncertainty in the probability distributions of parameters, explained in Section 3.2), where the worst-case line contingency is calculated by maximizing the expected cost of the third-level. Finally, the third-level minimizes the costs of operating the grid of every representative day in a post-contingency scenario. The relationships between these levels and what they stand for were summarized in Fig. 1.1.

3.1
First-level: investment planning problem under wildfire-related decision-dependent uncertainty

The objective function of the first-level minimization problem is defined as:

$$\sum_{r\in\mathcal{R}}\left(\Big(C_r^d(\cdot)+C_r^e(\cdot)\Big)w_r^1+\Big(C_r^s(\cdot)\Big)w_r^2\right)+C^i(\cdot)+C^h(\cdot), \tag{3-1}$$

where the first three cost functions are accounted for every r in the set of representative days $\mathcal{R}$: $C_r^d(\cdot)$ is the cost function of the prior operating point deficit/surplus at $t=0$; $C_r^e(\cdot)$ is the worst expected cost of the multiperiod operation; and $C_r^s(\cdot)$ is the switching actions costs. Investments are decided in the first stage for all of the representative days: $C^i(\cdot)$ is the function for line investments costs, and $C^h(\cdot)$ is for hardening investments costs. All of the costs can be considered in the same objective function by applying weights that every representative day r has in a year, and by considering investments costs annually levelized. Parameter w_r^1 is the weight of one hour and w_r^2 is the

weight of the switching action of the representative day in a year. Each of these cost functions is defined as:

$$C_r^d(\cdot) = \sum_{b\in\mathcal{N}} \Big(C^{p+}\Delta D_{b,0,r}^{p+} + C^{p-}\Delta D_{b,0,r}^{p-} + C^{q+}\Delta D_{b,0,r}^{q+} + C^{q-}\Delta D_{b,0,r}^{q-} \Big) \tag{3-2}$$

$$C_r^e(\cdot) = \sup_{\mathcal{Q}\in\mathcal{P}_r(\boldsymbol{f}_r^p,\boldsymbol{y}^{ha})} \mathbb{E}_{\mathcal{Q}}\Big[H_r(\boldsymbol{z}_r,\boldsymbol{a}_r)\Big] \tag{3-3}$$

$$C_r^s(\cdot) = \sum_{l\in\mathcal{L}^{sw}} C_l^{sw} y_{l,r}^{sw} \tag{3-4}$$

$$C^i(\cdot) = \sum_{l\in\mathcal{L}^{sw,c}} C_l^{sw,in} y_l^{sw,in} + \sum_{l\in\mathcal{L}^{c}} C_l^{in} y_l^{in} \tag{3-5}$$

$$C^h(\cdot) = \sum_{l\in\mathcal{L}^{ha}} \sum_{h\in\mathcal{H}_l} C_{l,h}^{ha}\ y_{l,h}^{ha}, \tag{3-6}$$

where, C^{p+}, C^{p-}, C^{q+}, C^{q-}, C^{sw}, $C^{sw,in}$, C^{in}, and C_h^{ha}, are respectively the cost of: active power surplus; active power deficit; reactive power surplus; reactive power deficit; switching action; investment to turn regular line into switchable; investment to construct a line; and investment of a line hardening action h. In this last case, different line hardening actions ($h \in \mathcal{H}_l$) can be considered with different costs and different impacts. Variables $\Delta D_{b,0,r}^{p+}$, $\Delta D_{b,0,r}^{p-}$, $\Delta D_{b,0,r}^{q+}$, and $\Delta D_{b,0,r}^{q-}$, are respectively the variables of active power surplus, active power deficit, reactive power surplus, and reactive power deficit, of each line l at each representative day r at the prior operating point $t = 0$. Binary variable $y_{l,r}^{sw}$ represents the switching action of each line $l \in \mathcal{L}$ at representative day $r \in \mathcal{R}$. And binary variables $y_l^{sw,in}$, y_l^{in}, and $y_{l,h}^{ha}$, are respectively investment decisions for turning a regular line into switchable, creating a new line, and making hardening action at each line $l \in \mathcal{L}$. These variables take the value 1 if the decision was made and 0 otherwise. Equation (3-3) represents the worst-case operation cost. The first-level problem is defined as follows:

$$\begin{aligned}
\underset{\substack{p_{b,0,r},q_{b,0,r},v_{b,0,r}^{\dagger},f_{l,0,r}^{p},f_{l,0,r}^{q},\\ \Delta D_{b,0,r}^{p+},\Delta D_{b,0,r}^{p-},\Delta D_{b,0,r}^{q+},\Delta D_{b,0,r}^{q-}\\ z_{l,r},y_{l,r}^{sw},y_l^{sw,in},y_l^{in},y_{l,h}^{ha}}}{\text{Minimize}}\ & \sum_{r\in\mathcal{R}} \Bigg\{ \Bigg(\sum_{b\in\mathcal{N}} \Big(C^{p+}\Delta D_{b,0,r}^{p+} + C^{p-}\Delta D_{b,0,r}^{p-} + C^{q+}\Delta D_{b,0,r}^{q+} + C^{q-}\Delta D_{b,0,r}^{q-} \Big) \\
& \qquad + \sup_{\mathcal{Q}\in\mathcal{P}_r(\boldsymbol{f}_r^p,\boldsymbol{y}^{ha})} \mathbb{E}_{\mathcal{Q}}\Big[H_r(\boldsymbol{z}_r,\boldsymbol{a}_r)\Big] \Bigg) w_r^1 + \Bigg(\sum_{l\in\mathcal{L}^{sw}} C_l^{sw} y_{l,r}^{sw} \Bigg) w_r^2 \Bigg\} \\
& + \sum_{l\in\mathcal{L}^{sw,c}} C_l^{sw,in} y_l^{sw,in} + \sum_{l\in\mathcal{L}^{c}} C_l^{in} y_l^{in} + \sum_{l\in\mathcal{L}^{ha}} \sum_{h\in\mathcal{H}_l} C_{l,h}^{ha}\ y_{l,h}^{ha}
\end{aligned} \tag{3-7}$$

subject to:

$$p_{b,0,r} + \sum_{l\in\mathcal{L}|to(l)=b} f^p_{l,0,r} - \sum_{l\in\mathcal{L}|fr(l)=b} f^p_{l,0,r} - D^p_{b,0,r} - \Delta D^{p+}_{b,0,r} + \Delta D^{p-}_{b,0,r} = 0; \\ \forall b \in \mathcal{N}^{sub}, r \in \mathcal{R} \quad (3\text{-}8)$$

$$q_{b,0,r} + \sum_{l\in\mathcal{L}|to(l)=b} f^q_{l,0,r} - \sum_{l\in\mathcal{L}|fr(l)=b} f^q_{l,0,r} - \tan(\arccos(PF_b))D^p_{b,0,r} \\ - \Delta D^{q+}_{b,0,r} + \Delta D^{q-}_{b,0,r} = 0; \forall b \in \mathcal{N}^{sub}, r \in \mathcal{R} \quad (3\text{-}9)$$

$$\sum_{l\in\mathcal{L}|to(l)=b} f^p_{l,0,r} - \sum_{l\in\mathcal{L}|fr(l)=b} f^p_{l,0,r} - D^p_{b,0,r} - \Delta D^{p+}_{b,0,r} + \Delta D^{p-}_{b,0,r} = 0; \\ \forall b \in \mathcal{N} \setminus \mathcal{N}^{sub}, r \in \mathcal{R} \quad (3\text{-}10)$$

$$\sum_{l\in\mathcal{L}|to(l)=b} f^q_{l,0,r} - \sum_{l\in\mathcal{L}|fr(l)=b} f^q_{l,0,r} - \tan(\arccos(PF_b))D^p_{b,0,r} \\ - \Delta D^{q+}_{b,0,r} + \Delta D^{q-}_{b,0,r} = 0; \forall b \in \mathcal{N} \setminus \mathcal{N}^{sub}, r \in \mathcal{R} \quad (3\text{-}11)$$

$$v^{\dagger}_{to(l),0,r} - v^{\dagger}_{fr(l),0,r} + 2(R_l f^p_{l,0,r} + X_l f^q_{l,0,r}) \leq (1 - z_{l,r})M; \forall l \in \mathcal{L}, r \in \mathcal{R} \quad (3\text{-}12)$$

$$v^{\dagger}_{fr(l),0,r} - v^{\dagger}_{to(l),0,r} - 2(R_l f^p_{l,0,r} + X_l f^q_{l,0,r}) \leq (1 - z_{l,r})M; \forall l \in \mathcal{L}, r \in \mathcal{R} \quad (3\text{-}13)$$

$$f^q_{l,0,r} - \cot\left(\left(\frac{1}{2} - e\right)\frac{\pi}{4}\right)\left(f^p_{l,0,r} - \cos\left(e\frac{\pi}{4}\right)\overline{F}_l\right) - \sin\left(e\frac{\pi}{4}\right)\overline{F}_l \leq 0; \\ \forall l \in \mathcal{L}, e \in \{1,\ldots,4\}, r \in \mathcal{R} \quad (3\text{-}14)$$

$$- f^q_{l,0,r} - \cot\left(\left(\frac{1}{2} - e\right)\frac{\pi}{4}\right)\left(f^p_{l,0,r} - \cos\left(e\frac{\pi}{4}\right)\overline{F}_l\right) - \sin\left(e\frac{\pi}{4}\right)\overline{F}_l \leq 0; \\ \forall l \in \mathcal{L}, e \in \{1,\ldots,4\}, r \in \mathcal{R} \quad (3\text{-}15)$$

$$0 \leq p_{b,0,r} \leq \overline{P}_b; \forall b \in \mathcal{N}^{sub}, r \in \mathcal{R} \quad (3\text{-}16)$$

$$\underline{Q}_b \leq q_{b,0,r} \leq \overline{Q}_b; \forall b \in \mathcal{N}^{sub}, r \in \mathcal{R} \quad (3\text{-}17)$$

$$\underline{V}^2_b \leq v^{\dagger}_{b,0,r} \leq \overline{V}^2_b; \forall b \in \mathcal{N} \setminus \mathcal{N}^{sub}, r \in \mathcal{R} \quad (3\text{-}18)$$

$$v^{\dagger}_{b,0,r} = V^{ref^2}; \forall b \in \mathcal{N}^{sub}, r \in \mathcal{R} \quad (3\text{-}19)$$

$$- z_{l,r}\overline{F}_l \leq f^p_{l,0,r} \leq z_{l,r}\overline{F}_l; \forall l \in \mathcal{L}, r \in \mathcal{R} \quad (3\text{-}20)$$

$$- z_{l,r}\overline{F}_l \leq f^q_{l,0,r} \leq z_{l,r}\overline{F}_l; \forall l \in \mathcal{L}, r \in \mathcal{R} \quad (3\text{-}21)$$

$$0 \leq \Delta D^{p+}_{b,0,r} \leq D^p_{b,0,r}; \forall b \in \mathcal{N}, r \in \mathcal{R} \quad (3\text{-}22)$$

$$0 \leq \Delta D^{p-}_{b,0,r} \leq D^p_{b,0,r}; \forall b \in \mathcal{N}, r \in \mathcal{R} \quad (3\text{-}23)$$

$$0 \leq \Delta D^{q+}_{b,0,r} \leq \tan(\arccos(PF_b))D^p_{b,0,r}; \forall b \in \mathcal{N}, r \in \mathcal{R} \quad (3\text{-}24)$$

$$0 \leq \Delta D^{q-}_{b,0,r} \leq \tan(\arccos(PF_b))D^p_{b,0,r}; \forall b \in \mathcal{N}, r \in \mathcal{R} \quad (3\text{-}25)$$

$$y^{sw}_{l,r} = 0; \forall l \in \mathcal{L} \setminus \mathcal{L}^{sw}, r \in \mathcal{R} \quad (3\text{-}26)$$

$$y^{sw,in}_{l} = 0; \forall l \in (\mathcal{L}^{sw,e}) \cup (\mathcal{L} \setminus \mathcal{L}^{sw}) \quad (3\text{-}27)$$

$$y^{in}_{l} = 0; \forall l \in \mathcal{L}^{e} \quad (3\text{-}28)$$

$$z_{l,r} = 1; \forall l \in \mathcal{L}^{e} \setminus \mathcal{L}^{sw}, r \in \mathcal{R} \quad (3\text{-}29)$$

$$y^{sw}_{l,r} \leq y^{sw,in}_{l}; \forall l \in \mathcal{L}^{sw,c}, r \in \mathcal{R} \quad (3\text{-}30)$$

$$y^{sw,in}_{l} \leq y^{in}_{l}; \forall l \in (\mathcal{L}^{c}) \cap (\mathcal{L}^{sw,c}) \quad (3\text{-}31)$$

$$y^{sw}_{l,r} \geq +z_{l,r} - z^{init}_{l,r}; \forall l \in \mathcal{L}^e, r \in \mathcal{R} \tag{3-32}$$

$$y^{sw}_{l,r} \geq -z_{l,r} + z^{init}_{l,r}; \forall l \in \mathcal{L}^e, r \in \mathcal{R} \tag{3-33}$$

$$y^{in}_{l} - y^{sw,in}_{l} \leq z_{l,r}; \forall l \in \mathcal{L}^c \setminus \mathcal{L}^{sw,e}, r \in \mathcal{R} \tag{3-34}$$

$$z_{l,r} \leq y^{in}_{l}; \forall l \in \mathcal{L}^c, r \in \mathcal{R} \tag{3-35}$$

$$\sum_{l \in \mathcal{L}^{forb}_k} z_{l,r} \leq |\mathcal{L}^{forb}_k| - 1; \forall k \in \mathcal{K}^{forb}, r \in \mathcal{R} \tag{3-36}$$

$$z_{l,r}, y^{sw}_{l,r} \in \{0,1\}; \forall l \in \mathcal{L}, r \in \mathcal{R} \tag{3-37}$$

$$y^{sw,in}_{l}, y^{in}_{l} \in \{0,1\}; \forall l \in \mathcal{L} \tag{3-38}$$

$$\sum_{h \in \mathcal{H}_l} y^{ha}_{l,h} \leq 1; \forall l \in \mathcal{L}^{ha} \tag{3-39}$$

$$y^{ha}_{l,h} \in \{0,1\}; \forall h \in \mathcal{H}_l, l \in \mathcal{L}^{ha}. \tag{3-40}$$

Constraints (3-8)–(3-11) model the active and reactive power balance in the buses with substations and in the buses without substations. Variables p and q represent active and reactive power at each substation, and variables f^p and f^q active and reactive power flow at each line, respectively. Parameters D^p and PF are the demand and the power factor at each bus. Constraints (3-12)–(3-13) model the voltage difference between buses, where variable $v^\dagger$ represents the squared voltage of the bus where a line starts (to) and the voltage where the line ends (from). Parameters R and X are respectively the resistance and the reactance of each line, and parameter M denotes a large number to relax these constraints when the line is off or was not created. Constraints (3-14)–(3-15) limit the active and reactive power flows according to the linearized AC power flow in [65]. Constraints (3-16)–(3-25) model the lower- and upper-bounds of all non-binary variables, where parameters $\overline{P}$, $\underline{Q}$, $\overline{Q}$, $\underline{V}$, $\overline{V}$, V^{ref}, and $\overline{F}$ represent the maximum active power at the substations, minimum reactive power at the substations, maximum reactive power at the substations, minimum voltage at every bus that is not a substation, maximum voltage at every bus that is not a substation, voltage reference at the substations, and maximum power flow in each line, respectively.

The group of constraints (3-26)–(3-38) models the behavior of the binary variables z, y^{sw}, $y^{sw,in}$, and y^{in}. Variable z represents the line status, where it takes the value 1 if the line is on, or 0 if the line is off. For example, if a line is switchable and the model chooses to turn off this line, variable z will assume value 0. The same will occur if a candidate line was not created. Parameter z^{init} represents the initial status of the line, where is 0 if the line starts off and 1 if the line starts on. Variable y^{sw} represents the action of turning a switchable line on or off, assuming value 1 if the action was made, and 0 otherwise. Variable

$y^{sw,in}$ represents the investment action of turning a line to become switchable, and y^{in} is the investment action of creating a new line, where they assume the value 1 if the investment was planned.

In this framework, a given line can be part of one of six different sets (see Fig. 3.1): 1) existing, 2) existing and switchable, 3) existing and candidate to become switchable, 4) candidate, 5) candidate that is switchable, and 6) candidate that can become switchable if an additional investment is made. The set of constraints (3-26)–(3-38) can model the status and investments of any line of a problem that has lines in any of these sets. Constraint (3-26) ensures that a line that is not switchable will not perform a switching action. Constraint (3-27) says that a line that is not a candidate to become switchable cannot make investments to become switchable, while constraint (3-28) ensures that the existing line cannot have line investment. Constraint (3-29) says that a line that exists and is not switchable, will always have its status on. For the lines that are candidates to become switchable, constraint (3-30) makes sure that a switching action is performed only if an investment for the line to become switchable happens. Similarly, for the lines that are candidates to be created and to become switchable, constraint (3-31) makes sure that a switching investment can be made only if the line is created. Constraints (3-32)–(3-33) model the behavior of the switching actions for the lines that are existent, signaling that a switching action was performed when the line status variable (z) is different from the initial status (z^{init}). Constraint (3-34) limits the behavior of status variable z when a line is created but does not become switchable, where the line must be on. Constraint (3-35) makes sure that if a line is not created, the status variable will be 0. Constraint (3-36) avoids the simultaneous activation of line segments that can result in the formation of loops within the network, i.e., given a rule $k \in \mathcal{K}^{forb}$, at least one line of the set $\mathcal{L}_k^{forb}$ must be off ($z = 0$). This is made since the problem is applied to a distribution network. For any given grid, this set can be easily calculated with a depth-first search (DFS) algorithm [66]. Constraints (3-37) and (3-38) state the binary nature of these 4 binary variables.

Finally, constraint (3-39) imposes that no more than one binary variable $y_{l,h}^{ha}$ can have the value 1, i.e., the model is allowed to choose only one line hardening investment out of the set $\mathcal{H}_l$. This type of investment directly affects the second-level of the problem, by changing the probability of a line to fail given an environmental scenario (explored in the next section). Constraint (3-40) states the binary nature of this binary variable.

It is important to notice that the first-level problem is at the first-stage, and as shown in Fig. 1.1, the horizon in this stage is one period. The sub-

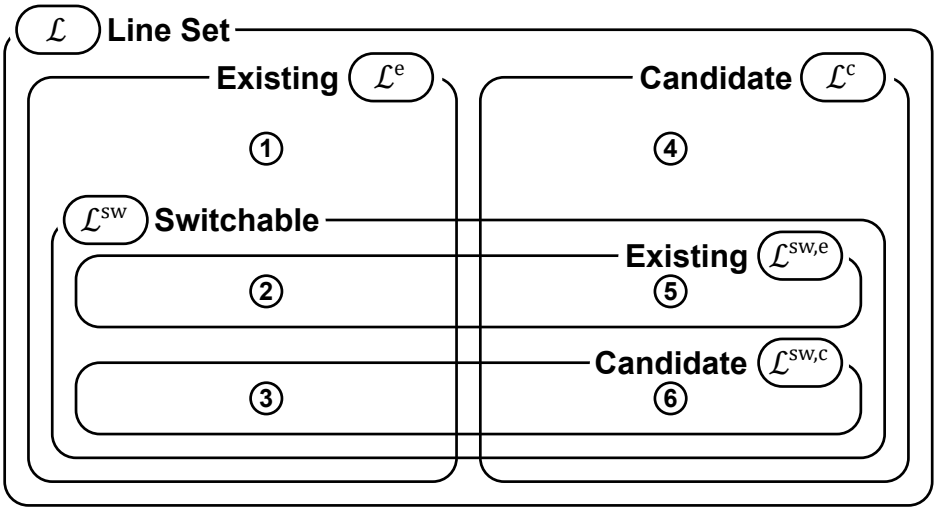

Figure 3.1: All the sets a line can belong.

index "0" that appears in the problem's variables represents that the problem is optimizing the operation of the grid considering only single period 0, based on the demand at this period (D_0^p). Index r that appears in some variables and some constraints is modeling the problem for every representative day r of the set $\mathcal{R}$. Besides the operation variables, only binary variables z and y^{sw} have index r, this means that topology configuration can be decided differently for each representative day, while investment decisions are made the same for the entire period.

3.2 Second-level: worst expected cost problem under ambiguous uncertainty

This level calculates the worst expected cost of the multiperiod operation (H_r) considering the ambiguity set $\mathcal{P}_r$ for each representative day r. The term that represents this level is located at the objective function of the first-level:

$$\sup_{\mathcal{Q}\in\mathcal{P}_r(\boldsymbol{f}_r^p,\boldsymbol{y}^{ha})} \mathbb{E}_{\mathcal{Q}}\Big[H_r(\boldsymbol{z_r},\boldsymbol{a_r})\Big]. \tag{3-41}$$

This maximization problem is defined at the ambiguity set $\mathcal{P}_r(\boldsymbol{f}_r^p,\boldsymbol{y}^{ha}) \in \mathcal{M}_+$ for every representative day r. This set is composed of a collection of probability distributions that characterizes the limited knowledge of failure probabilities and the endogenous/exogenous uncertain impact factors, similar to the set defined in [12]. In our methodology, we robustly plan the grid considering not only the probability of a line contingency alone but also considering the fact that environmental conditions can create a wildfire-prone environment, which can influence line availability. Under these circumstances, we argue that line availability uncertainty is endogenously impacted by the

power flow decisions of the lines. The probability of a line to start a fire and going unavailable increases as the active power of this line is increased. Besides that, in this work, we acknowledge that investment decisions can be made prior to the operation so the probability of a line failure can be reduced under extreme weather circumstances. Formally, the proposed ambiguity set can be expressed as:

$$\mathcal{P}_r(\boldsymbol{f}_r^p, \boldsymbol{y}^{ha}) = \Big\{ \mathcal{Q} \in \mathcal{M}_+(\mathcal{A}_r) \;\Big|\; \mathbb{E}_{\mathcal{Q}}\big[\boldsymbol{S}\hat{\boldsymbol{a}}_r\big] \leq \overline{\boldsymbol{\mu}}_r(\cdot) \Big\}, \tag{3-42}$$

where matrix $\boldsymbol{S}$ is an auxiliary matrix of coefficients:

$$\boldsymbol{S} = \big[\, \mathbb{I} \mid -\mathbb{I} \,\big]^{\top}_{2|\mathcal{L}|\times|\mathcal{L}|}, \tag{3-43}$$

where $\mathbb{I}$ is the identity matrix of size $|\mathcal{L}|$. Vector $\hat{\boldsymbol{a}}_r$ indicates a random vector of line unavailability that can be defined as:

$$\hat{\boldsymbol{a}}_r = \mathbb{1} - \boldsymbol{a}_r, \tag{3-44}$$

with $\mathbb{1}$ being a vector of ones and $\boldsymbol{a}_r$ a binary vector of size $|\mathcal{L}|$ for every representative day r. The support of the random vector $\hat{\boldsymbol{a}}_r$, is defined as:

$$\mathcal{A}_r = \Big\{ \boldsymbol{a}_r \in \{0,1\}^{|\mathcal{L}|} \;\Big|\; \sum_{l\in\mathcal{L}} a_{l,r} \geq |\mathcal{L}| - K \Big\}, \tag{3-45}$$

where binary variable $a_{l,r}$ indicates if a line l is available (1) or unavailable (0). The term $|\mathcal{L}| - K$ represents the security criteria as used in [67], with K indicating the maximum number of lines that can go simultaneously unavailable.

Following the ambiguity set definition in (3-42), function $\overline{\boldsymbol{\mu}}_r$ defines the exogenous and endogenous dependency vector of means of each representative day r, and is defined as:

$$\overline{\boldsymbol{\mu}}_r(f^p, y^{ha}) = \boldsymbol{\gamma} + \operatorname{diag}\Big(\boldsymbol{\beta}_{0,r} w^{\beta}\Big) |\boldsymbol{f}_{0,r}^p|, \tag{3-46}$$

where vector $\boldsymbol{\gamma}$ represents an estimated nominal probability of failure associated with each line segment $l \in \mathcal{L}$, extracted from the set of available information (e.g., failures per year). This parameter characterizes the exogenous nature of failure that is not related to any decision variable. This vector is defined as:

$$\boldsymbol{\gamma} = \big[\, \gamma_l \mid \mathbb{0} \,\big]^{\top}_{1\times 2|\mathcal{L}|}, \tag{3-47}$$

with $\mathbb{0}$ representing a vector of zeros of size $|\mathcal{L}|$.

Vector β is the probability of failure parameter related to the scheduled active power flow in each line at period 0, for every representative day r. The interaction between this parameter and the active power flow represents how the uncertainty is modeled endogenously dependent on the model's decision. Parameter β can be adjusted considering an expected weather condition for such representative day that the operator wants to be resilient to a higher β would mean that a higher probability of failure will happen as the power flow of a line increases. Besides that, the weight w^β is defined as:

$$w_l^\beta = 1 - \sum_{h \in \mathcal{H}_l} w_{l,h}^{ha} y_{l,h}^{ha}; \forall l \in \mathcal{L}^{ha} \tag{3-48}$$

$$w_l^\beta = 1; \forall l \in \mathcal{L} \setminus \mathcal{L}^{ha}, \tag{3-49}$$

where (3-48) represents the decrease of β parameter for the lines that have the option of hardening investments ($\mathcal{L}^{ha}$), and (3-49) represents the weight for the lines that do not have this option, i.e., the β is not reduced. The way we model this function allows the user to input different options of hardening investment strategies for a given line l (set $\mathcal{H}_l$). For example, we can give the model the option to consider two different investments in line 8, one that decreases the probability of failure by half and another that decreases by 20% the probability of failure. In this case, w_8^β would be equal to $1-0.5y_{8,1}^{har}-0.2y_{8,2}^{har}$. As we use constraint (3-39), the model can choose at most one investment. If the model chooses the first investment, variable $y_{8,1}^{har}$ would be equal to 1, and the weight function w_8^β would be equal to 0.5, reducing β_8 by half for this line example. The same goes if the model chooses to invest in the second option, where variable $y_{8,2}^{har}$ would be equal to 1, and the weight function would be w_8^β equal to 0.8, reducing β_8 by 20%. If the user would like to consider in this example both hardening investments at once, it would be necessary to include a third hardening investment option with a weight ($w_{8,3}^{ha}$) that represents the decrease of failure probability if both investments are made, and a cost ($C_{8,3}^{ha}$) associated to this two investments at once. This line hardening investment can include different types of actions, such as line undergrounding, line coating, or even vegetation management near the lines, that although it cannot be defined properly as a line hardening, it fits in this model as it can reduce the probability of wildfire disruption. It is important to highlight that these decisions made in the first stage are valid for all of the representative days r.

The product of β and the weight w^β are inside the function diag$(\cdot)$, a function that returns a diagonal matrix of size $|\mathcal{L}| \times 2|\mathcal{L}|$. This diagonal matrix is then multiplied by $|\boldsymbol{f}^p|$, modeling the fact that the higher the power flow is

(no matter its direction), the higher the value of μ_r.

Considering these definitions, function μ_r (3-46) can be defined as:

$$\overline{\mu}_{l,0,r} = \gamma_{l,0} + \beta_{l,0,r} w_l^{\beta} |f_{l,0,r}^{p}| \; ; \forall l \in \mathcal{L}^{ha}, r \in \mathcal{R} \tag{3-50}$$

$$\overline{\mu}_{l,0,r} = \gamma_{l,0} + \beta_{l,0,r} |f_{l,0,r}^{p}| \; ; \forall l \in \mathcal{L} \setminus \mathcal{L}^{ha}, r \in \mathcal{R} \tag{3-51}$$

$$\overline{\mu}_{(l+|\mathcal{L}|),0,r} = 0; \forall l \in \mathcal{L}, r \in \mathcal{R}. \tag{3-52}$$

This means that every line can have a different probability of failure, which is constructed differently for every representative day r. Besides that, the failure probability is based on the representative day power flow (f^p) and weather conditions (β) at period $t = 0$. This information is carried out for the whole period in the second-stage operation.

Finally, the resulting ambiguity set for every representative day r can be defined as:

$$\mathcal{P}_r(\boldsymbol{f}_r^p, \boldsymbol{y}^{ha}) = \Big\{ \mathcal{Q} \in \mathcal{M}_+(\mathcal{A}_r) \;\Big|\; 0 \leq \mathbb{E}_{\mathcal{Q}}[\hat{a}_{l,r}] \leq \gamma_l + \beta_{l,0,r} w_l^{\beta} |f_{l,0,r}^{p}| \; ; \forall l \in \mathcal{L}^{ha}, \\ 0 \leq \mathbb{E}_{\mathcal{Q}}[\hat{a}_{l,r}] \leq \gamma_l + \beta_{l,0,r} |f_{l,0,r}^{p}| \; ; \forall l \in \mathcal{L} \setminus \mathcal{L}^{ha} \Big\}. \tag{3-53}$$

Since $\hat{\boldsymbol{a}}_r$ is a Bernoulli-type random vector, the structural specification of (3-53) implies that a fault probability in each line $l \in \mathcal{L}$ for each representative day $r \in \mathcal{R}$ is constrained between 0 and the factor $\gamma + \beta w^{\beta} |f^p|$, thus dependent on the scheduled active power flow f^p, and contextual information γ and β at period $t = 0$.

Considering the definition of the ambiguity set in (3-53), maximization problem (3-41) can be defined for every representative day r as:

$$\underset{\mathcal{Q} \in \mathcal{M}^+}{\text{Maximize}} \quad \sum_{\boldsymbol{a}_r \in \mathcal{A}_r} H_r(\boldsymbol{z_r}, \boldsymbol{a_r}) \mathcal{Q}(\boldsymbol{a_r}) \tag{3-54}$$

subject to:

$$\sum_{\boldsymbol{a}_r \in \mathcal{A}_r} (S \hat{\boldsymbol{a}}_r) \mathcal{Q}(\boldsymbol{a}_r) \leq \overline{\mu}_r : (\boldsymbol{\psi}_r) \tag{3-55}$$

$$\sum_{\boldsymbol{a}_r \in \mathcal{A}_r} \mathcal{Q}(\boldsymbol{a}_r) = 1 : (\varphi_r), \tag{3-56}$$

where the objective function maximizes the expected cost of the third-level (H_r). The third-level function represents the operation cost of the multiperiod representative day r considering the grid topology decided at the first stage (z) and a line availability scenario a. To give this, the problem maximizes the sum for every scenario in $a_r \in \mathcal{A}_r$ of the product between H_r and the probability of each scenario $\mathcal{Q}(\boldsymbol{a_r})$. Constraint (3-55) states that the

probability of each scenario is contained between 0 and function (3-46), with ψ being the dual variable associated with this constraint. Constraint (3-56) says that the summation of the probability of all scenarios must be 100%, where φ is the dual variable associated with this constraint.

3.3 Third-level: multiperiod operational post-contingency problem

This level formulation is developed to represent function H_r for a given representative day $r \in \mathcal{R}$. The model is similar to the first-level operation model, except that a multiperiod operation is considered and the topology information (z) and line availability (a) are inputs. The primal formulation of the third-level is defined as:

$$\underset{\substack{p^c_{b,t,r},q^c_{b,t,r},v^{\dagger^c}_{b,t,r},\\ f^{p^c}_{l,t,r},f^{q^c}_{l,t,r},\Delta D^{p-^c}_{b,t,r},\\ \Delta D^{p+^c}_{b,t,r},\Delta D^{q-^c}_{b,t,r},\Delta D^{q+^c}_{b,t,r}}}{\text{Minimize}} \quad \frac{1}{|\mathcal{T}|}\left(\sum_{t\in\mathcal{T}}\sum_{b\in\mathcal{N}^{sub}} C^{tr}_b p^c_{b,t,r} + \sum_{t\in\mathcal{T}}\sum_{b\in\mathcal{N}}\left(C^{p+}\Delta D^{p+^c}_{b,t,r} + C^{p-}\Delta D^{p-^c}_{b,t,r} + C^{q+}\Delta D^{q+^c}_{b,t,r} + C^{q-}\Delta D^{q-^c}_{b,t,r}\right)\right) \tag{3-57}$$

subject to:

$$p^c_{b,t,r} + \sum_{l\in\mathcal{L}|to(l)=b} f^{p^c}_{l,t,r} - \sum_{l\in\mathcal{L}|fr(l)=b} f^{p^c}_{l,t,r} - D^p_{b,t,r} - \Delta D^{p+^c}_{b,t,r} + \Delta D^{p-^c}_{b,t,r} = 0 : (\eta^1_{b,t,r}); \forall b \in \mathcal{N}^{sub}, t \in \mathcal{T} \tag{3-58}$$

$$q^c_{b,t,r} + \sum_{l\in\mathcal{L}|to(l)=b} f^{q^c}_{l,t,r} - \sum_{l\in\mathcal{L}|fr(l)=b} f^{q^c}_{l,t,r} - \tan(\arccos(PF_b))D^p_{b,t,r} - \Delta D^{q+^c}_{b,t,r} + \Delta D^{q-^c}_{b,t,r} = 0 : (\eta^2_{b,t,r}); \forall b \in \mathcal{N}^{sub}, t \in \mathcal{T} \tag{3-59}$$

$$\sum_{l\in\mathcal{L}|to(l)=b} f^{p^c}_{l,t,r} - \sum_{l\in\mathcal{L}|fr(l)=b} f^{p^c}_{l,t,r} - D^p_{b,t,r} - \Delta D^{p+^c}_{b,t,r} + \Delta D^{p-^c}_{b,t,r} = 0 : (\eta^3_{b,t,r}); \forall b \in \mathcal{N}\setminus\mathcal{N}^{sub}, t \in \mathcal{T} \tag{3-60}$$

$$\sum_{l\in\mathcal{L}|to(l)=b} f^{q^c}_{l,t,r} - \sum_{l\in\mathcal{L}|fr(l)=b} f^{q^c}_{l,t,r} - \tan(\arccos(PF_b))D^p_{b,t,r} - \Delta D^{q+^c}_{b,t,r} + \Delta D^{q-^c}_{b,t,r} = 0 : (\eta^4_{b,t,r}); \forall b \in \mathcal{N}\setminus\mathcal{N}^{sub}, t \in \mathcal{T} \tag{3-61}$$

$$-v^{\dagger^c}_{fr(l),t,r} + v^{\dagger^c}_{to(l),t,r} + 2(R_l f^{p^c}_{l,t,r} + X_l f^{q^c}_{l,t,r}) - (1-a_{l,r})M - (1-z_{l,r})M \le 0 : (\eta^5_{l,t,r}); \forall l \in \mathcal{L}, t \in \mathcal{T} \tag{3-62}$$

$$v^{\dagger^c}_{fr(l),t,r} - v^{\dagger^c}_{to(l),t,r} - 2(R_l f^{p^c}_{l,t,r} + X_l f^{q^c}_{l,t,r}) - (1-a_{l,r})M - (1-z_{l,r})M \le 0 : (\eta^6_{l,t,r}); \forall l \in \mathcal{L}, t \in \mathcal{T} \tag{3-63}$$

$$f^{q^c}_{l,t,r} - \cot\left(\left(\frac{1}{2}-e\right)\frac{\pi}{4}\right)\left(f^{p^c}_{l,t,r} - \cos\left(e\frac{\pi}{4}\right)\overline{F}_l\right) - \sin\left(e\frac{\pi}{4}\right)\overline{F}_l \le 0 : (\eta^7_{l,e,t,r}); \forall l \in \mathcal{L}, e \in \{1,\ldots,4\}, t \in \mathcal{T} \tag{3-64}$$

$$- f^{q^c}_{l,t,r} - \cot\left(\left(\frac{1}{2} - e\right)\frac{\pi}{4}\right)\left(f^{p^c}_{l,t,r} - \cos\left(e\frac{\pi}{4}\right)\overline{F}_l\right) - \sin\left(e\frac{\pi}{4}\right)\overline{F}_l \leq 0 : (\eta^8_{l,e,t,r}); \forall l \in \mathcal{L}, e \in \{1,\ldots,4\}, t \in \mathcal{T} \quad (3\text{-}65)$$

$$0 \leq p^c_{b,t,r} \leq \overline{P}_b : (\eta^9_{b,t,r}, \eta^{10}_{b,t,r}); \forall b \in \mathcal{N}^{sub}, t \in \mathcal{T} \quad (3\text{-}66)$$

$$\underline{Q}_b \leq q^c_{b,t,r} \leq \overline{Q}_b : (\eta^{11}_{b,t,r}, \eta^{12}_{b,t,r}); \forall b \in \mathcal{N}^{sub}, t \in \mathcal{T} \quad (3\text{-}67)$$

$$\underline{V}^2_b \leq v^{\dagger^c}_{b,t,r} \leq \overline{V}^2_b : (\eta^{13}_{b,t,r}, \eta^{14}_{b,t,r}); \forall b \in \mathcal{N} \setminus \mathcal{N}^{sub}, t \in \mathcal{T} \quad (3\text{-}68)$$

$$v^{\dagger^c}_{b,t,r} = V^{ref^2} : (\eta^{15}_{b,t,r}); \forall b \in \mathcal{N}^{sub}, t \in \mathcal{T} \quad (3\text{-}69)$$

$$- z_{l,r}a_{l,r}\overline{F}_l \leq f^{p^c}_{l,t,r} \leq z_{l,r}a_{l,r}\overline{F}_l : (\eta^{16}_{l,t,r}, \eta^{17}_{l,t,r}); \forall l \in \mathcal{L}, t \in \mathcal{T} \quad (3\text{-}70)$$

$$- z_{l,r}a_{l,r}\overline{F}_l \leq f^{q^c}_{l,t,r} \leq z_{l,r}a_{l,r}\overline{F}_l : (\eta^{18}_{l,t,r}, \eta^{19}_{l,t,r}); \forall l \in \mathcal{L}, t \in \mathcal{T} \quad (3\text{-}71)$$

$$0 \leq \Delta D^{p+^c}_{b,t,r} \leq D^p_{b,t,r} : (\eta^{20}_{b,t,r}, \eta^{21}_{b,t,r}); \forall b \in \mathcal{N}, t \in \mathcal{T} \quad (3\text{-}72)$$

$$0 \leq \Delta D^{p-^c}_{b,t,r} \leq D^p_{b,t,r} : (\eta^{22}_{b,t,r}, \eta^{23}_{b,t,r}); \forall b \in \mathcal{N}, t \in \mathcal{T} \quad (3\text{-}73)$$

$$0 \leq \Delta D^{q+^c}_{b,t,r} \leq \tan(\arccos(PF_b))D^p_{b,t,r} : (\eta^{24}_{b,t,r}, \eta^{25}_{b,t,r}); \forall b \in \mathcal{N}, t \in \mathcal{T} \quad (3\text{-}74)$$

$$0 \leq \Delta D^{q-^c}_{b,t,r} \leq \tan(\arccos(PF_b))D^p_{b,t,r} : (\eta^{26}_{b,t,r}, \eta^{27}_{b,t,r}); \forall b \in \mathcal{N}, t \in \mathcal{T}, \quad (3\text{-}75)$$

where continuous decision variables p^c, q^c, $v^{\dagger^c}$, f^{p^c}, f^{q^c}, ΔD^{p+^c}, ΔD^{p-^c}, ΔD^{q+^c}, and ΔD^{q-^c} have the same role as the continuous decision variables of the first level problem (3-7)–(3-40), but in the third level these variables are accounted for every period $t \in \mathcal{T}$, of a given representative day $r \in \mathcal{R}$. Besides that, as the third-level receives the contingency information a as an input, the problem operates the grid in a post-contingency scenario. Therefore, superscript c is used to highlight that the variables in this level are being optimized considering contingencies, thus differentiating them from the first-level variables.

The objective function (3-57) minimizes the cost of electricity purchase at every substation for each period and the cost of active and reactive deficit/surplus. The objective function in this level is divided by the number of periods $|\mathcal{T}|$, providing the average cost of one hour in the multiperiod operation. This is made since we are comparing in the objective function of the first-level the costs of single period $t = 0$ and the worst expected cost of the third level. Analogously to the first-level, constraints (3-58)–(3-61) model the active and reactive power balances for every bus. Constraints (3-62)–(3-63) model the voltage differences between two buses connected by a line, where they are considered under a given contingency state associated with vector a and a first-stage topology decision z. Constraints (3-64)–(3-65) enforce limits to active and reactive flows. Finally, constraints (3-66)–(3-75) imposes the upper and lower limits of each decision variable. Variables η represent the dual variable of this problem associated with each constraint. As will be shown in the next section, this is important as we will need to dualize problem (3-57)–(3-75) to be able to solve the whole model. It is worth mentioning that the

third-level problem is always feasible since one of the solutions is to curtail all demand.

4
Solution methodology

The two-stage formulation (3-7)–(3-40) proposed in Section 3 is intended to optimally decide line investments and topology aiming to increase wildfire resilience. As the formulated problem is also a three-level problem, with a min-max-min configuration, it is necessary to develop a methodology to solve this problem. In this section we present the same iterative procedure of an outer approximation as in [12], using Benders decomposition [68]. First, the master is developed and then the subproblem is presented (the complete formulation of both problems is provided in Appendices A and B, respectively). Finally, the solution algorithm is shown.

4.1
Master problem

As the three-level problem is a min-max-min problem, the first step to solve it is by transforming the second-level problem into a minimization problem. This is done by developing the dual problem of second-level (3-54)–(3-56) for each representative day r:

$$\underset{\psi_{l,r},\varphi_r}{\text{Minimize}} \quad \boldsymbol{\psi}_r^\top \overline{\mu}_r + \varphi_r \tag{4-1}$$

subject to:

$$\boldsymbol{\psi}_r^\top S\hat{\boldsymbol{a}}_r + \varphi_r \geq H_r(\boldsymbol{z}_r, \boldsymbol{a}_r); \forall \boldsymbol{a}_r \in \mathcal{A}_r \tag{4-2}$$

$$\psi_{l,r} \geq 0; \forall l = \{1, \ldots, 2|\mathcal{L}|\} \tag{4-3}$$

$$\varphi_r \in \mathbb{R}, \tag{4-4}$$

where variables ψ and φ are the dual variables associated to constraints (3-55) and (3-56), respectively.

As the strong duality theorem is valid, primal and dual formulation of problem (3-41) are equivalent and, therefore, interchangeable. First, the second-level primal objective function is exchanged with its dual formulation objective function. Then, constraints (4-2)–(4-4) are considered in the first-level set of constraints for every $r \in \mathcal{R}$. The problem is now defined as:

$$\underset{\substack{p_{b,0,r}, q_{b,0,r}, v^{\dagger}_{b,0,r}, f^{p}_{l,0,r}, f^{q}_{l,0,r}, \\ \Delta D^{p+}_{b,0,r}, \Delta D^{p-}_{b,0,r}, \Delta D^{q+}_{b,0,r}, \Delta D^{q-}_{b,0,r} \\ z_{l,r}, y^{sw}_{l,r}, y^{sw,in}_{l}, y^{in}_{l}, y^{ha}_{l,h} \\ \psi_{l,r}, \varphi_r}}{\text{Minimize}}$$

$$\sum_{r\in\mathcal{R}}\Bigg\{\Bigg(\sum_{b\in\mathcal{N}}\Big(C^{p+}\Delta D^{p+}_{b,0,r}+C^{p-}\Delta D^{p-}_{b,0,r}+C^{q+}\Delta D^{q+}_{b,0,r}+C^{q-}\Delta D^{q-}_{b,0,r}\Big)+\boldsymbol{\psi}_r^{\top}\overline{\mu}_r+\varphi_r\Bigg)w^1_r+\Bigg(\sum_{l\in\mathcal{L}^{sw}}C^{sw}_l y^{sw}_{l,r}\Bigg)w^2_r\Bigg\}$$
$$+\sum_{l\in\mathcal{L}^{sw,c}}C^{sw,in}_l y^{sw,in}_l+\sum_{l\in\mathcal{L}^{c}}C^{in}_l y^{in}_l+\sum_{l\in\mathcal{L}^{ha}}\sum_{h\in\mathcal{H}_l}C^{ha}_{l,h}\ y^{ha}_{l,h} \tag{4-5}$$

subject to:

$$\text{Constraints (3-8)–(3-40)} \tag{4-6}$$
$$\boldsymbol{\psi}_r^{\top}S\hat{\boldsymbol{a}}_r+\varphi_r\geq H_r(\boldsymbol{z}_r,\boldsymbol{a}_r);\forall\boldsymbol{a}_r\in\mathcal{A}_r,r\in\mathcal{R} \tag{4-7}$$
$$\psi_{l,r}\geq 0;\forall l=\{1,\ldots,2|\mathcal{L}|\},r\in\mathcal{R} \tag{4-8}$$
$$\varphi_r\in\mathbb{R};\forall r\in\mathcal{R}. \tag{4-9}$$

To withstand the intractability caused by the combinatorial nature of the support set $\mathcal{A}_r$ defined in (3-45), we can robustly pick the worst contingency case. To do that, constraints (4-7) can be remodeled as:

$$\varphi_r\geq\max_{\boldsymbol{a}\in\mathcal{A}}\Big\{H_r(\boldsymbol{z}_r,\boldsymbol{a}_r)-\boldsymbol{\psi}_r^{\top}S\hat{\boldsymbol{a}}_r\Big\};\forall r\in\mathcal{R}. \tag{4-10}$$

Besides that, following the definitions of second-level, the product $\boldsymbol{\psi}_r^{\top}\overline{\mu}_r$ in (4-5) can be first expressed as:

$$\sum_{l\in\mathcal{L}\setminus\mathcal{L}^{ha}}\Big(\gamma_{l,0,r}\psi_{l,r}+\beta_{l,0,r}|f^{p}_{l,0,r}|\psi_{l,r}\Big)+\sum_{l\in\mathcal{L}^{ha}}\Big(\gamma_{l,0,r}\psi_{l,r}+\beta_{l,0,r}w^{\beta}_l|f^{p}_{l,0,r}|\psi_{l,r}\Big);\forall r\in\mathcal{R}, \tag{4-11}$$

and with function w^{β} definition (3-48)–(3-49), the product $\boldsymbol{\psi}_r^{\top}\overline{\mu}_r$ becomes:

$$\sum_{l\in\mathcal{L}}\Big(\gamma_{l,0,r}\psi_{l,r}+\beta_{l,0,r}|f^{p}_{l,0,r}|\psi_{l,r}\Big)-\sum_{l\in\mathcal{L}^{ha}}\Bigg(\beta_{l,0,r}\sum_{h\in\mathcal{H}_l}w^{ha}_{l,h}y^{ha}_{l,h}|f^{p}_{l,0,r}|\psi_{l,r}\Bigg);\forall r\in\mathcal{R}. \tag{4-12}$$

Considering this, the first-level problem can now be defined as:

$$\underset{\substack{p_{b,0,r},q_{b,0,r},v^{\dagger}_{b,0,r},f^{p}_{l,0,r},f^{q}_{l,0,r},\\ \Delta D^{p+}_{b,0,r},\Delta D^{p-}_{b,0,r},\Delta D^{q+}_{b,0,r},\Delta D^{q-}_{b,0,r}\\ z_{l,r},y^{sw}_{l,r},y^{sw,in}_{l},y^{in}_{l},y^{ha}_{l,h}\\ \psi_{l,r},\varphi_r}}{\text{Minimize}}$$

$$\sum_{r\in\mathcal{R}}\Bigg\{\Bigg(\sum_{b\in\mathcal{N}}\Big(C^{p+}\Delta D^{p+}_{b,0,r}+C^{p-}\Delta D^{p-}_{b,0,r}+C^{q+}\Delta D^{q+}_{b,0,r}+C^{q-}\Delta D^{q-}_{b,0,r}\Big)$$
$$+\sum_{l\in\mathcal{L}}\Big(\gamma_{l,0,r}\psi_{l,r}+\beta_{l,0,r}|f^{p}_{l,0,r}|\psi_{l,r}\Big)$$
$$-\sum_{l\in\mathcal{L}^{ha}}\Big(\beta_{l,0,r}\sum_{h\in\mathcal{H}_l}w^{ha}_{l,h}y^{ha}_{l,h}|f^{p}_{l,0,r}|\psi_{l,r}\Big)+\varphi_r\Bigg)w^1_r$$
$$+\Bigg(\sum_{l\in\mathcal{L}^{sw}}C^{sw}_{l}y^{sw}_{l,r}\Bigg)w^2_r\Bigg\}$$
$$+\sum_{l\in\mathcal{L}^{sw,c}}C^{sw,in}_{l}y^{sw,in}_{l}+\sum_{l\in\mathcal{L}^{c}}C^{in}_{l}y^{in}_{l}+\sum_{l\in\mathcal{L}^{ha}}\sum_{h\in\mathcal{H}_l}C^{ha}_{l,h}\ y^{ha}_{l,h} \tag{4-13}$$

subject to:

$$\text{Constraints (3-8)–(3-40)} \tag{4-14}$$
$$\varphi_r\geq\max_{\boldsymbol{a}\in\mathcal{A}}\Big\{H_r(\boldsymbol{z}_r,\boldsymbol{a}_r)-\boldsymbol{\psi}_r^{\top}S\hat{\boldsymbol{a}}_r\Big\};\forall r\in\mathcal{R} \tag{4-15}$$
$$\psi_{l,r}\geq 0;\forall l=\{1,\ldots,2|\mathcal{L}|\},r\in\mathcal{R} \tag{4-16}$$
$$\varphi_r\in\mathbb{R};\forall r\in\mathcal{R}. \tag{4-17}$$

With expression (4-12), the first-level objective function (4-13) becomes non-linear. This non-linearity appears first with the product of the two decision variables ψ and f^p, and later with the product of the three decision variables ψ, f^p, and y^{ha}. Not only that but variable f^p appears in these products with its absolute value. To avoid this, these two products need to be replaced with other variables and constraints that can model their behavior without adding non-linearity to the problem. This linearization process is described next.

4.1.1 Linearization of first-level objective function

The process starts by first handling the product $|f^p|\psi$ non-linearity. The main idea is to replace it with a new variable χ that is modeled through a set of constraints.

First, we need to linearize the absolute value of the power flow variable f^p. In [69], it is proved that every irrestrict variable can be defined as the difference of two non-negative variables. Considering this, variable f^p can be redefined with two new auxiliary variables:

$$f^{p}_{l,0,r}=f^{p+}_{l,0,r}-f^{p-}_{l,0,r};\forall l\in\mathcal{L},r\in\mathcal{R} \tag{4-18}$$
$$f^{p+}_{l,0,r}\geq 0;\forall l\in\mathcal{L},r\in\mathcal{R} \tag{4-19}$$
$$f^{p-}_{l,0,r}\geq 0;\forall l\in\mathcal{L},r\in\mathcal{R}. \tag{4-20}$$

Besides setting a lower bound for each of the two new variables as zero, it is possible to also construct an upper bound for them. Considering that f^p is constrained between $-\overline{F}$ and $+\overline{F}$, and using an auxiliary binary variable called ξ, we define:

$$f^{p+}_{l,0,r} \leq \overline{F}_l(\xi_{l,0,r}); \forall l \in \mathcal{L}, r \in \mathcal{R} \tag{4-21}$$

$$f^{p-}_{l,0,r} \leq \overline{F}_l(1 - \xi_{l,0,r}); \forall l \in \mathcal{L}, r \in \mathcal{R} \tag{4-22}$$

$$\xi_{l,0,r} \in \{0, 1\}; \forall l \in \mathcal{L}, r \in \mathcal{R}. \tag{4-23}$$

With this, the new auxiliary binary variable ξ is modeled to assume value 1 if variable f^p has a positive value and value 0 if variable f^p has a negative value, as in the following sketch:

$$\begin{aligned} &\text{if } f^p \geq 0 \rightarrow \xi = 1 \begin{cases} 0 \leq f^{p+} \leq \overline{F} \\ 0 \leq f^{p-} \leq 0 \end{cases} \rightarrow f^{p-} = 0 \rightarrow f^p = +f^{p+} \\ &\text{if } f^p \leq 0 \rightarrow \xi = 0 \begin{cases} 0 \leq f^{p+} \leq 0 \\ 0 \leq f^{p-} \leq \overline{F} \end{cases} \rightarrow f^{p+} = 0 \rightarrow f^p = -f^{p-}. \end{aligned} \tag{4-24}$$

Finally, by using constraints (4-18)–(4-23), the module of variable f^p can be replaced by the sum of f^{p+} and f^{p-}:

$$|f^p_{l,0,r}| \equiv f^{p+}_{l,0,r} + f^{p-}_{l,0,r}. \tag{4-25}$$

After that, the product of variables ψ and $|f^p|$ is handled. An approach for that is to approximate the value of one of the variables using auxiliary binary variables. By doing that, the linearization process can be easily done since there will be the product of continuous variables and binary variables. In this case, the approximation can be made with variable $|f^p|$ since this is the variable with defined bounds. The procedure for that is called binary expansion, as in [70], and is done by defining:

$$f^{p+}_{l,0,r} + f^{p-}_{l,0,r} = s \sum_{e=1}^{E_l} \left(2^{e-1} \delta_{l,0,e,r}\right); \forall l \in \mathcal{L}, r \in \mathcal{R} \tag{4-26}$$

$$\delta_{l,0,e,r} \in \{0, 1\}; \forall l \in \mathcal{L}, e \in \{1, \cdots, E_l\}, r \in \mathcal{R}, \tag{4-27}$$

where δ is a new auxiliary binary variable that has size E for each line l at each representative day r. The parameter E is the number of digits necessary in the binary form to represent a number in the decimal form. For example, the number $(5)_{10}$ in the decimal form is equal to $(101)_2$ in the binary form, requiring three digits. Given that, index e represents each digit in the binary

representation of a number. Parameter s is used to allow representations of rational numbers using this expression, it means the steps between the numbers that the binary expansion can represent. The choice of parameter s and parameter E is made according to the lower and upper bound of the variable that is going to be represented. If a value of s is chosen as 0.01, for example, in the case of a $E = 3$, the highest number that could be represented is 0.07 (when all binaries are equal to 1), and the lowest number would be 0 (when all binaries are 0). If a higher value for s is chosen, the number represented can be more accurate but would require higher E and therefore more binaries. Following the criterion developed in [70], the expression to calculate the value of parameter E can be adapted for our problem given a required accuracy and the upper bound $\overline{F}$ of variable $|f^p|$:

$$E_l = \left\lceil \log_2 \left(\frac{\overline{F}_l}{s} \right) \right\rceil ; \forall l \in \mathcal{L}, \tag{4-28}$$

where function $\lceil \cdot \rceil$ returns the ceiling of a rational number.

As stated before, the main objective is to be able to replace the product $|f^p|\psi$ with variable χ. Considering all that has been done so far, this replacement is done considering the following sketch:

$$\begin{aligned} & |f^p|\psi = \chi \\ & s \sum_{e=1}^{E} \left(2^{e-1} \delta \right) \psi = \chi \\ & s \sum_{e=1}^{E} \left(2^{e-1} \delta \psi \right) = \chi. \end{aligned} \tag{4-29}$$

By doing this, the product $\delta\psi$ appears. As explained before, this product can be easily linearized since one of the variables is binary. To deal with this, first, a new auxiliary variable ρ is introduced to replace them:

$$\chi_{l,0,r} = s \sum_{e=1}^{E_l} \left(2^{e-1} \rho_{l,0,e,r} \right) ; \forall l \in \mathcal{L}, r \in \mathcal{R}. \tag{4-30}$$

To end this characterization, it is only required to model the behavior of variable ρ without any non-linear constraints. This procedure is done by characterizing the values that this product can have. For a given l, e and r, the following sketch represents this:

$$\begin{aligned} & \text{if } \delta = 0 \ \rightarrow \ \rho = 0 \cdot \psi \ \rightarrow \ \rho = 0 \\ & \text{if } \delta = 1 \ \rightarrow \ \rho = 1 \cdot \psi \ \rightarrow \ \rho = \psi. \end{aligned} \tag{4-31}$$

To ensure this performance, it is required the following set of constraints, where M represents a sufficiently big number:

$$-(1-\delta_{l,0,e,r})M \leq \psi_{l,r} - \rho_{l,0,e,r} \leq (1-\delta_{l,0,e,r})M; \quad \forall l \in \mathcal{L}, e \in \{1,\cdots,E_l\}, r \in \mathcal{R} \tag{4-32}$$

$$-\delta_{l,0,e,r}M \leq \rho_{l,0,e,r} \leq \delta_{l,0,e,r}M; \forall l \in \mathcal{L}, e \in \{1,\cdots,E_l\}, r \in \mathcal{R}. \tag{4-33}$$

Finally, the set of constraints (4-18)–(4-23), (4-26)–(4-27), (4-30), and (4-32)–(4-33) can be added to the first-level problem and the non-linear product $|f^p|\psi$ can be approximated by variable χ. After doing this, the product between variable y^{ha} and χ still keeps the non-linear nature of the objective function. As said previously, this is easily handled since y^{ha} is a binary variable. The procedure to that linearization is similar to the one defined at (4-32)–(4-33) and is done by using the auxiliary variable ρ^{ha} for every hardening action h:

$$-(1-y^{ha}_{l,h})M \leq \chi_{l,0,r} - \rho^{ha}_{l,0,r,h} \leq (1-y^{ha}_{l,h})M; \forall l \in \mathcal{L}^{ha}, r \in \mathcal{R}, h \in \mathcal{H}_l \tag{4-34}$$

$$-y^{ha}_{l,h}M \leq \rho^{ha}_{l,0,r,h} \leq y^{ha}_{l,h}M; \forall l \in \mathcal{L}^{ha}, r \in \mathcal{R}, h \in \mathcal{H}_l. \tag{4-35}$$

With the proposed linearization, the first-level problem can now be defined as:

$$\begin{aligned}
&\underset{\substack{p_{b,0,r},q_{b,0,r},v^{\dagger}_{b,0,r},f^{p}_{l,0,r},f^{q}_{l,0,r},\\ \Delta D^{p+}_{b,0,r},\Delta D^{p-}_{b,0,r},\Delta D^{q+}_{b,0,r},\Delta D^{q-}_{b,0,r}\\ z_{l,r},y^{sw}_{l,r},y^{sw,in}_{l},y^{in}_{l},y^{ha}_{l,h}\\ \psi_{l,r},\varphi_r,f^{p+}_{l,0,r},f^{p-}_{l,0,r},\xi_{l,0,r},\\ \delta_{l,0,e,r},\rho_{l,0,e,r},\rho^{ha}_{l,0,r,h},\chi_{l,0,r}}}{\text{Minimize}} \\
&\sum_{r\in\mathcal{R}}\Bigg\{\Bigg(\sum_{b\in\mathcal{N}}\left(C^{p+}\Delta D^{p+}_{b,0,r}+C^{p-}\Delta D^{p-}_{b,0,r}+C^{q+}\Delta D^{q+}_{b,0,r}+C^{q-}\Delta D^{q-}_{b,0,r}\right)\\
&\quad+\sum_{l\in\mathcal{L}}\left(\gamma_{l,0,r}\psi_{l,r}+\beta_{l,0,r}\chi_{l,0,r}\right)-\sum_{l\in\mathcal{L}^{ha}}\left(\beta_{l,0,r}\sum_{h\in\mathcal{H}_l}w^{ha}_{l,h}\rho^{ha}_{l,0,r,h}\right)\\
&\quad+\varphi_r\Bigg)w^1_r+\left(\sum_{l\in\mathcal{L}^{sw}}C^{sw}_l y^{sw}_{l,r}\right)w^2_r\Bigg\}\\
&+\sum_{l\in\mathcal{L}^{sw,c}}C^{sw,in}_l y^{sw,in}_l+\sum_{l\in\mathcal{L}^{c}}C^{in}_l y^{in}_l+\sum_{l\in\mathcal{L}^{ha}}\sum_{h\in\mathcal{H}_l}C^{ha}_{l,h}\,y^{ha}_{l,h}
\end{aligned} \tag{4-36}$$

subject to:

Constraints (3-8)–(3-40) (4-37)

$$\varphi_r \geq \max_{\boldsymbol{a}\in\mathcal{A}} \left\{ H_r(\boldsymbol{z}_r, \boldsymbol{a}_r) - \boldsymbol{\psi}_r^\top S\hat{\boldsymbol{a}}_r \right\}; \forall r \in \mathcal{R} \tag{4-38}$$

$$\psi_{l,r} \geq 0; \forall l = \{1, \ldots, 2|\mathcal{L}|\}, r \in \mathcal{R} \tag{4-39}$$

$$\varphi_r \in \mathbb{R}; \forall r \in \mathcal{R} \tag{4-40}$$

$$f^p_{l,0,r} = f^{p+}_{l,0,r} - f^{p-}_{l,0,r}; \forall l \in \mathcal{L}, r \in \mathcal{R} \tag{4-41}$$

$$0 \leq f^{p+}_{l,0,r} \leq \overline{F}_l \xi_{l,0,r}; \forall l \in \mathcal{L}, r \in \mathcal{R} \tag{4-42}$$

$$0 \leq f^{p-}_{l,0,r} \leq \overline{F}_l (1 - \xi_{l,0,r}); \forall l \in \mathcal{L}, r \in \mathcal{R} \tag{4-43}$$

$$f^{p+}_{l,0,r} + f^{p-}_{l,0,r} = s \sum_{e=1}^{E_l} \left(2^{e-1} \delta_{l,0,e,r} \right); \forall l \in \mathcal{L}, r \in \mathcal{R} \tag{4-44}$$

$$\chi_{l,0,r} = s \sum_{e=1}^{E_l} \left(2^{e-1} \rho_{l,0,e,r} \right); \forall l \in \mathcal{L}, r \in \mathcal{R} \tag{4-45}$$

$$-(1 - \delta_{l,0,e,r})M \leq \psi_{l,r} - \rho_{l,0,e,r} \leq (1 - \delta_{l,0,e,r})M; \quad \forall l \in \mathcal{L}, e \in \{1, \cdots, E_l\}, r \in \mathcal{R} \tag{4-46}$$

$$-\delta_{l,0,e,r} M \leq \rho_{l,0,e,r} \leq \delta_{l,0,e,r} M; \forall l \in \mathcal{L}, e \in \{1, \cdots, E_l\}, r \in \mathcal{R} \tag{4-47}$$

$$-(1 - y^{ha}_{l,h})M \leq \chi_{l,0,r} - \rho^{ha}_{l,0,r,h} \leq (1 - y^{ha}_{l,h})M; \forall l \in \mathcal{L}^{ha}, r \in \mathcal{R}, h \in \mathcal{H}_l \tag{4-48}$$

$$-y^{ha}_{l,h} M \leq \rho^{ha}_{l,0,r,h} \leq y^{ha}_{l,h} M; \forall l \in \mathcal{L}^{ha}, r \in \mathcal{R}, h \in \mathcal{H}_l \tag{4-49}$$

$$\xi_{l,0,r} \in \{0, 1\}; \forall l \in \mathcal{L}, r \in \mathcal{R} \tag{4-50}$$

$$\delta_{l,0,e,r} \in \{0, 1\}; \forall l \in \mathcal{L}, e \in \{1, \cdots, E_l\}, r \in \mathcal{R} \tag{4-51}$$

$$\chi_{l,0,r} \in \mathbb{R}; \forall l \in \mathcal{L}, r \in \mathcal{R} \tag{4-52}$$

$$\rho_{l,0,e,r} \in \mathbb{R}; \forall l \in \mathcal{L}, e \in \{1, \cdots, E_l\}, r \in \mathcal{R} \tag{4-53}$$

$$\rho^{ha}_{l,0,r,h} \in \mathbb{R}; \forall l \in \mathcal{L}^{ha}, r \in \mathcal{R}, h \in \mathcal{H}_l. \tag{4-54}$$

Finally, to solve problem (4-36)-(4-54), we use decomposition techniques to iteratively approximate the right-hand side of constraint (4-38). First a relaxed version of problem (4-36)-(4-54) is developed, named the "Master Problem":

$$\underset{\substack{p_{b,0,r}, q_{b,0,r}, v^\dagger_{b,0,r}, f^p_{l,0,r}, f^q_{l,0,r}, \\ \Delta D^{p+}_{b,0,r}, \Delta D^{p-}_{b,0,r}, \Delta D^{q+}_{b,0,r}, \Delta D^{q-}_{b,0,r} \\ z_{l,r}, y^{sw}_{l,r}, y^{sw,in}_l, y^{in}_l, y^{ha}_{l,h} \\ \psi_{l,r}, \varphi_r, f^{p+}_{l,0,r}, f^{p-}_{l,0,r}, \xi_{l,0,r}, \\ \delta_{l,0,e,r}, \rho_{l,0,r}, \rho^{ha}_{l,0,r,h}, \chi_{l,0,r}}}{\text{Minimize}}$$

$$\sum_{r\in\mathcal{R}} \left\{ \left(\sum_{b\in\mathcal{N}} \left(C^{p+} \Delta D^{p+}_{b,0,r} + C^{p-} \Delta D^{p-}_{b,0,r} + C^{q+} \Delta D^{q+}_{b,0,r} + C^{q-} \Delta D^{q-}_{b,0,r} \right) \right. \right.$$

$$\left. + \sum_{l\in\mathcal{L}} \left(\gamma_{l,0,r} \psi_{l,r} + \beta_{l,0,r} \chi_{l,0,r} \right) - \sum_{l\in\mathcal{L}^{ha}} \left(\beta_{l,0,r} \sum_{h\in\mathcal{H}_l} w^{ha}_{l,h} \rho^{ha}_{l,0,r,h} \right) \right.$$

$$+ \varphi_r \Bigg) w_r^1 + \Bigg(\sum_{l \in \mathcal{L}^{sw}} C_l^{sw} y_{l,r}^{sw} \Bigg) w_r^2 \Bigg\}$$
$$+ \sum_{l \in \mathcal{L}^{sw,c}} C_l^{sw,in} y_l^{sw,in} + \sum_{l \in \mathcal{L}^c} C_l^{in} y_l^{in} + \sum_{l \in \mathcal{L}^{ha}} \sum_{h \in \mathcal{H}_l} C_{l,h}^{ha} \; y_{l,h}^{ha} \tag{4-55}$$

subject to:

$$\text{Constraints (3-8)–(3-40)} \tag{4-56}$$

$$\text{Constraints (4-39)–(4-54)} \tag{4-57}$$

$$\varphi_r \geq \text{Cutting Plane}_r^{(j)}; \forall j \in \mathcal{J}, \forall r \in \mathcal{R} \tag{4-58}$$

$$\sum_{l \in \mathcal{L}} \Big(\gamma_{l,0,r} \psi_{l,r} + \beta_{l,0,r} \chi_{l,0,r} \Big) - \sum_{l \in \mathcal{L}^{ha}} \Big(\beta_{l,0,r} \sum_{h \in \mathcal{H}_l} w_{l,h}^{ha} \rho_{l,0,r,h}^{ha} \Big) + \varphi_r \geq 0;$$
$$\forall r \in \mathcal{R}, \tag{4-59}$$

where, constraint (4-58) is considered for every representative day r for all the iterations needed j in $\mathcal{J}$. Constraint (4-59) is added to provide a lower bound of the second-level, stating that the expected worst cost of the operation is non-negative. This is helpful for the algorithm since it is not possible to affirm that variable φ – the variable that we want to approximate at each iteration – is non-negative. Considering this, solving this problem can be hard if we do not provide a lower bound for this variable. The complete formulation of the "Master Problem" is provided in Appendix A.

The so-called "Subproblem" is developed to solve the right-hand side of (4-38). This process is developed in the next section (4.2). By solving the subproblem at each iteration, cutting planes are constructed and added to the Master problem (4.3) for each representative day r. The solution algorithm for this is shown in section 4.4.

4.2 Subproblem

As explained before, we construct at each iteration an approximation of the right-hand side of constraint (4-38), in the so-called "Subproblem" defined for every r in $\mathcal{R}$:

$$\underset{\boldsymbol{a} \in \mathcal{A}}{\text{Maximize}} \quad \Big\{ H_r(\boldsymbol{z}_r, \boldsymbol{a}_r) - \boldsymbol{\psi}_r^\top S \hat{\boldsymbol{a}}_r \Big\}. \tag{4-60}$$

Problem (4-60) is a maximization problem in $\boldsymbol{a} \in \mathcal{A}$. This information reveals the characterization of the security criterion defined in (3-45). Thus, this maximization problem is now defined:

$$\underset{a}{\text{Maximize}} \quad \Big\{ H_r(\boldsymbol{z}_r, \boldsymbol{a}_r) - \boldsymbol{\psi}_r^\top S \hat{\boldsymbol{a}}_r \Big\} \tag{4-61}$$

subject to:

$$\sum_{l\in\mathcal{L}} a_{l,r} \geq |\mathcal{L}| - K \tag{4-62}$$

$$a_{l,r} \in \{0,1\}; \forall l \in \mathcal{L}. \tag{4-63}$$

Besides that, function H_r models the third-level problem, with the multiperiod post-contingency operation (section 3.3). This problem receives as inputs the grid topology (represented by first-level variable z) and the random binary vector (a) associated with line availability. As shown, this problem is a minimization problem. When considering inside the objective function (4-61), the subproblem becomes a max-min problem. To solve that, once again we rely on the duality theory, where the dual of the third-level problem (3-57)–(3-75) is calculated and put in the place of H_r in the objective function of problem (4-61)–(4-63). With this, the subproblem for each representative day r can now be defined as:

$$\begin{aligned}
&\underset{\substack{\eta^1_{b,t,r},\eta^2_{b,t,r},\eta^3_{b,t,r},\eta^4_{b,t,r},\eta^5_{l,t,r},\eta^6_{l,t,r},\eta^7_{l,e,t,r},\\ \eta^8_{l,e,t,r},\eta^9_{b,t,r},\eta^{10}_{b,t,r},\eta^{11}_{b,t,r},\eta^{12}_{b,t,r},\eta^{13}_{b,t,r},\eta^{14}_{b,t,r},\\ \eta^{15}_{b,t,r},\eta^{16}_{l,t,r},\eta^{17}_{l,t,r},\eta^{18}_{l,t,r},\eta^{19}_{l,t,r},\eta^{20}_{b,t,r},\eta^{21}_{b,t,r},\\ \eta^{22}_{b,t,r},\eta^{23}_{b,t,r},\eta^{24}_{b,t,r},\eta^{25}_{b,t,r},\eta^{26}_{b,t,r},\eta^{27}_{b,t,r},a}}{\text{Maximize}} \\
&\sum_{t\in\mathcal{T}}\sum_{b\in\mathcal{N}^{sub}}\Big(- D^p_{b,t,r}\eta^1_{b,t,r} - \tan\left(\arccos\left(PF_b\right)\right)D^p_{b,t,r}\eta^2_{b,t,r} \\
&\qquad - \overline{P}_b\eta^{10}_{b,t,r} + \underline{Q}_b\eta^{11}_{b,t,r} - \overline{Q}_b\eta^{12}_{b,t,r} - {V^{ref}}^2\eta^{15}_{b,t,r} \\
&\qquad - D^p_{b,t,r}\eta^{21}_{b,t,r} - D^p_{b,t,r}\eta^{23}_{b,t,r} - \tan(\arccos(PF_b))D^p_{b,t,r}\eta^{25}_{b,t,r} \\
&\qquad - \tan(\arccos(PF_b))D^p_{b,t,r}\eta^{27}_{b,t,r}\Big) \\
&+\sum_{t\in\mathcal{T}}\sum_{b\in\mathcal{N}\setminus\mathcal{N}^{sub}}\Big(- D^p_{b,t,r}\eta^3_{b,t,r} - \tan\left(\arccos\left(PF_b\right)\right)D^p_{b,t,r}\eta^4_{b,t,r} \\
&\qquad + \underline{V}^2_b\eta^{13}_{b,t,r} - \overline{V}^2_b\eta^{14}_{b,t,r} - D^p_{b,t,r}\eta^{21}_{b,t,r} - D^p_{b,t,r}\eta^{23}_{b,t,r} \\
&\qquad - \tan(\arccos(PF_b))D^p_{b,t,r}\eta^{25}_{b,t,r} \\
&\qquad - \tan(\arccos(PF_b))D^p_{b,t,r}\eta^{27}_{b,t,r}\Big) \\
&+\sum_{t\in\mathcal{T}}\sum_{l\in\mathcal{L}}\Bigg(- ((1-a_{l,r})M + (1-z_{l,r})M)\eta^5_{l,t,r} \\
&\qquad - ((1-a_{l,r})M + (1-z_{l,r})M)\eta^6_{l,t,r} \\
&\qquad + \sum_{e\in\{1,2,3,4\}}\Bigg[\overline{F}_l\Big(\cot\Big((1/2-e)(\pi/4)\Big)\cos\Big(e(\pi/4)\Big) \\
&\qquad\qquad - \sin\Big(e(\pi/4)\Big)\Big)(\eta^7_{l,e,t,r} + \eta^8_{l,e,t,r})\Bigg]
\end{aligned}$$

$$- z_{l,r} a_{l,r} \overline{F}_l (\eta^{16}_{l,t,r} + \eta^{17}_{l,t,r} + \eta^{18}_{l,t,r} + \eta^{19}_{l,t,r}) \Bigg)$$

$$- \boldsymbol{\psi}_r^\top S \hat{\boldsymbol{a}}_r \tag{4-64}$$

subject to:

$$\sum_{l \in \mathcal{L}} a_{l,r} \geq |\mathcal{L}| - K \tag{4-65}$$

$$a_{l,r} \in \{0,1\}; \forall l \in \mathcal{L} \tag{4-66}$$

$$C^{tr}_b / |\mathcal{T}| + \eta^1_{b,t,r} - \eta^9_{b,t,r} + \eta^{10}_{b,t,r} = 0 : (p^c_{b,t,r}); \forall b \in \mathcal{N}^{sub}, t \in \mathcal{T} \tag{4-67}$$

$$\eta^2_{b,t,r} - \eta^{11}_{b,t,r} + \eta^{12}_{b,t,r} = 0 : (q^c_{b,t,r}); \forall b \in \mathcal{N}^{sub}, t \in \mathcal{T} \tag{4-68}$$

$$\sum_{l \in \mathcal{L} | b = fr(l)} \Big(\eta^6_{l,t,r} - \eta^5_{l,t,r} \Big) + \sum_{l \in \mathcal{L} | b = to(l)} \Big(\eta^5_{l,t,r} - \eta^6_{l,t,r} \Big) - \eta^{13}_{b,t,r} + \eta^{14}_{b,t,r} = 0 : (v^{\dagger^c}_{b,t,r}); \forall b \in \mathcal{N} \setminus \mathcal{N}^{sub}, t \in \mathcal{T} \tag{4-69}$$

$$\sum_{l \in \mathcal{L} | b = fr(l)} \Big(\eta^6_{l,t,r} - \eta^5_{l,t,r} \Big) + \sum_{l \in \mathcal{L} | b = to(l)} \Big(\eta^5_{l,t,r} - \eta^6_{l,t,r} \Big) + \eta^{15}_{b,t,r} = 0 : (v^{\dagger^c}_{b,t,r}); \forall b \in \mathcal{N}^{sub}, t \in \mathcal{T} \tag{4-70}$$

$$\sum_{b \in \mathcal{N}^{sub} | b = to(l)} \eta^1_{b,t,r} - \sum_{b \in \mathcal{N}^{sub} | b = fr(l)} \eta^1_{b,t,r} + \sum_{b \in \mathcal{N} \setminus \mathcal{N}^{sub} | b = to(l)} \eta^3_{b,t,r} - \sum_{b \in \mathcal{N} \setminus \mathcal{N}^{sub} | b = fr(l)} \eta^3_{b,t,r} + 2R_l \eta^5_{l,t,r} - 2R_l \eta^6_{l,t,r} + \sum_{e \in \{1,2,3,4\}} \Big[- \cot\Big((1/2 - e)(\pi/4) \Big) \Big(\eta^7_{l,e,t,r} \Big) - \cot\Big((1/2 - e)(\pi/4) \Big) \Big(\eta^8_{l,e,t,r} \Big) \Big] - \eta^{16}_{l,t,r} + \eta^{17}_{l,t,r} = 0 : (f^{p^c}_{l,t,r}); \forall l \in \mathcal{L}, t \in \mathcal{T} \tag{4-71}$$

$$\sum_{b \in \mathcal{N}^{sub} | b = to(l)} \eta^2_{b,t,r} - \sum_{b \in \mathcal{N}^{sub} | b = fr(l)} \eta^2_{b,t,r} + \sum_{b \in \mathcal{N} \setminus \mathcal{N}^{sub} | b = to(l)} \eta^4_{b,t,r} - \sum_{b \in \mathcal{N} \setminus \mathcal{N}^{sub} | b = fr(l)} \eta^4_{b,t,r} + 2X_l \eta^5_{l,t,r} - 2X_l \eta^6_{l,t,r} + \sum_{e \in \{1,2,3,4\}} \Big(\eta^7_{l,e,t,r} - \eta^8_{l,e,t,r} \Big) - \eta^{18}_{l,t,r} + \eta^{19}_{l,t,r} = 0 : (f^{q^c}_{l,t,r}); \forall l \in \mathcal{L}, t \in \mathcal{T} \tag{4-72}$$

$$C^{p+} / |\mathcal{T}| - \eta^1_{b,t,r} - \eta^{20}_{b,t,r} + \eta^{21}_{b,t,r} = 0 : (\Delta D^{p+^c}_{b,t,r}); \forall b \in \mathcal{N}^{sub}, t \in \mathcal{T} \tag{4-73}$$

$$C^{p+} / |\mathcal{T}| - \eta^3_{b,t,r} - \eta^{20}_{b,t,r} + \eta^{21}_{b,t,r} = 0 : (\Delta D^{p+^c}_{b,t,r}); \forall b \in \mathcal{N} \setminus \mathcal{N}^{sub}, t \in \mathcal{T} \tag{4-74}$$

$$C^{p-} / |\mathcal{T}| + \eta^1_{b,t,r} - \eta^{22}_{b,t,r} + \eta^{23}_{b,t,r} = 0 : (\Delta D^{p-^c}_{b,t,r}); \forall b \in \mathcal{N}^{sub}, t \in \mathcal{T} \tag{4-75}$$

$$C^{p-} / |\mathcal{T}| + \eta^3_{b,t,r} - \eta^{22}_{b,t,r} + \eta^{23}_{b,t,r} = 0 : (\Delta D^{p-^c}_{b,t,r}); \forall b \in \mathcal{N} \setminus \mathcal{N}^{sub}, t \in \mathcal{T} \tag{4-76}$$

$$C^{q+} / |\mathcal{T}| - \eta^2_{b,t,r} - \eta^{24}_{b,t,r} + \eta^{25}_{b,t,r} = 0 : (\Delta D^{q+^c}_{b,t,r}); \forall b \in \mathcal{N}^{sub}, t \in \mathcal{T} \tag{4-77}$$

$$C^{q+} / |\mathcal{T}| - \eta^4_{b,t,r} - \eta^{24}_{b,t,r} + \eta^{25}_{b,t,r} = 0 : (\Delta D^{q+^c}_{b,t,r}); \forall b \in \mathcal{N} \setminus \mathcal{N}^{sub}, t \in \mathcal{T} \tag{4-78}$$

$$C^{q-} / |\mathcal{T}| + \eta^2_{b,t,r} - \eta^{26}_{b,t,r} + \eta^{27}_{b,t,r} = 0 : (\Delta D^{q-^c}_{b,t,r}); \forall b \in \mathcal{N}^{sub}, t \in \mathcal{T} \tag{4-79}$$

$$C^{q-} / |\mathcal{T}| + \eta^4_{b,t,r} - \eta^{26}_{b,t,r} + \eta^{27}_{b,t,r} = 0 : (\Delta D^{q-^c}_{b,t,r}); \forall b \in \mathcal{N} \setminus \mathcal{N}^{sub}, t \in \mathcal{T} \tag{4-80}$$

$$\eta^{1}_{b,t,r}, \eta^{2}_{b,t,r}, \eta^{15}_{b,t,r} \in \mathbb{R}; \forall b \in \mathcal{N}^{sub}, t \in \mathcal{T} \tag{4-81}$$

$$\eta^{3}_{b,t,r}, \eta^{4}_{b,t,r} \in \mathbb{R}; \forall b \in \mathcal{N} \setminus \mathcal{N}^{sub}, t \in \mathcal{T} \tag{4-82}$$

$$\eta^{20}_{b,t,r}, \eta^{21}_{b,t,r}, \eta^{22}_{b,t,r}, \eta^{23}_{b,t,r}, \eta^{24}_{b,t,r}, \eta^{25}_{b,t,r}, \eta^{26}_{b,t,r}, \eta^{27}_{b,t,r} \geq 0; \forall b \in \mathcal{N}, t \in \mathcal{T} \tag{4-83}$$

$$\eta^{13}_{b,t,r}, \eta^{14}_{b,t,r} \geq 0; \forall b \in \mathcal{N} \setminus \mathcal{N}^{sub}, t \in \mathcal{T} \tag{4-84}$$

$$\eta^{9}_{b,t,r}, \eta^{10}_{b,t,r}, \eta^{11}_{b,t,r}, \eta^{12}_{b,t,r} \geq 0; \forall b \in \mathcal{N}^{sub}, t \in \mathcal{T} \tag{4-85}$$

$$\eta^{5}_{l,t,r}, \eta^{6}_{l,t,r}, \eta^{16}_{l,t,r}, \eta^{17}_{l,t,r}, \eta^{18}_{l,t,r}, \eta^{19}_{l,t,r} \geq 0; \forall l \in \mathcal{L}, t \in \mathcal{T} \tag{4-86}$$

$$\eta^{7}_{l,e,t,r}, \eta^{8}_{l,e,t,r} \geq 0; \forall l \in \mathcal{L}, \forall e \in \{1,2,3,4\}, t \in \mathcal{T}. \tag{4-87}$$

It is important to mention that, although the inner maximization problem (a representation of function H_r) receives both variables z and a as inputs, the outer maximization problem considers variable a as a decision variable. When we turn this problem into one single maximization problem, it is required to consider a as a decision variable inside H_r problem. By doing this, this inner problem becomes non-linear, as there is the product between different decision variables (η) with the binary variable a in the objective function (4-64). To linearize these products, we use the same methodology done in (4-32)–(4-33), replacing them with new auxiliary variables λ and a set of constraints.

Besides that, expression $\boldsymbol{\psi}_r^{\top} S \hat{\boldsymbol{a}}_r$ can be reformulated considering the definition of $\hat{\boldsymbol{a}}_r$ in (3-44) and the definition of S in (3-43). As first-stage variable $\psi_r^{\top}$ is a vector of size $2|\mathcal{L}|$, the final Subproblem formulation is defined as:

$$\begin{aligned}
&\underset{\substack{\eta^{1}_{b,t,r},\eta^{2}_{b,t,r},\eta^{3}_{b,t,r},\eta^{4}_{b,t,r},\eta^{5}_{l,t,r},\eta^{6}_{l,t,r},\eta^{7}_{l,e,t,r},\\ \eta^{8}_{l,e,t,r},\eta^{9}_{b,t,r},\eta^{10}_{b,t,r},\eta^{11}_{b,t,r},\eta^{12}_{b,t,r},\eta^{13}_{b,t,r},\eta^{14}_{b,t,r},\\ \eta^{15}_{b,t,r},\eta^{16}_{l,t,r},\eta^{17}_{l,t,r},\eta^{18}_{l,t,r},\eta^{19}_{l,t,r},\eta^{20}_{b,t,r},\eta^{21}_{b,t,r},\\ \eta^{22}_{b,t,r},\eta^{23}_{b,t,r},\eta^{24}_{b,t,r},\eta^{25}_{b,t,r},\eta^{26}_{b,t,r},\eta^{27}_{b,t,r},a\\ \lambda^{5}_{l,t,r},\lambda^{6}_{l,t,r},\lambda^{16}_{l,t,r},\lambda^{17}_{l,t,r},\lambda^{18}_{l,t,r},\lambda^{19}_{l,t,r}}}{\text{Maximize}} \\
&\sum_{t\in\mathcal{T}}\sum_{b\in\mathcal{N}^{sub}}\Big(- D^{p}_{b,t,r}\eta^{1}_{b,t,r} - \tan\left(\arccos\left(PF_b\right)\right)D^{p}_{b,t,r}\eta^{2}_{b,t,r} \\
&\qquad - \overline{P}_b\eta^{10}_{b,t,r} + \underline{Q}_b\eta^{11}_{b,t,r} - \overline{Q}_b\eta^{12}_{b,t,r} - {V^{ref}}^2\eta^{15}_{b,t,r} \\
&\qquad - D^{p}_{b,t,r}\eta^{21}_{b,t,r} - D^{p}_{b,t,r}\eta^{23}_{b,t,r} - \tan(\arccos(PF_b))D^{p}_{b,t,r}\eta^{25}_{b,t,r} \\
&\qquad - \tan(\arccos(PF_b))D^{p}_{b,t,r}\eta^{27}_{b,t,r}\Big) \\
&+\sum_{t\in\mathcal{T}}\sum_{b\in\mathcal{N}\setminus\mathcal{N}^{sub}}\Big(- D^{p}_{b,t,r}\eta^{3}_{b,t,r} - \tan\left(\arccos\left(PF_b\right)\right)D^{p}_{b,t,r}\eta^{4}_{b,t,r} \\
&\qquad + \underline{V}^{2}_{b}\eta^{13}_{b,t,r} - \overline{V}^{2}_{b}\eta^{14}_{b,t,r} - D^{p}_{b,t,r}\eta^{21}_{b,t,r} - D^{p}_{b,t,r}\eta^{23}_{b,t,r} \\
&\qquad - \tan(\arccos(PF_b))D^{p}_{b,t,r}\eta^{25}_{b,t,r} \\
&\qquad - \tan(\arccos(PF_b))D^{p}_{b,t,r}\eta^{27}_{b,t,r}\Big)
\end{aligned}$$

$$
\begin{aligned}
&+\sum_{t\in\mathcal{T}}\sum_{l\in\mathcal{L}}\Bigg(-((1-a_{l,r})M+(1-z_{l,r})M)\eta^{5}_{l,t,r}\\
&\qquad-((1-a_{l,r})M+(1-z_{l,r})M)\eta^{6}_{l,t,r}\\
&\qquad+\sum_{e\in\{1,2,3,4\}}\Bigg[\overline{F}_l\Big(\cot\Big((1/2-e)(\pi/4)\Big)\cos\Big(e(\pi/4)\Big)\\
&\qquad\qquad-\sin\Big(e(\pi/4)\Big)\Big)(\eta^{7}_{l,e,t,r}+\eta^{8}_{l,e,t,r})\Bigg]\\
&\qquad-z_{l,r}a_{l,r}\overline{F}_l(\eta^{16}_{l,t,r}+\eta^{17}_{l,t,r}+\eta^{18}_{l,t,r}+\eta^{19}_{l,t,r})\Bigg)\\
&-\sum_{l\in\mathcal{L}}\Big((\psi_{l,r}-\psi_{l+|\mathcal{L}|,r})(1-a_{l,r})\Big) \qquad (4\text{-}88)
\end{aligned}
$$

subject to:

$$\text{Constraints (4-65)–(4-87)} \qquad (4\text{-}89)$$

$$-(1-a_{l,r})M\le\eta^{5}_{l,t,r}-\lambda^{5}_{l,t,r}\le(1-a_{l,r})M;\forall l\in\mathcal{L},t\in\mathcal{T} \qquad (4\text{-}90)$$

$$-a_{l,r}M\le\lambda^{5}_{l,t,r}\le a_{l,r}M;\forall l\in\mathcal{L},t\in\mathcal{T} \qquad (4\text{-}91)$$

$$-(1-a_{l,r})M\le\eta^{6}_{l,t,r}-\lambda^{6}_{l,t,r}\le(1-a_{l,r})M;\forall l\in\mathcal{L},t\in\mathcal{T} \qquad (4\text{-}92)$$

$$-a_{l,r}M\le\lambda^{6}_{l,t,r}\le a_{l,r}M;\forall l\in\mathcal{L},t\in\mathcal{T} \qquad (4\text{-}93)$$

$$-(1-a_{l,r})M\le\eta^{16}_{l,t,r}-\lambda^{16}_{l,t,r}\le(1-a_{l,r})M;\forall l\in\mathcal{L},t\in\mathcal{T} \qquad (4\text{-}94)$$

$$-a_{l,r}M\le\lambda^{16}_{l,t,r}\le a_{l,r}M;\forall l\in\mathcal{L},t\in\mathcal{T} \qquad (4\text{-}95)$$

$$-(1-a_{l,r})M\le\eta^{17}_{l,t,r}-\lambda^{17}_{l,t,r}\le(1-a_{l,r})M;\forall l\in\mathcal{L},t\in\mathcal{T} \qquad (4\text{-}96)$$

$$-a_{l,r}M\le\lambda^{17}_{l,t,r}\le a_{l,r}M;\forall l\in\mathcal{L},t\in\mathcal{T} \qquad (4\text{-}97)$$

$$-(1-a_{l,r})M\le\eta^{18}_{l,t,r}-\lambda^{18}_{l,t,r}\le(1-a_{l,r})M;\forall l\in\mathcal{L},t\in\mathcal{T} \qquad (4\text{-}98)$$

$$-a_{l,r}M\le\lambda^{18}_{l,t,r}\le a_{l,r}M;\forall l\in\mathcal{L},t\in\mathcal{T} \qquad (4\text{-}99)$$

$$-(1-a_{l,r})M\le\eta^{19}_{l,t,r}-\lambda^{19}_{l,t,r}\le(1-a_{l,r})M;\forall l\in\mathcal{L},t\in\mathcal{T} \qquad (4\text{-}100)$$

$$-a_{l,r}M\le\lambda^{19}_{l,t,r}\le a_{l,r}M;\forall l\in\mathcal{L},t\in\mathcal{T} \qquad (4\text{-}101)$$

$$\lambda^{5}_{l,t,r},\lambda^{6}_{l,t,r},\lambda^{16}_{l,t,r},\lambda^{17}_{l,t,r},\lambda^{18}_{l,t,r},\lambda^{19}_{l,t,r}\in\mathbb{R};\forall l\in\mathcal{L},t\in\mathcal{T}. \qquad (4\text{-}102)$$

It is worth highlighting that in the constructed Subproblem, ψ and z are not decision variables, instead they are input from the Master problem. Besides that, the recourse function associated with the resulting Subproblem is convex with respect to the first-stage decision as it is a maximum of affine functions, therefore rendering the description of the right-hand side of Equation (4-38) is suitable with cutting planes approximation. The complete formulation of the "Subproblem" is provided in Appendix B.

4.3 Cutting plane

The Master relaxation (4-55)–(4-59) is improved by the iterative inclusion of cutting planes in Equation (4-58). These cutting planes are constructed in the form of the objective function of the Subproblem (4-88), which is added at each iteration j in $\mathcal{J}$. As the third-level is always feasible, these cuts are optimality cuts, and there is no need to construct viability cuts. The cutting planes are presented as:

$$
\begin{aligned}
&\text{Cutting Plane}_r^{(j)} = \\
&\sum_{t\in\mathcal{T}}\sum_{b\in\mathcal{N}^{sub}}\Big(-D^p_{b,t,r}\eta^{1(j)}_{b,t,r} - \tan\left(\arccos\left(PF_b\right)\right)D^p_{b,t,r}\eta^{2(j)}_{b,t,r} \\
&\qquad - \overline{P}_b\eta^{10(j)}_{b,t,r} + \underline{Q}_b\eta^{11(j)}_{b,t,r} - \overline{Q}_b\eta^{12(j)}_{b,t,r} - V^{ref^2}\eta^{15(j)}_{b,t,r} \\
&\qquad - D^p_{b,t,r}\eta^{21(j)}_{b,t,r} - D^p_{b,t,r}\eta^{23(j)}_{b,t,r} \\
&\qquad - \tan(\arccos(PF_b))D^p_{b,t,r}\eta^{25(j)}_{b,t,r} \\
&\qquad - \tan(\arccos(PF_b))D^p_{b,t,r}\eta^{27(j)}_{b,t,r}\Big) \\
&+\sum_{t\in\mathcal{T}}\sum_{b\in\mathcal{N}\setminus\mathcal{N}^{sub}}\Big(-D^p_{b,t,r}\eta^{3(j)}_{b,t,r} - \tan\left(\arccos\left(PF_b\right)\right)D^p_{b,t,r}\eta^{4(j)}_{b,t,r} \\
&\qquad + \underline{V}^2_b\eta^{13(j)}_{b,t,r} - \overline{V}^2_b\eta^{14(j)}_{b,t,r} - D^p_{b,t,r}\eta^{21(j)}_{b,t,r} - D^p_{b,t,r}\eta^{23(j)}_{b,t,r} \\
&\qquad - \tan(\arccos(PF_b))D^p_{b,t,r}\eta^{25(j)}_{b,t,r} \\
&\qquad - \tan(\arccos(PF_b))D^p_{b,t,r}\eta^{27(j)}_{b,t,r}\Big) \\
&+\sum_{t\in\mathcal{T}}\sum_{l\in\mathcal{L}}\Bigg(-((1-a^{(j)}_{l,r})M + (1-z_{l,r})M)\eta^{5(j)}_{l,t,r} \\
&\qquad - ((1-a^{(j)}_{l,r})M + (1-z_{l,r})M)\eta^{6(j)}_{l,t,r} \\
&\qquad + \sum_{e\in\{1,2,3,4\}}\Bigg[\overline{F}_l\Big(\cot\Big((1/2-e)(\pi/4)\Big)\cos\Big(e(\pi/4)\Big) \\
&\qquad\qquad - \sin\Big(e(\pi/4)\Big)\Big)(\eta^{7(j)}_{l,e,t,r} + \eta^{8(j)}_{l,e,t,r})\Bigg] \\
&\qquad - z_{l,r}a^{(j)}_{l,r}\overline{F}_l(\eta^{16(j)}_{l,t,r} + \eta^{17(j)}_{l,t,r} + \eta^{18(j)}_{l,t,r} + \eta^{19(j)}_{l,t,r})\Bigg) \\
&-\sum_{l\in\mathcal{L}}\Big((\psi_{l,r} - \psi_{l+|\mathcal{L}|,r})(1-a^{(j)}_{l,r})\Big). \qquad (4\text{-}103)
\end{aligned}
$$

4.4 Algorithm

Following the Master and Subproblem descriptions, the algorithm is carried out until the approximation provided by the inclusion of the cutting planes (4-103) is sufficient to make the solution of the relaxed Master problem close enough to optimality. This proposed outer approximation algorithm is illustrated in Fig. 4.1 and summarized in Algorithm 1.

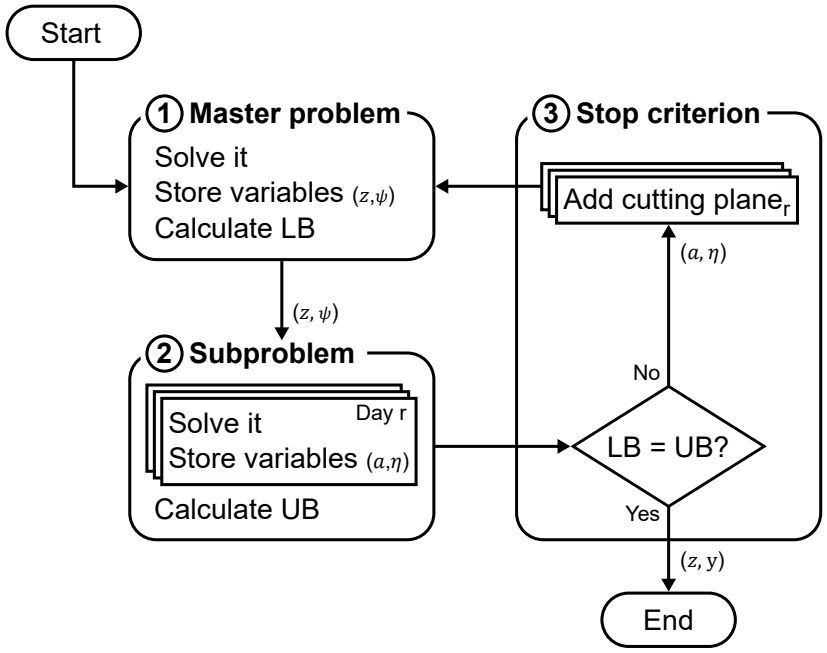

Figure 4.1: Algorithm illustration to solve the decomposed problem.

First Master problem (4-55)-(4-59) is solved. The lower-bound (LB) of the algorithm is calculated as the objective function (4-55) result in this iteration. After that, the subproblem (4-88)–(4-102) is solved for every representative day $r \in \mathcal{R}$, considering as input the previous values of variables z and ψ, calculated in the Master problem. The upper-bound (UB) of the algorithm is calculated considering the Master's objective function (4-55) solution minus the term with variable φ plus the Subproblem's objective function (4-88) solution (the approximation of φ). With the LB and UB calculated, the stopping criterion can be tested. If the bounds are close enough to a preset parameter ϵ, the problem stops and gives the current topology configuration z for each representative day and investment decisions y as the final solution. If the bounds are not close enough, considering the calculated values from dual variables η and the contingency vector a from the Subproblem, a cutting plane (4-103) is added for every representative day r in $\mathcal{R}$. After

this addition, the algorithm runs the Master problem again and continues the mentioned process until the bounds are close enough.

Algorithm 1: Iterative process

Initialization:
  Set $j \leftarrow 0$ and $\mathcal{J} \leftarrow \emptyset$

Iteration $j \geq 1$:
  Step 1 – Master problem:
    Solve problem (4-55)-(4-59)
    Store variables $\boldsymbol{z}_r^{(j)}$, $\boldsymbol{\psi}_r^{(j)}$, $\varphi_r^{(j)}$
    Compute $LB^{(j)} = \text{Eq. (4-55)}^{(j)}$
  Step 2 – Subproblems:
    for $r \in \mathcal{R}$ **do**
      Get stored variables $\boldsymbol{z}_r^{(j)}$, $\boldsymbol{\psi}_r^{(j)}$
      Solve problem (4-88)–(4-102)
      Identify worst case contingency $\boldsymbol{a}_r$
      Store variables $\boldsymbol{\eta}_r^{(j)}$, $\boldsymbol{a}_r$
    Compute $UB^{(j)} = LB^{(j)} - \sum_{r\in\mathcal{R}} \varphi_r^{(j)} w_r^1 + \sum_{r\in\mathcal{R}} \text{Eq.(4-88)}_r^{(j)} w_r^1$
  Step 3 – Stop criterion:
    if $\left(UB^{(j)} - LB^{(j)}\right)/UB^{(j)} \geq \epsilon$ **then**
    for $r \in \mathcal{R}$ **do**
      Get stored variables $\boldsymbol{\eta}_r^{(j)}$, $\boldsymbol{a}_r$
      Include cutting planes $(4\text{-}103)_r$ in Master
      Set $j \leftarrow j+1$ and $\mathcal{J} \leftarrow \mathcal{J} \cup \{j\}$
    Go to **Step 1**
    else
      Return solution $\boldsymbol{z}_r^{(j)}$, $\boldsymbol{y}^{sw,in^{(j)}}$, $\boldsymbol{y}^{in^{(j)}}$, $\boldsymbol{y}_h^{ha^{(j)}}$

4.5 Complimentary algorithms

In this section, two complimentary algorithms we developed are presented. The first describes the steps to construct the forbidden switching set used in the first-stage. And the second shows the out-of-sample analysis made for the cases studies (Chapter 5) to evaluate the model we propose.

4.5.1 Grid forbidden patterns

As explained before, the model developed here is made considering the operation of distribution systems. The set of constraints used is valid for operating only this type of system. As we consider topology changes, it is manda-

tory to ensure that no cycles are created in the final grid configuration. Also, no path between substations should be possible. To ensure these situations, constraint (3-36) is used in the first-level, where the topology is decided. For this constraint, it is necessary to construct set $\mathcal{K}^{forb}$ of forbidden patterns that cannot exist. An algorithm using depth-first search (DFS) [66] was developed. The steps are summarized in Algorithm 2.

Algorithm 2: Forbidden patterns set construction

Step 1 – Graph creation:
    Create a graph where buses are nodes and lines are edges
    Get indexes of existing lines that are non-switchable
    Get indexes of buses that are substations

Step 2 – Forbidden cycles:
    Use DFS to find all cycles (closed paths) in the graph
    Remove cycles with same edges
    Remove duplicated cycles
    Transform cycle information from nodes to edges (lines)
    Filter out existing lines that are non-switchable
    Get remaining rules of forbidden cycles

Step 3 – Forbidden paths:
    Find all paths between pairs of substations using DFS
    Transform paths information from nodes to edges (lines)
    Filter out existing lines that are non-switchable
    Get remaining rules of forbidden paths

Step 4 – Forbidden set creation:
    Combine forbidden cycles and paths into a single set
    Remove duplicates rules
    Assign unique rule IDs to each forbidden pattern

4.5.2 Out-of-sample analysis

To compare the results that a case study would have if we consider the operation based on the results from the decision-dependent model developed here, it is necessary to compare it with the results obtained by a model that does not consider this type of uncertainty. This model is constructed exactly the same as the "with DDU" model, but considering parameter β as zero for every line in every case, leaving the probability of failure only with the term γ (named "without DDU" model). Therefore, the uncertainty is not affected by any decisions made within the model.

After obtaining the results of each model (grid topology and investments), we perform an out-of-sample analysis using Monte Carlo simulation

[71]. Considering the final grid topology, first, the regular operation of the distribution grid of each representative day is analyzed, and the power flow of each line in each period t and each representative day r is calculated. With this, we calculate the probability of failure of each line in each period t and each representative day r. For both models, we calculate the probability of failure based on the definition made in expressions (3-50)–(3-51), with the same value of β used in the model "with DDU". Although in the construction of the model's ambiguity set, we only consider the failure associated with the power flow at period 0, here we calculate individually the failure rate of each period t. After that, we generated 2000 scenarios of failure following a Bernoulli trial for the line states (1 in service; 0 otherwise) with the computed probabilities. Once again, the operation of the case is evaluated in each scenario and the deficit proportion of the entire demand is calculated. By doing this, we are able to verify the impacts on the demand that would not be possible to deliver if we made decisions without considering the DDU model. All the steps to address this analysis are summarized in Algorithm 3.

Algorithm 3: Out-of-sample analysis

Initialization:
  Step 1 – Grid topology:
    Solve problem with and without DDU
    Store final topology configuration of each model (z_r) for each r in $\mathcal{R}$

Operation Analysis:
  Step 2 – Probability of failure:
    for each model **do**
      for r in $\mathcal{R}$ **do**
        Set a as vectors of 1 (no contingencies)
        Get z_r
        Solve third-level $H_r(z_r, a)$
        Store power flow variables $f^p_{l,t,r}$ for each period t and line l
        Compute failure probability for each period t and line l:
          $\mu_{l,t,r} = \gamma_l + \beta_{l,r} w_l^{\beta} |f^p_{l,t,r}|$
  Step 3 – Scenario generation $a_{\omega,l} \sim Bern(p)$:
    for each model **do**
      for ω in $1:2000$ **do**
        for t in $\mathcal{T}, l$ in $\mathcal{L}, r$ in $\mathcal{R}$ **do**
          Sample x in $X \sim \mathcal{U}(0,1)$
          if $x \leq \mu_{l,t,r}$ **then**
            Set $a_{\omega,l,t,r} = 0$
          if $x > \mu_{l,t,r}$ **then**
            Set $a_{\omega,l,t,r} = 1$
  Step 4 – Impact at each scenario:
    for r in $\mathcal{R}$ **do**
      Solve $H_r(z_r, a_{\omega,r})$ for each model and scenario ω
      Store deficit variables
      Compute deficit percentage of the demand
  Step 5 – Results analysis:
    Compare data from each model of each representative day r in $\mathcal{R}$

5
Results

The proposed methodology is illustrated in this section with three case studies. In all of them, we consider that a part of the grid is vulnerable to the ignition of a wildfire, which can be influenced by the levels of power flows passing through the line segments within the region. Furthermore, in the numerical experiments, we assume $K = 1$ in expression (3-45) to characterize the support set $\mathcal{A}$. The first case study is based on a 54-bus distribution system, whereas the second one comprises a 138-bus distribution system. The two cases aim to analyze the methodology considering the operation of one hour in one representative day, with no investment options. The third case study is a 54-bus distribution system, but considering the operation of 24 hours, in 3 different representatives days. In this last study, we consider investment options. For replicability purposes, the input data can be downloaded from [72]. The solution algorithm for the model described in Chapter 3 was implemented in Julia 1.9 and solved on a server with one Intel® Core® i7-10700K processor @ 3.80GHz and 64 GB of RAM, using Gurobi 9.0.3. under JuMP.

5.1
Case 1: 54-bus system, 1 representative day

In the first case study, we analyze the operation of a 54-bus distribution system (depicted in Fig. 5.1) based on the data provided in [73]. Here, we consider only one representative day with one period, and no investment options. The reason we do this is to first study the behavior of the model considering the topology reconfiguration in a more simple problem. In this system, there are 54 buses, from which 3 are substations (buses 51, 53, and 54). The total demand of the system is 5400 kW for the single period of the single representative day. Besides that, there are 11 switchable lines and 46 lines that are non-switchable. In Fig. 5.1, the switchable lines are represented by blue lines, where the dashed lines are initially open and the solid lines are initially closed. To enforce radiality, we used a DFS algorithm to create forbidden rules as explained in Chapter 4.5.1. The switching action cost is \$100 and the energy price is 0.01 \$/kWh. The weights parameters of the master function were used as 1 for both w_1 and w_2.

We consider an event of adverse climate conditions approaching that includes extreme dry weather and consistent wind speed at the southeast region of the grid (lines 6, 7, 8, 9, 10, 12, 13, 36, 37, 43, 45, 46, 47, and 52). This

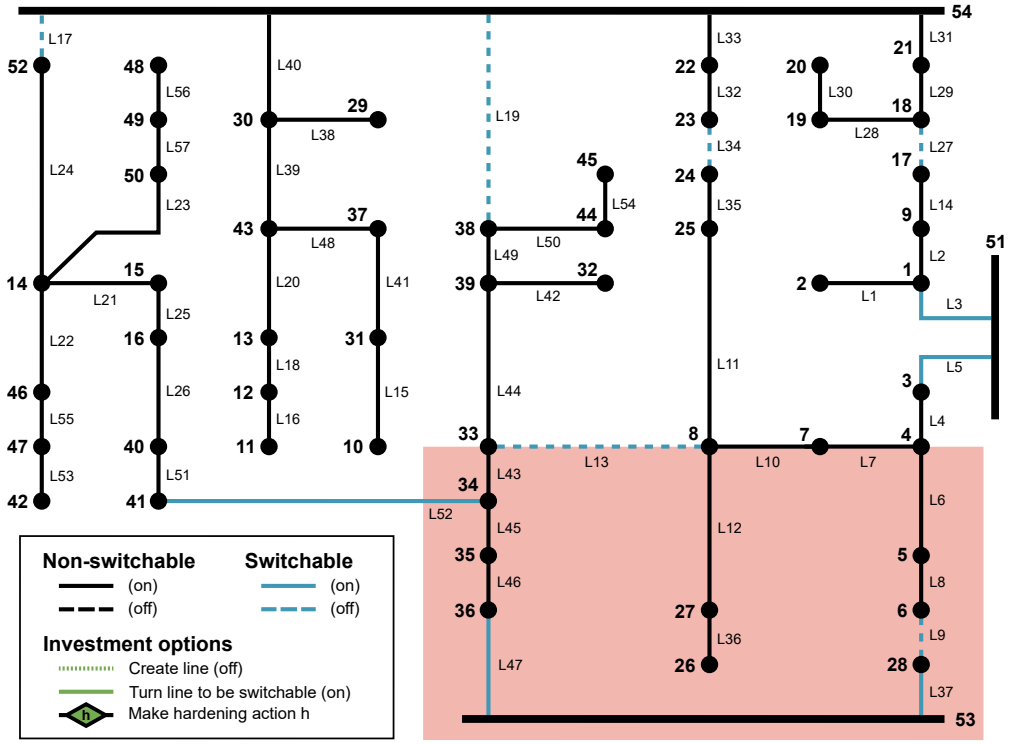

Figure 5.1: Case 1 distribution system.

unusual environmental condition in this area is expressed with a higher value for the β parameter in the failure probability expression (3-46). In each of the aforementioned lines, we consider an increase of 3% in its probability of failure for each 0.01 pu (100kW) of scheduled active power flow ($\beta = 300\%$). The remaining lines outside this critical region have an increase of only $10^{-4}\%$ in their probabilities of failure per 0.01 pu of scheduled active power flow ($\beta = 0.01\%$). We also consider that every line has a nominal rate of failure equal to 0.4 failures per year. Using the exponential probability distribution (5-1), this rate of failure translates into a failure probability of 0.12% (γ) for each line in the next 24 hours.

$$FailureProb = 1 - e^{\left(\frac{-1}{1/FailureRate}\right)} \tag{5-1}$$

We consider in this first study three possible modeling structures to determine the status of switchable lines. In the first one, hereinafter referred to as "without DDU", the operator ignores the decision-dependent influence of line flows and probabilities of failures in the modeling and, therefore, only considers the nominal probabilities previously described ($\beta = 0$). In the second one, hereinafter referred to as "with DDU", the operator explicitly considers the aforementioned increase in failure probability corresponding to line usage according to (3-46). In the third one, hereinafter referred to as "with

DDU+WU", decision-dependency is considered exactly as in the "with DDU" case but the cutting planes of the "without DDU" case are included in the master problem since the beginning of the execution of the solution algorithm. This reuse of cutting planes works as a warm-up phase and can help the model to achieve the same solution of the "with DDU" method in less time.

The resulting topology statuses for every model considered are depicted in Table 5.1, where 1 means a line is closed and 0 means a line is open. As expected, when DDU is ignored there is no incentive to change the status of any line. Nonetheless, when DDU is considered, six lines have their statuses changed.

Table 5.1: Case 1 topology results (1 for closed and 0 for open)

	Switchable Lines										
	3	**5**	**9**	**13**	**17**	**19**	**27**	**34**	**37**	**47**	**52**
W/out DDU	1	1	0	0	0	0	0	0	1	1	1
With DDU	1	0	0	0	1	1	0	1	1	0	0
With DDU+WU	1	0	0	0	1	1	0	1	1	0	0

In a simplified representation, Figure 5.2a shows how the grid would be if no switching actions were performed, same result as the "without DDU" case. In this configuration, the demand of the buses inside the red area (wildfire-prone environment) is mostly being supplied by substations 53 and 51. Figure 5.2b shows the configuration of the grid when the switching actions proposed by the "with DDU" model are performed. In this case, most of the grid demand is supplied by substation 54.

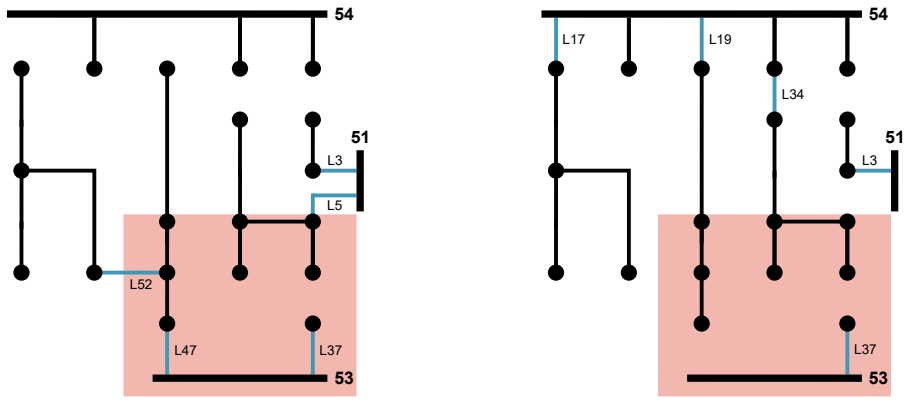

(a) Without DDU (b) With DDU

Figure 5.2: Case 1 simplified diagram of topology reconfiguration results. The left figure (a) represents the solution for the case "without DDU", where no switching actions were performed. The right figure (b) represents the solution for the case "with DDU", where lines 17, 19, and 34 were closed and lines 5, 47, and 52 were opened.

This change of topology incurs a reduction of the average power flow of lines across the system, as seen in Fig. 5.3. This reduction occurs since by recognizing that the power flows through the lines inside a wildfire-prone environment can increase failure probabilities, the proposed methodology better distributes the power flow level across all line segments of the system while minimizing the system's loss of load. By considering the information about which lines are inside an area that is vulnerable to wildfires, the proposed methodology is able to strategically decrease power flow levels in this area, and increase power flow levels in safer areas to compensate the demand supply (see Fig. 5.3).

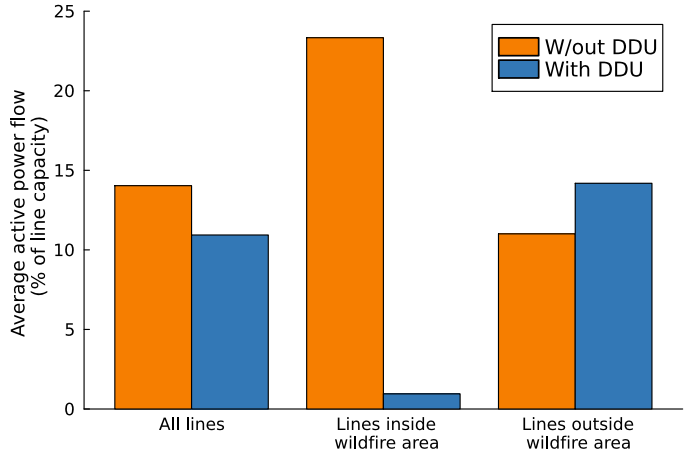

Figure 5.3: Case 1 power flows results for the solutions *without* and *with* DDU.

Considering the operation of the grid in this single representative day, the cost would be \$54 for the "without DDU" case, and \$654 for the "with DDU" solution. This last cost includes not only the cost of feeding loads but also the cost of performing 6 switching actions. The "with DDU+WU" solution results in exactly the same costs and topology decisions as the "with DDU" solution. The solutions "without DDU", "with DDU", and "with DDU+WU", were obtained in 2.3, 3.7, and 1.2 minutes, respectively. While the master problem of the "with DDU" case had 961 continuous variables and 570 binary variables, the master problem for the "without DDU" case had 505 continuous variables and 228 binary variables. For both models, the subproblem had 1,797 continuous variables and 57 binary variables.

5.1.1 Out-of-sample analysis

To compare the performance of both solutions, "without DDU" and "with DDU", we conduct the out-of-sample analysis as shown in Chapter 4.5.2. The average loss of load (% of total demand) for the solutions "without DDU" and

"with DDU" are 44.21% and 0.68%, respectively. In addition, the $\text{CVaR}_{95\%}$ of loss of load (% of total demand) for the solutions "without DDU" and "with DDU" are 58.20% and 9.06%, respectively. Moreover, according to Fig. 5.4, the solution "with DDU" has 83% probability to incur in null loss of load and 96% probability of resulting in up to 2% of loss of load, whereas the solution "without DDU" has 98% probability to incur in any loss of load and 93% probability to result in more than 30% of loss of load.

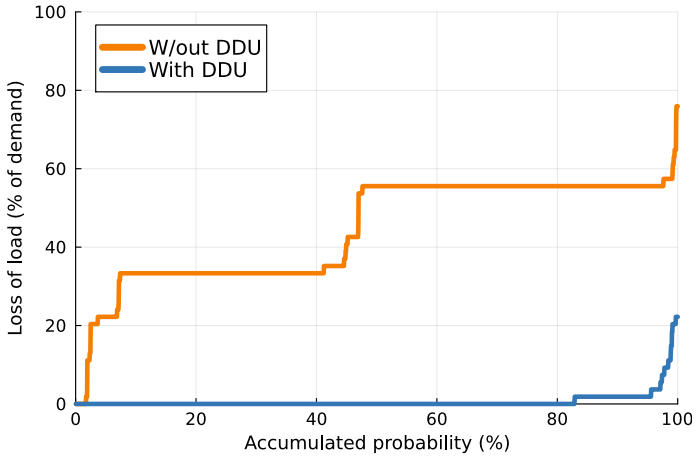

Figure 5.4: Case 1 out-of-sample inverse cumulative distribution of the system loss of load for the solutions *without* and *with DDU*.

We note that the magnitude of the impact on loss of load probability is rooted in the topology reconfiguration prescribed by the two cases under analysis. More specifically, note from Fig. 5.2a that the cost-effective action prescribed under the *without DDU* case is to feed customers using power mostly from substation Bus 53, by keeping lines 47 and 52 closed, i.e., no switching action is taken. Since the substation Bus 53 is in a wildfire-prone area, the likelihood of line failure closely linked to feeding part of the system with power coming from this feeding bus is high. This fact is due to the context and the relatively higher power flow needed to feed almost the whole system. Therefore, this topology reconfiguration potentially triggers the failure of important line segments, magnifying the system loss of load for several operating conditions (scenarios), and inducing the observed high loss of load probability. It should be highlighted, nevertheless, that by appropriately taking into account wildfire-prone conditions when prescribing the topology reconfiguration (the *with DDU* case), the same performance metric was significantly improved for the same system and context conditions. In fact, the topology reconfiguration prescribed under the *with DDU* case is to feed customers using power mostly from substation Bus 54, located in an area without critical wildfire conditions (as shown in Fig. 5.2b). This proposed reconfiguration is constituted by opening

lines 5, 47, and 52 and closing lines 17, 19, and 34. Therefore, we argue that our proposed methodology can properly recognize the appropriate switching actions that are needed to significantly decrease the risk of loss of load within a decision-dependent uncertainty framework.

5.2 Case 2: 138-bus system, 1 representative day

The second case study considers a 138-bus distribution system (Fig. 5.5), also adapted from the data provided in [73]. This study was made to evaluate the benefits and effectiveness of the proposed methodology in larger and more complex systems. Besides that, we evaluate the sensitivity of the β parameter. In this system, there are 3 substations, 138 buses, and 142 lines, from which 12 are switchable. As in the first case study, we consider only one representative day with a single period operation and no investment options. The total demand of the system is 56,900 kW and the energy price is 0.20 \$/kWh. We consider a penalty of 2 \$/kWh for loss and surplus of both active and reactive power, and each switching action costs \$200. The DFS algorithm is used to identify the 12 rules that avoid the simultaneous activation of line segments and result in the formation of cycles within the network. All branches have a nominal rate of failure equal to 0.15 per year and, analogously to Subsection 5.1, this rate of failure translates into a 0.0411% of failure probability (γ) for each line in the next 24 hours using the exponential probability distribution. Furthermore, the northwest part of the system is more likely to initiate a wildfire. This area of the grid includes lines 1–5 and 17–24. As showed in the first case study (Subsection 5.1), the model with the DDU can be helped by the inclusion of the warm-up phase with the cutting planes from the model without DDU, providing the same solution in a shorter time. As we increase the complexity of the case studies, hereinafter the results we show for the DDU model are already considering the warm-up phase.

In this numerical experiment, we conduct a sensitivity analysis of the impact of the β parameter in the solution by running the model "with DDU" 27 times, considering different values for β in the mentioned area. The range of the chosen values is defined considering the maximum failure probability ($\gamma + \beta\overline{F}$). This probability indicates how likely a line failure is to happen if the power flow in the feeder is at its maximum capacity. Given that, we choose β values for the lines in the wildfire area considering $\beta \times \overline{F}$ to range from 1% to 2% by 0.1%, from 2% to 10% by 1%, and from 10% to 90% by 10%. All the lines from outside the wildfire-prone area are assumed to have a $\beta \times \overline{F}$ as 0.1% in all cases.

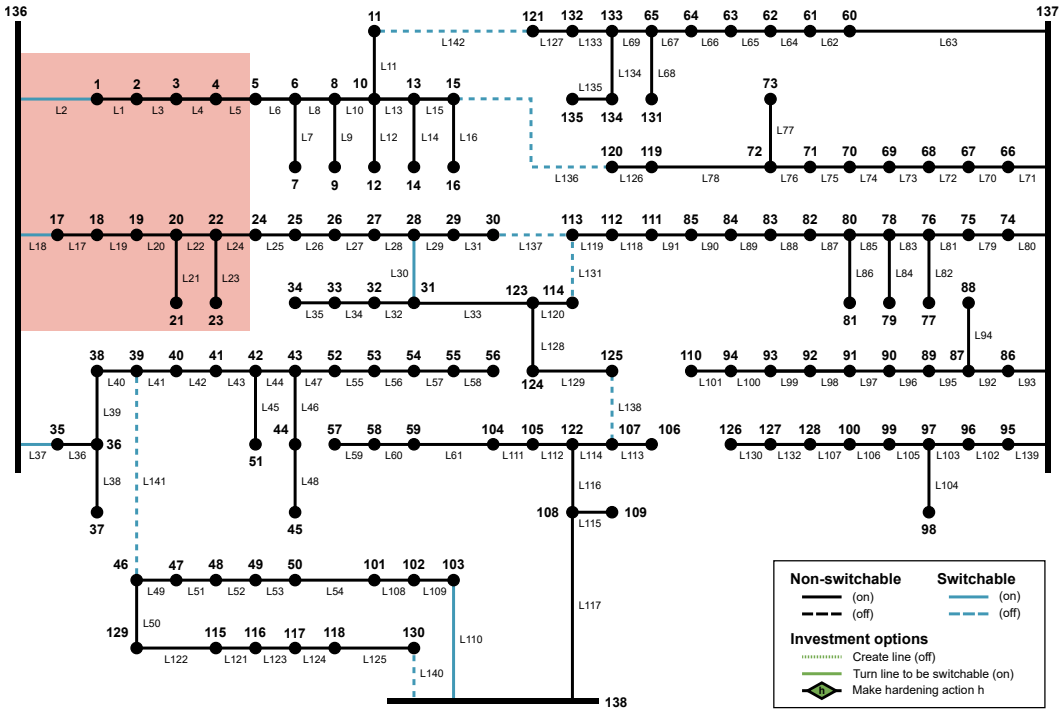

Figure 5.5: Case 2 distribution system.

The main results are depicted in Table 5.2, where, for expository purposes, only the results for 8 cases are shown. These cases of maximum failure probability are important as they resulted in an operation change in terms of switching actions, for example, the cases between 1.1% and 1.8% resulted in the same switching decision, and so on. The first line shows the maximum failure probability, and the second the switching actions performed in each case. Next, the master objective function costs are shown, with the respective terms presented in the master function: C^d as the cost of prior operating point deficit/surplus at $t = 0$; C^e as the worst expected cost of the multiperiod operation; C^s as the switching actions costs; C^i as the line investments costs; and C^h as the hardening investments costs. Finally, the computing time of each case is presented in minutes.

As depicted in Table 5.2, as the value of β increases (maximum failure probability), the line risk of failure also increases, thus the solution is to change the grid by switching some strategical lines. By changing the grid topology, the model decreases the power flow in critical lines (inside the wildfire-prone area), decreasing the risk of failure associated with $\boldsymbol{\beta}$. The four possible topology configurations are depicted in Figure 5.6. Figure 5.6a shows the simplified diagram of the grid configuration result for the cases with maximum line failure probability between 0% and 1%. In this topology, substation 136 is being used to provide energy for the branches that start in lines 2 and 18. Figure 5.6b shows the topology for the cases with maximum line failure probability between

1.1% and 1.8%. Now, by switching lines 30 and 138, part of the branch that started in line 18 is being supplied by substation 138. Figure 5.6c shows the topology for the cases with maximum line failure probability between 1.9% and 3%, where by additionally switching lines 2 and 136, all the branches that started in line 2 is being supplied by substation 137. Figure 5.6d shows the topology for the cases with maximum line failure probability between 4% and 90%, where by additionally switching lines 18 and 137, both branches that started in lines 2 and 18 are totally being energized by substations 137 and 138.

This change of configuration can be understood also by looking at the cost terms of the objective function. As we increase the level of $\boldsymbol{\beta}$, the worst-case expected value of post-contingency operation cost increases until it is worth performing switching actions. For instance, in the cases where only 4 lines are switched, between 1.9% and 3%, the worst-case expected value increases up to \$12,543. At 4%, it is more economically viable to afford further two switching actions and have a lower worst-case expected value. Therefore, as we increase the influence of the power flow levels through some line segments on their corresponding failure probabilities, the proposed methodology is able to recognize the impact and perform the appropriate switching actions, yielding more risk-averse solutions. These switching actions are intended to decrease the power flows through the most vulnerable line segments, which, as a consequence, results in dramatically lower metrics of average and $\text{CVaR}_{95\%}$ of loss of load as can be seen in our further discussion out-of-sample analysis. These lower levels of loss of load can be translated into avoiding large costs for

Table 5.2: Case 2 main results

	Without DDU	**With DDU[a]**						
Max. failure prob.	**0.0%**	**1.0%**	**1.1%**	**1.8%**	**1.9%**	**3%**	**4%**	**90%**
Sw. actions (line index)	-	-	30; 138	30; 138	2; 30; 136; 138	2; 30; 136; 138	2; 18; 30; 136; 137; 138	2; 18; 30; 136; 137; 138
Master ($)	11,721	12,721	12,802	13,126	13,154	13,343	13,463	14,792
C^d	0	0	0	0	0	0	0	0
C^e	11,721	12,721	12,402	12,726	12,354	12,543	12,263	13,592
C^s	0	0	400	400	800	800	1,200	1,200
C^i	0	0	0	0	0	0	0	0
C^h	0	0	0	0	0	0	0	0
Time (min)	7.3	2.7	4.2	7.5	9.1	11.0	11.6	13.9

[a] The results shown for the "with DDU" model considered the warm-up phase reusing the "without DDU" cutting planes, therefore, the real elapsed time for the "with DDU" model should add the "without DDU" elapsed time.

not serving the demand, which is an economic benefit of our methodology.

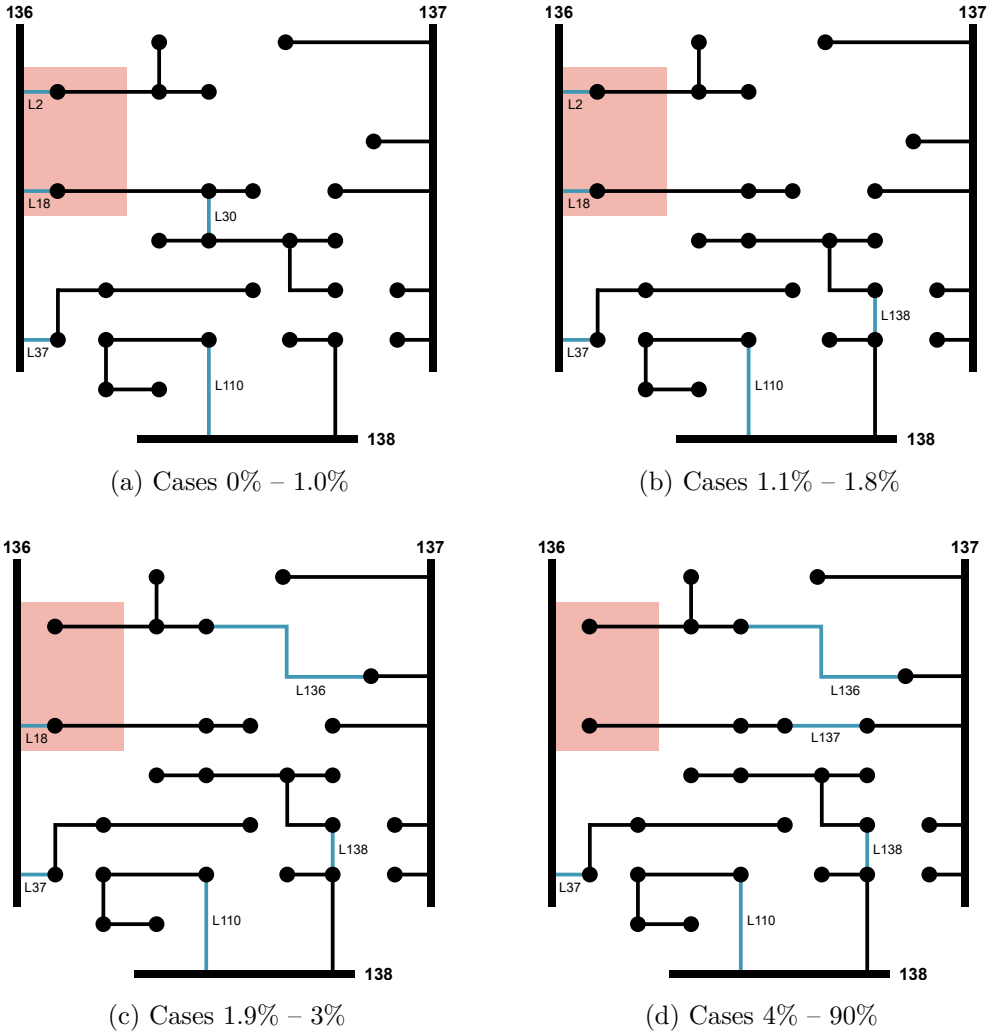

(a) Cases 0% – 1.0%

(b) Cases 1.1% – 1.8%

(c) Cases 1.9% – 3%

(d) Cases 4% – 90%

Figure 5.6: Simplified diagram for topology reconfiguration results of case 2. In Figure (a) no switching action was performed, in Figure (b) lines 30 and 138 were switched, in Figure (c) lines 2, 30, 136, and 138 were switched, and in Figure (d) lines 2, 18, 30, 136, 137, and 138 were switched.

In general, the solution time of each case also increases with the $\boldsymbol{\beta}$ levels, reaching a maximum elapsed time of roughly 14 minutes. Essentially, when decision-dependent uncertainty is neglected ($\beta = 0$ for all lines), the impact of power flow levels on failure probabilities is not considered. Therefore, the switching decisions are the only first-stage decision variables to influence the outcome of the worst-case expected value of post-contingency costs. With $\beta = 0$ for all lines, γ is the only remaining parameter in the line failure probability affine function, defined in expression (3-46). Since in our case studies, we consider γ as a low routine failure probability for all lines, different first-stage switching decisions lead to the same outcome of the worst-case expected value of post-contingency costs when $\beta = 0$. The

solution algorithm can then efficiently recognize that no switching decision would decrease the worst-case expected value of post-contingency costs and, since switching decisions have an associated cost, switching is not performed. It is worth mentioning that switching actions only take place when the decrease in the worst-case expected value of post-contingency costs offsets the switching costs. On the other hand, when we consider that power flow levels can impact line failure probabilities ($\beta \geq 0$), the solution algorithm needs more information from the subproblem to better describe in the master problem how the worst-case expected value of post-contingency costs could decrease depending on the first-stage switching actions. In this case, different combinations of switching actions can decrease the worst-case expected value of post-contingency costs. Consequently, the solution algorithm needs more iterations to determine the least-cost combination of switching actions that can lead to the highest decrease in the worst-case expected value of post-contingency costs. Moreover, the impact of power flow levels on line failure probabilities increases as we consider higher values of β, which prompts the solution algorithm to usually require more time to approximate the worst-case expected value of post-contingency costs so as to identify the optimal combination of switching actions.

While the master problem of the "with DDU" case had 3,253 continuous variables and 2,272 binary variables, the master problem for the "without DDU" case had 1,265 continuous variables and 568 binary variables. For both models, the subproblem had 4,505 continuous variables and 142 binary variables.

5.2.1 Out-of-sample analysis

In this 138-bus system, we consider the results of using each parameter $\boldsymbol{\beta}$. Firstly, in Fig. 5.7, we showcase the average load shedding for the out-of-sample analysis for a few levels of maximum failure probability ($\gamma + \beta\overline{F}$). Note that, as the environmental conditions for a wildfire worsen, the impact of the average loss of load when disregarding the DDU increases significantly. For instance, for a maximum failure probability of 90%, the average loss of load would be roughly 23% of total demand if no actions were considered ("without DDU"), while it would be roughly 1% if the actions suggested by the DDU model were implemented. Furthermore, Fig. 5.8 depicts a similar analysis, but highlighting the associated $\text{CVaR}_{95\%}$ level. Note that, for the setup "without DDU", a value between 20% and 30% in loss of load (in % of total demand) can be observed in the most critical scenarios. On the other hand, the system

topology prescribed by the "with DDU" setup significantly mitigates the load shedding occurrence and, consequently, the system operation cost. Considering once more the maximum failure probability of 90%, the average cost in the "without DDU" setup is around $26,000 (Fig. 5.7). This value is even higher than the expected cost of around $13,000 in the 5% worst-valued scenarios ($\text{CVaR}_{95\%}$) when prescribing the "with DDU" setup (Fig. 5.8).

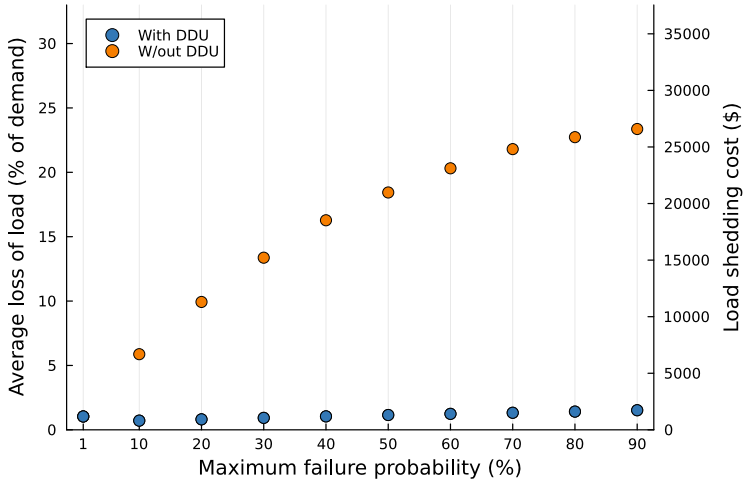

Figure 5.7: Case 2 average loss of load (% total demand) in the out-of-sample analysis for the solution setup *with DDU* and *without DDU* for different levels of maximum failure probability.

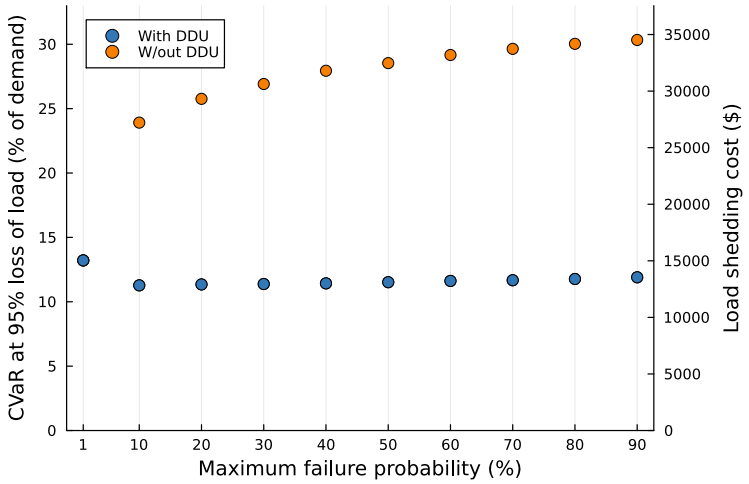

Figure 5.8: Case 2 $\text{CVaR}_{95\%}$ loss of load (% total demand) in the out-of-sample analysis for the solution setup *with DDU* and *without DDU* for different levels of maximum failure probability.

5.3
Case 3: 54-bus system, 3 representative days

The last case study aims to illustrate the full potential of the methodology we propose. We use the same grid as in the first case study (Section 5.1), a distribution system with 54 buses and 57 lines. In this case, only lines 13, 17, 47, and 52 are already switchable. Existing lines 3, 5, and 37 need an additional investment to become switchable, and lines 9, 19, 27, and 34 are candidate lines that needs an additional investment to be constructed. In this case example, candidate lines become switchable lines if they are created. Besides that, lines 10, 11, and 12 have the option of hardening investment 1, and lines 11, 12, 22, and 24 have the option of hardening investment 2. While hardening investment 1 can reduce the failure probability by 50%, hardening option 2 can reduce the failure probability by 100%. This grid configuration can be seen in Figure 5.9.

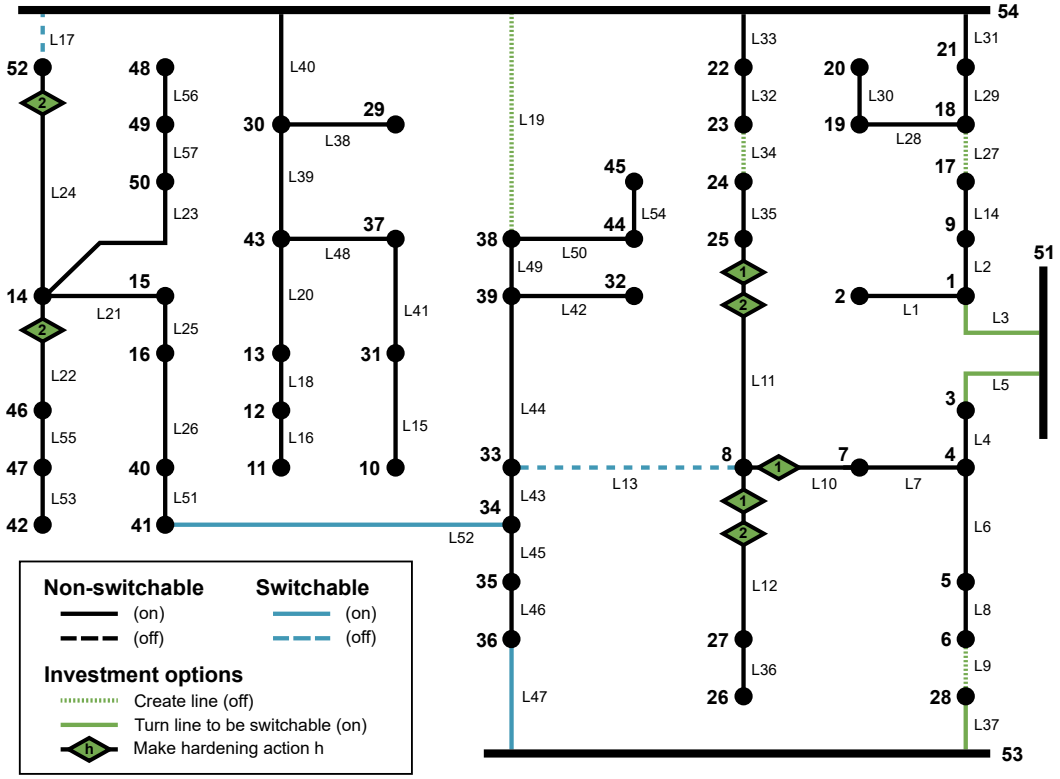

Figure 5.9: Case 3 distribution system.

In this case study we consider 3 different representative days in the problem formulation. Each of these days considers different demands and different wildfire area-prone environment inputs. The demand for each day is hourly accounted for, with 24 periods. The demand profile was constructed based on the first case study, but adapting the profile of the total demand considering the CAISO profile for days 05-jan-2022, 05-may-2022, and 05-sep-2022, for days 1, 2, and 3, respectively. We chose the prior operating point

($t = 0$) considering the hour with the highest demand in each day. While the peak demand on days 1 and 3 was at 7 pm, on day 2 the peak was at 9 pm. The total demand profile of the system for each day can be seen in Figure 5.10.

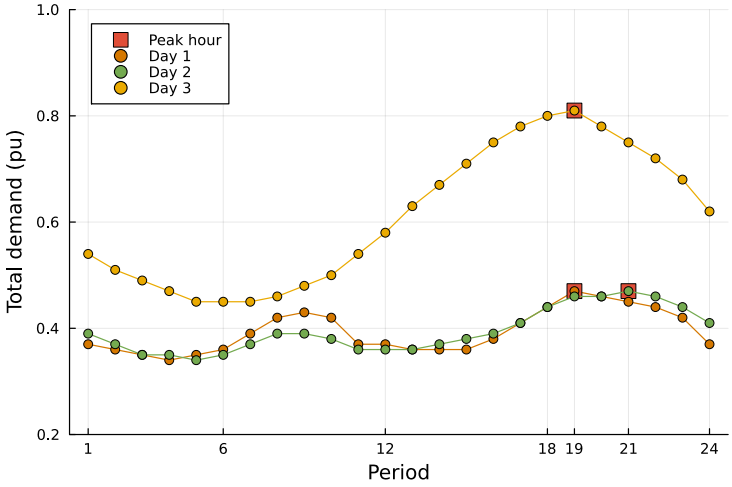

Figure 5.10: Case 3 total demand profile of each representative day.

The wildfire risk conditions are different for each representative day. In representative day 1, it is expected extreme weather conditions in the southwest part of the grid (lines 21, 22, 25, 26, 51, 53, and 55) that highly affect the failure probability of the lines inside this area. East from this part of the grid, it is expected a more mild weather condition (lines 13, 43, 45, 46, 47, and 52), that although affects line failure probability, has a lower intensity. For the first area we chose a β that would represent a maximum failure probability ($\gamma + \beta\overline{F}$) of 50%, while in the second area, the β chosen represents a maximum failure probability of 10%. All the other lines outside these areas were considered to have a minimum β parameter for a maximum failure probability of 0.003%. These different wildfire-prone areas can be seen in the simplified diagram in Fig. 5.11a, where the dark red shade represents the more extreme weather condition. In the representative day 2, depicted in Fig. 5.11b, an extreme weather condition is expected in the southeast part of the grid (lines 6, 7, 8, 9, 10, 12, 13, 36, 37, 43, 45, 46, 47, and 52). In the lines inside of this area, the β parameter was also chosen considering a maximum failure probability of 50%. Finally, the representative day 3 has a wildfire area only in part of the grid (lines 6, 7, 8, 9, 10, 12, 36, and 37), as depicted in Fig. 5.11c. In this part, we chose a β that would represent a maximum failure probability of 70%.

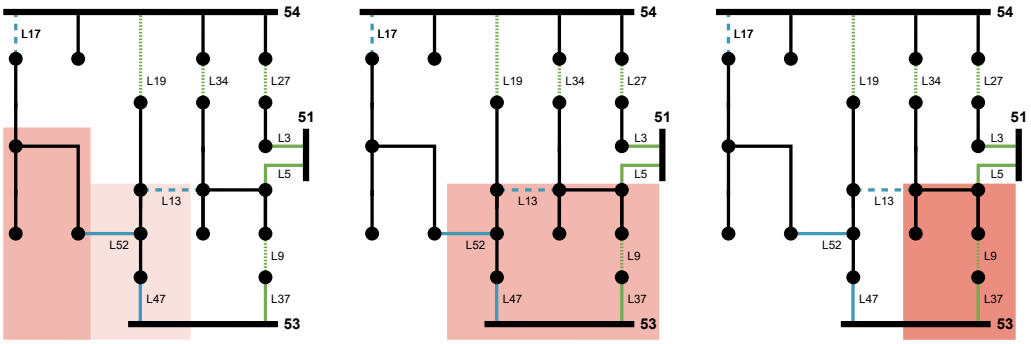

(a) Representative day 1 (b) Representative day 2 (c) Representative day 3

Figure 5.11: Simplified diagram of wildfire-prone area in each representative day of case 3.

The cost for creating a new line was considered to be \$10,000, the cost for turning a regular line to be switchable \$1,000, and the switching action cost \$100. The investment cost for the hardening option 1 was considered to be \$1,000, while for the hardening option 2, \$100,000. The energy price is 0.01 \$/kWh. We considered each representative day with the same weight in a typical year, where the weights parameters of the master function were chosen to be 2920 for both w_1 and w_2. This value represents the hours in a year that each day represents. All other parameters were used the same as in case 1.

The main results can be seen in Table 5.3. The first column shows the results for the model without DDU and the second for the model with DDU. The last column shows the result for the model with DDU but locking all the switching and investment binary variables to be zero.

In the model without DDU, no investment or switching action was made, as there is no incentive to change the topology. The model with DDU returns a solution with investments for creating lines 19 and 34, and turning line 5 to be switchable. These investments allow the model to change the topology differently for each day. Hardening investments were made only in the model with DDU, where line 10 had the hardening investment 1, and lines 12 and 22 had the investment 2. When we analyze the cost functions of the master problem for the models with DDU, we can see that the expected cost of the post-contingency operation (C^e) reduces drastically when we allow the model to invest and perform switching actions. In this case, the reduction is from \$78,805,000 to \$5,532,000. The cost for line investments and switching actions is lower than this difference, and therefore, the model prefers to pay for these actions than to have a high expected cost for the second-level. The expected cost for the case without DDU is lower since the model ignores the decision dependency of the failure. Besides that, as lines 19 and 34 were created in the

Table 5.3: Case 3 main results

		W/out DDU	With DDU	With DDU [a]
New lines		-	19; 34	-
New switchable lines		-	5	-
Sw. actions (line index)	**Day 1**	-	17; 19; 47; 52	-
	Day 2	-	5; 17; 19; 34; 47; 52	-
	Day 3	-	5; 34	-
Hardening investments	**1**	-	10	-
	2	-	12; 22	-
Master ($K)		2,781	8,090	78,805
C^d		0	0	0
C^e		2,781	5,532	78,805
C^s		0	2,336	0
C^i		0	21	0
C^h		0	201	0
Time (min)		23.0	43.3 [b]	20.3

[a] The results for this case were obtained locking all y variables to be zero, i.e., no switching actions and investments were allowed to be performed.

[b] The results shown for the "with DDU" considered the warm-up phase reusing the "without DDU" cutting planes, therefore, the real elapsed time for the "with DDU" model should add the "without DDU" elapsed time.

model with DDU, no switching costs were considered for both lines. Therefore, the total switching costs (C^s) considered 3 switching actions for day 1, 4 actions for day 2, and 1 action for day 3. With a cost of \$100 per switching action and a weight $w_2 = 2920$, the total cost for the switching actions in the master objective function is \$2,336 thousand. Lines investments cost in total \$21,000, where \$20,000 is for the creation of two lines and \$1,000 for turning line 5 to be switchable. Finally, the hardening investment cost (C^h) accounts for \$1,000 for hardening line 10 with option 1 and \$200,000 for hardening lines 12 and 22 with option 2. The elapsed time for the case without DDU is 23 minutes, and for the case with DDU is 43.3 minutes. In the "with DDU" case shown in this section the warm-up phase is considered, and therefore, the elapsed time for the "with DDU" case should add the time necessary to run the case "without DDU". While the master problem of the "with DDU" case had 3,225 continuous variables and 1,296 binary variables, the master problem for the "without DDU" case had 1,515 continuous variables and 570 binary variables. For both models, the subproblem of each representative day had 43,128 continuous variables and 57 binary variables.

The topology reconfiguration results can be better seen in the simplified diagrams in Fig. 5.12 for each representative day and for each model. In these figures, lines that were not created or were not turned on are not shown. As in

the "without DDU" case no investments were made, and lines 9, 19, 34, and 27, were not created, so they are not shown in Figures 5.12a–5.12c. Lines 3, 5, and 37 did not turn to be switchable in this case, and they are shown in solid black lines in Figures 5.12a–5.12c. In the "with DDU" model, as line 5 were turned to be switchable and lines 19 and 34 were created, they are shown in solid blue line when they are turned on. In the topology configuration for day 1, if no switching action is performed (Fig. 5.12a), the buses inside the wildfire-prone area are entirely supplied by bus 53. If the "with DDU" switching action is performed (Fig. 5.12d), these buses have their energy supplied by bus 54. In this configuration, these buses are at the end of their branches, which helps in reducing the power flow of the lines inside this red area. For day 2, a similar result as in Case 1 can be seen, the buses inside the wildfire-prone area that were mostly being supplied by bus 53 (Fig. 5.12b), are now being supplied mostly by bus 54 (Fig. 5.12e). For day 3, as the wildfire-prone area changes in location and intensity, only two switching actions are necessary (lines 5 and 34). With these actions, part of the buses in the red area that was being supplied by bus 51 (Fig. 5.12c), is now being supplied by bus 54 (Fig. 5.12f).

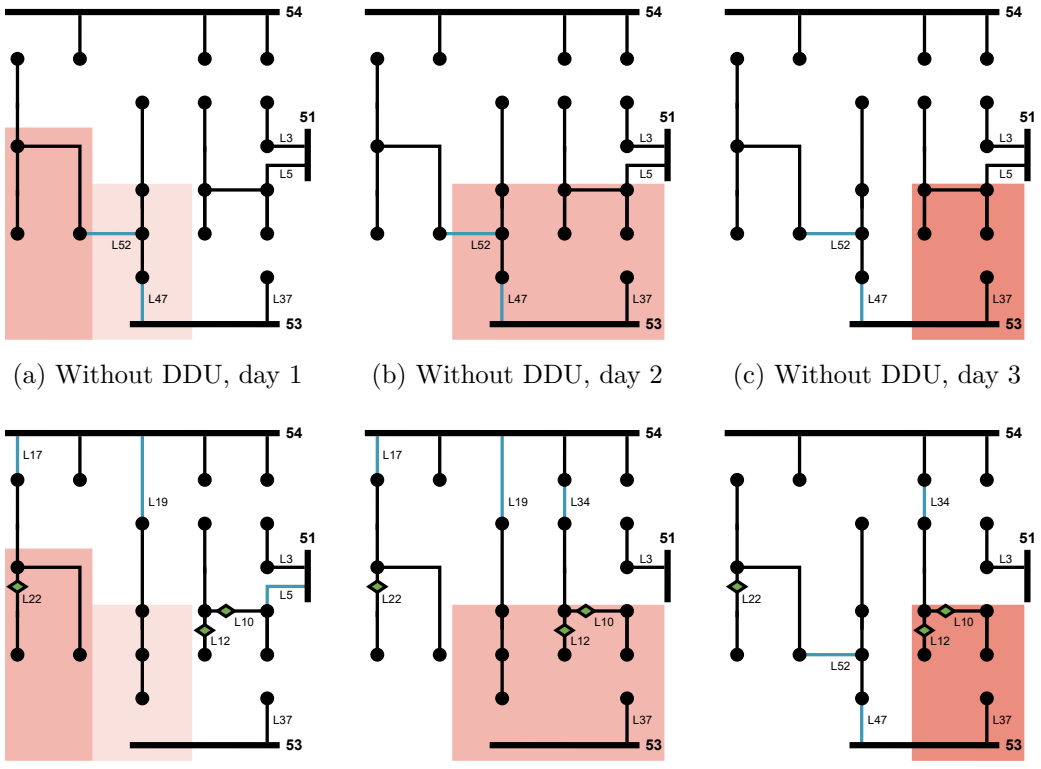

(a) Without DDU, day 1 (b) Without DDU, day 2 (c) Without DDU, day 3

(d) With DDU, day 1 (e) With DDU, day 2 (f) With DDU, day 3

Figure 5.12: Simplified diagram for topology reconfiguration results of each representative day of case 3.

In Figure 5.12 it can also be seen the lines that received investment to be

hardened, line 10 with hardening action 1, and lines 12 and 22 with hardening action 2. Line 22 is inside the wildfire-prone area in the first representative day (Fig. 5.12d), and lines 10 and 12 are both inside the wildfire-prone areas for days 2 and 3 (Fig. 5.12e and 5.12f). As explained before, hardening investments are decided in the first-stage of the problem and therefore are the same for all the representative days considered.

5.3.1 Out-of-sample analysis

Similar to cases 1 and 2, in this last case, we also perform an out-of-sample analysis following Algorithm 3. We evaluate the performance of the solutions "without DDU" and "with DDU" in terms of loss of active load for each representative day r. In this case, the analysis is made not only considering the topology change but also considering the hardening investments that directly affect line unavailability uncertainty construction. The average loss of load for each day as well as the $\text{CVaR}_{95\%}$ of loss of load can be seen in Table 5.4. It is clear that as we consider the investments and topology reconfiguration of the "with DDU" model, we decrease the probability of having a loss of load. In day 2 for example, there is a reduction from 24% of loss of load if no action was taken against only 1% of loss of load if the actions from the DDU model were taken. This reduction can be perceived in all days and also evaluating the loss of load in terms of $\text{CVaR}_{95\%}$.

Table 5.4: Case 3 out-of-sample analysis results

		W/out DDU	**With DDU**
Average loss of active load (% of demand)	**Day 1**	11	1
	Day 2	24	1
	Day 3	7	1
$\text{CVaR}_{95\%}$ loss of active load (% of demand)	**Day 1**	17	3
	Day 2	31	3
	Day 3	10	3

The complete out-of-sample results can be seen for each day in Fig. 5.13 through the inverse cumulative distribution of the system loss of load. We can perceive that the loss of load in this case is in general lower than the first case study (see 5.4). This is due to the fact that the ambiguity set that defines the uncertainty probability is constructed using the peak demand. In the out-of-sample analysis, we calculate the line unavailability considering the power flow for each hour. As the hours outside the peak hour usually had lower power flows, the total loss of load in the whole period can be reduced.

Although when we operate more than one hour, like in this third case study, the benefits of using the case with DDU are reduced, it is still more reliable than the solution of the model that ignores the decision-dependency nature of this type of uncertainty. Besides that, in this case study, lower failure probability values for β were chosen to be lower.

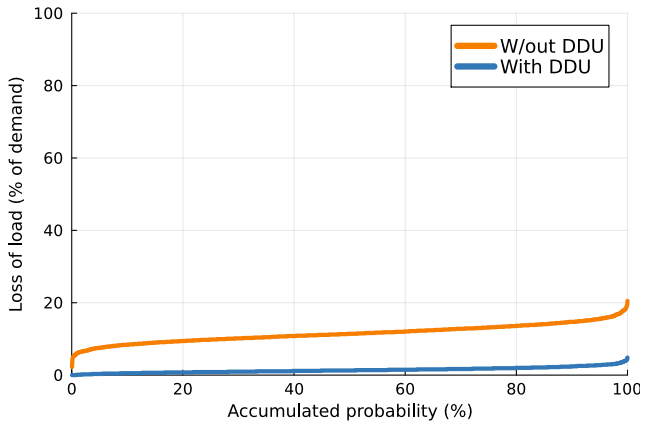

(a) Representative day 1

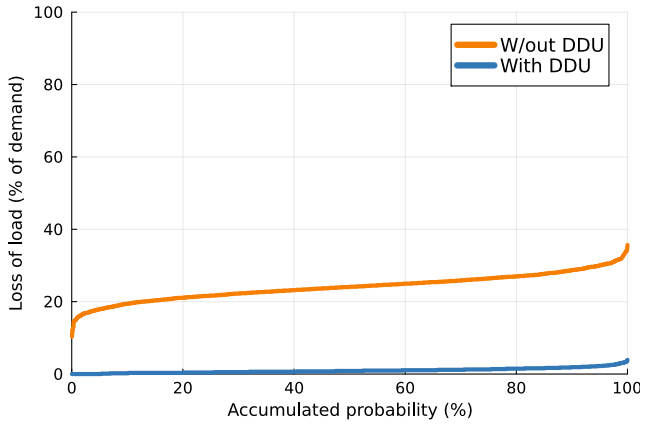

(b) Representative day 2

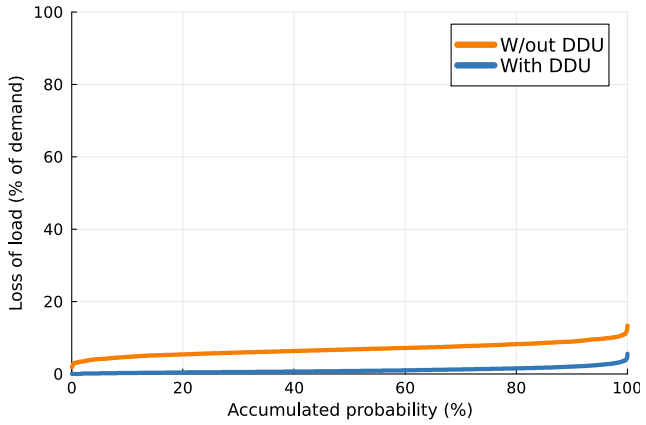

(c) Representative day 3

Figure 5.13: Case 3 out-of-sample inverse cumulative distribution of the system loss of load for the solutions *without* and *with DDU*.

6
Conclusion

This dissertation proposes a novel methodology to better plan the operation of distribution systems considering wildfire-prone environments. We acknowledge that the likelihood of a line failing is dependent on its power flow levels. Because of that, we leverage a decision-dependent uncertainty framework to characterize this aspect. In this framework, the model can properly prescribe optimal switching actions to decrease power flow values of lines inside areas with extreme weather conditions. Besides that, the model can decide for line investments that increase the grid's topology flexibility and for hardening investments that decrease the dependency of failure probability with the power flow levels.

Three numerical experiments were conducted to illustrate the effectiveness of the proposed methodology. We compared the results of the model we propose with a model that ignores this decision-dependency aspect. The first case study presented how the model works regarding the topology configuration aspect. The second case study proved that the model could be used in a grid with more buses and lines, and presented a sensitivity test for β, the parameter that represents the wildfire-prone weather conditions. The last case study aimed to demonstrate the interaction between the topology decisions and the investment options. In this case, we also tested the capability of the model to work with 3 representative days and a multiperiod operation. In general, the results demonstrated that by considering the wildfire information in the way constructed by our model, we can reduce the risk of failure and therefore the expected loss of load. We can extrapolate this analysis and claim that this would lead to less wildfire disruption caused by power lines.

This line of research can be enhanced or adapted in different aspects. For future work, the following topics can be evaluated:

1. Test the model in a case study with a more realistic grid. More representative cost values and a better representation of the extreme weather conditions can also be addressed. With bigger grids, heuristics approaches can be developed to decrease the computational time;

2. Adapt the framework to different topological conditions such as distribution systems operated as meshed networks and transmission systems;

3. Model the switching actions as recourse decisions and correlated cascading failures;

4. Consider the operation of batteries and DERs for microgrid formation;

5. Consider other ways to linearize the problem. The binary expansion approach increased significantly the number of binary variables needed, which increased the computational burden. Approaches such as McCormick envelopes can be evaluated in this framework;

6. Investigate other ways to construct the ambiguity set. We modeled the line failure probability of the whole multiperiod operation based on a single period, which can be unsuitable for some cases.

7
Bibliography

1 JAHN, W.; URBAN, J. L.; REIN, G. Powerlines and wildfires: overview, perspectives, and climate change: could there be more electricity blackouts in the future? **IEEE Power and Energy Magazine**, IEEE, v. 20, n. 1, p. 16–27, 2022.

2 CHIU, B.; ROY, R.; TRAN, T. Wildfire resiliency: California case for change. **IEEE Power and Energy Magazine**, v. 20, n. 1, p. 28–37, 2022.

3 DALE, L. et al. Assessing the impact of wildfires on the california electricity grid. **California Energy Commission. CCCA4-CEC-2018-002**, v. 1, 2018.

4 National Interagency Coordination Center. **Wildland fire summary and statistics annual report 2021**. [S.l.], 2022. Disponível em: <https://www.texaslawyers.com/coomer/Bastrop%20Complex%20Fire%20-%20Report.pdf>.

5 SERRANO, R. et al. Fighting against wildfires in power systems: Lessons and resilient practices from the chilean and brazilian experiences. **IEEE Power and Energy Magazine**, IEEE, v. 20, n. 1, p. 38–51, 2022.

6 SHORT, K. C. **Spatial wildfire occurrence data for the United States, 1992-2020 [FPA_FOD_20221014]**. [S.l.]: Fort Collins, CO: Forest Service Research Data Archive, 2022.

7 MITCHELL, J. W. Power line failures and catastrophic wildfires under extreme weather conditions. **Engineering Failure Analysis**, Elsevier, v. 35, p. 726–735, 2013.

8 RUSSELL, B. D.; BENNER, C. L.; WISCHKAEMPER, J. A. Distribution feeder caused wildfires: Mechanisms and prevention. In: **2012 65th Annual Conference for Protective Relay Engineers**. [S.l.: s.n.], 2012. p. 43–51.

9 PG&E. **Fire Incident Data 2022**. [S.l.], 2023. Disponível em: <https://www.cpuc.ca.gov/industries-and-topics/wildfires>.

10 SDG&E. **Fire Incident Data 2022**. [S.l.], 2023. Disponível em: <https://www.cpuc.ca.gov/industries-and-topics/wildfires>.

11 SCE. **Fire Incident Data 2022**. [S.l.], 2023. Disponível em: <https://www.cpuc.ca.gov/industries-and-topics/wildfires>.

12 MOREIRA, A. et al. Distribution system operation amidst wildfire-prone climate conditions under decision-dependent line availability uncertainty. **IEEE Transactions on Power Systems**, p. 1–16, 2024.

13 WANG, X.; BOCCHINI, P. Predicting wildfire ignition induced by dynamic conductor swaying under strong winds. **Scientific Reports**, Nature Publishing Group UK London, v. 13, n. 1, p. 3998, 2023.

14 MUHS, J. W. et al. Characterizing probability of wildfire ignition caused by power distribution lines. **IEEE Transactions on Power Delivery**, IEEE, v. 36, n. 6, p. 3681–3688, 2020.

15 VICTORIAN BUSHFIRES ROYAL COMMISSION. **Power line Bushfire Safety Taskforce, Final Report**. [S.l.], 2011. Disponível em: <https://www.energy.vic.gov.au/__data/assets/pdf_file/0035/594098/Powerline-Bushfire-Safety-Taskforce-Report.pdf>.

16 TEAGUE, B.; MCLEOD, R.; PASCOE, S. Final report, 2009 victorian bushfires royal commission. **Parliament of Victoria, Melbourne Victoria, Australia**, v. 1, 2010. Disponível em: <https://bit.ly/2JWEjON>.

17 RIDENOUR, K. et al. **Bastrop complex wildfire case study**. [S.l.], 2011. Disponível em: <https://www.co.bastrop.tx.us/upload/page/0019/docs/Bastrop%20case%20study05212012%20FinalVersion.pdf>.

18 Texas Forest Service. **Investigation Report - Bastrop Complex**. [S.l.], 2012. Disponível em: <https://www.texaslawyers.com/coomer/Bastrop%20Complex%20Fire%20-%20Report.pdf>.

19 STATHI, E.; PAPASPYROPOULOS, K. Corporate social responsibility, sustainability reporting and forest fires: Evidence from the 2018 megafires. In: . [S.l.: s.n.], 2022.

20 MARRIS, E. Hawaii wildfires: did scientists expect maui to burn? **Nature**, ePub, n. ePub, p. ePub–ePub, 2023. ISSN 0028-0836. Disponível em: <http://dx.doi.org/10.1038/d41586-023-02571-z>.

21 Hawaiian Electric. **News Release - Hawaiian Electric provides update on Lahaina fires, response**. 2023. Disponível em: <https://www.hawaiianelectric.com/documents/about_us/news/2023/20230827_lahaina_fires_update.pdf>.

22 MARANGHIDES, A. et al. A case study of the camp fire–fire progression timeline. Alexander Maranghides, Eric Link, William Mell, Steven Hawks, Mike Wilson, 2021.

23 RAMSEY, M.; MURPHY, M.; DIAZ, J. **The Camp Fire Public Report: A Summary of the Camp Fire Investigation**. [S.l.], 2020. Disponível em: <https://htv-prod-media.s3.amazonaws.com/files/pge-the-camp-fire-public-report-1592448040.pdf>.

24 California Department of Forestry and Fire Protection. **CAL FIRE investigators determine cause of the camp fire**. [S.l.], 2022. Disponível em: <https://web.archive.org/web/20220118192820/https://www.fire.ca.gov/media/edwez51p/dixie_fire_release.pdf>.

25 California Department of Forestry and Fire Protection. **Investigation Report - Dixie (Case No. 21CABTU009205-58)**. [S.l.], 2021.

26 KEELEY, J. E.; SYPHARD, A. D. Twenty-first century california, usa, wildfires: fuel-dominated vs. wind-dominated fires. **Fire Ecology**, Springer, v. 15, n. 1, p. 1–15, 2019.

27 California Department of Forestry and Fire Protection. **Top 20 most destructive California wildfires**. Sacramento, CA, 2018. Disponível em: <https://34c031f8-c9fd-4018-8c5a-4159cdff6b0d-cdn-endpoint.azureedge.net/-/media/calfire-website/our-impact/fire-statistics/featured-items/top20_destruction.pdf?rev=ee6ea855632a4b56a46adea1d3c8022f&hash=5B8B3A1A35CBB52CB0ED7A010F0B52E0>.

28 GEOCARIS, M. **Assessing Power System Reliability in a Changing Grid, Environment**. 2022. Disponível em: <https://www.nrel.gov/news/program/2022/assessing-power-system-reliability-in-a-changing-grid-environment.html>.

29 Electrical Power Research Institute (EPRI). **Power System Supply Resilience: The Need for Definitions and Metrics in Decision Making**. [S.l.], 2020. Disponível em: <https://www.epri.com/research/products/000000003002014963>.

30 PANTELI, M.; MANCARELLA, P. The grid: Stronger, bigger, smarter?: Presenting a conceptual framework of power system resilience. **IEEE Power and Energy Magazine**, v. 13, n. 3, p. 58–66, 2015.

31 WANG, Y. et al. Research on resilience of power systems under natural disasters—a review. **IEEE Transactions on Power Systems**, v. 31, n. 2, p. 1604–1613, 2016.

32 HUANG, G. et al. Integration of preventive and emergency responses for power grid resilience enhancement. **IEEE Transactions on Power Systems**, v. 32, n. 6, p. 4451–4463, 2017.

33 ARAB, A. et al. Three lines of defense for wildfire risk management in electric power grids: A review. **IEEE Access**, v. 9, p. 61577–61593, 2021.

34 SHARAFI, D. et al. Wildfires down under: Impacts and mitigation strategies for australian electricity grids. **IEEE Power and Energy Magazine**, v. 20, n. 1, p. 52–63, 2022.

35 UDREN, E. A. et al. Managing wildfire risks: Protection system technical developments combined with operational advances to improve public safety. **IEEE Power and Energy Magazine**, v. 20, n. 1, p. 64–77, 2022.

36 PG&E. **2023 to 2025 Electrical Corporation Wildfire Mitigation Plans**. [S.l.], 2023. Disponível em: <https://www.pge.com/pge_global/common/pdfs/safety/emergency-preparedness/natural-disaster/wildfires/wildfire-mitigation-plan/pge-wmp-r3-redline-092723.pdf>.

37 HUANG, C. et al. A review of public safety power shutoffs (psps) for wildfire mitigation: Policies, practices, models and data sources. **IEEE Transactions on Energy Markets, Policy and Regulation**, v. 1, n. 3, p. 187–197, 2023.

38 MORENO, R. et al. Microgrids against wildfires: Distributed energy resources enhance system resilience. **IEEE Power and Energy Magazine**, v. 20, n. 1, p. 78–89, Jan.-Feb. 2022.

39 ROMERO, N. R. et al. Transmission and generation expansion to mitigate seismic risk. **IEEE Transactions on Power Systems**, v. 28, n. 4, p. 3692–3701, 2013.

40 LAGOS, T. et al. Identifying optimal portfolios of resilient network investments against natural hazards, with applications to earthquakes. **IEEE Transactions on Power Systems**, v. 35, n. 2, p. 1411–1421, 2020.

41 NAZEMI, M. et al. Energy storage planning for enhanced resilience of power distribution networks against earthquakes. **IEEE Transactions on Sustainable Energy**, v. 11, n. 2, p. 795–806, 2020.

42 LIN, Y.; BIE, Z. Tri-level optimal hardening plan for a resilient distribution system considering reconfiguration and dg islanding. **Applied Energy**, v. 210, p. 1266–1279, 2018. ISSN 0306-2619. Disponível em: <https://www.sciencedirect.com/science/article/pii/S0306261917308048>.

43 BERTOLETTI, A. Z.; PRADO, J. C. do. Transmission system expansion planning under wildfire risk. **2022 North American Power Symposium (NAPS)**, p. 1–6, 2022. Disponível em: <https://api.semanticscholar.org/CorpusID:255993699>.

44 BAYANI, R. et al. Quantifying the risk of wildfire ignition by power lines under extreme weather conditions. **IEEE Systems Journal**, v. 17, n. 1, p. 1024–1034, 2023.

45 DIAN, S. et al. Integrating wildfires propagation prediction into early warning of electrical transmission line outages. **IEEE Access**, v. 7, p. 27586–27603, 2019.

46 ABDELMALAK, M.; BENIDRIS, M. A markov decision process to enhance power system operation resilience during wildfires. In: **2021 IEEE Industry Applications Society Annual Meeting (IAS)**. [S.l.: s.n.], 2021. p. 1–6.

47 TRAKAS, D. N.; HATZIARGYRIOU, N. D. Optimal distribution system operation for enhancing resilience against wildfires. **IEEE Transactions on Power Systems**, v. 33, n. 2, p. 2260–2271, 2018.

48 NAZEMI, M. et al. Resilient operation of electric power distribution grids under progressive wildfires. **IEEE Transactions on Industry Applications**, v. 58, n. 2, p. 1632–1643, 2022.

49 IZADI, M. et al. Resiliency-oriented operation of distribution networks under unexpected wildfires using multi-horizon information-gap decision theory. **Applied Energy**, v. 334, p. 120536, 2023. ISSN 0306-2619. Disponível em: <https://www.sciencedirect.com/science/article/pii/S0306261922017937>.

50 CHEN, C. et al. Resilient distribution system by microgrids formation after natural disasters. **IEEE Transactions on Smart Grid**, v. 7, n. 2, p. 958–966, 2016.

51 LEI, S. et al. Radiality constraints for resilient reconfiguration of distribution systems: Formulation and application to microgrid formation. **IEEE Transactions on Smart Grid**, v. 11, n. 5, p. 3944–3956, 2020.

52 YUAN, Y. et al. Resilience-oriented transmission expansion planning with optimal transmission switching under typhoon weather. **CSEE Journal of Power and Energy Systems**, p. 1–10, 2022.

53 NAGARAJAN, H. et al. Optimal resilient transmission grid design. In: **2016 Power Systems Computation Conference (PSCC)**. [S.l.: s.n.], 2016. p. 1–7.

54 BYEON, G. et al. Communication-constrained expansion planning for resilient distribution systems. **INFORMS Journal on Computing**, v. 32, n. 4, p. 968–985, 2020. Disponível em: <https://doi.org/10.1287/ijoc.2019.0899>.

55 BAYANI, R.; MANSHADI, S. D. Resilient expansion planning of electricity grid under prolonged wildfire risk. **IEEE Transactions on Smart Grid**, v. 14, n. 5, p. 3719–3731, 2023.

56 KAVOUSI-FARD, A.; WANG, M.; SU, W. Stochastic resilient post-hurricane power system recovery based on mobile emergency resources and reconfigurable networked microgrids. **IEEE Access**, v. 6, p. 72311–72326, 2018.

57 BIE, Z. et al. Battling the extreme: A study on the power system resilience. **Proceedings of the IEEE**, v. 105, n. 7, p. 1253–1266, 2017.

58 LUO, F.; MEHROTRA, S. Distributionally robust optimization with decision dependent ambiguity sets. **Optimization Letters**, Springer, v. 14, p. 2565–2594, 2020.

59 RAHIMIAN, H.; MEHROTRA, S. Frameworks and Results in Distributionally Robust Optimization. **Open Journal of Mathematical Optimization**, Université de Montpellier, v. 3, 2022. Disponível em: <https://ojmo.centre-mersenne.org/articles/10.5802/ojmo.15/>.

60 MA, S. et al. Resilience enhancement of distribution grids against extreme weather events. **IEEE Transactions on Power Systems**, v. 33, n. 5, p. 4842–4853, 2018.

61 YIN, W. et al. A decision-dependent stochastic approach for joint operation and maintenance of overhead transmission lines after sandstorms. **IEEE Systems Journal**, v. 17, n. 1, p. 1489–1500, 2023.

62 ZHANG, W. et al. Transmission defense hardening against typhoon disasters under decision-dependent uncertainty. **IEEE Transactions on Power Systems**, v. 38, n. 3, p. 2653–2665, 2023.

63 ALVARADO, D. et al. Co-optimizing substation hardening and transmission expansion against earthquakes: A decision-dependent probability approach. **IEEE Transactions on Power Systems**, v. 38, n. 3, p. 2058–2070, 2023.

64 SHI, W.; LIANG, H.; BITTNER, M. Stochastic planning for power distribution system resilience enhancement against earthquakes considering mobile energy resources. **IEEE Transactions on Sustainable Energy**, p. 1–14, 2023.

65 MASHAYEKH, S. et al. Security-Constrained Design of Isolated Multi-Energy Microgrids. **IEEE Transactions on Power Systems**, v. 33, n. 3, p. 2452–2462, 2018.

66 TARJAN, R. Depth-first search and linear graph algorithms. **SIAM Journal on Computing**, v. 1, n. 2, p. 146–160, 1972. Disponível em: <https://doi.org/10.1137/0201010>.

67 MOREIRA, A.; FANZERES, B.; STRBAC, G. Energy and reserve scheduling under ambiguity on renewable probability distribution. **Electric Power Systems Research**, v. 160, p. 205–218, 2018. ISSN 0378-7796. Disponível em: <https://www.sciencedirect.com/science/article/pii/S0378779618300324>.

68 BENDERS, J. F. Partitioning procedures for solving mixed-variables programming problems. **Numerische Mathematik**, v. 4, p. 238–252, 1962.

69 BERTSIMAS, D.; TSITSIKLIS, J. N. **Introduction to linear optimization**. [S.l.]: Athena scientific Belmont, MA, 1997. v. 6.

70 PEREIRA, M. et al. Strategic bidding under uncertainty: a binary expansion approach. **IEEE Trans. Power Syst.**, v. 20, n. 1, p. 180–188, Feb. 2005.

71 MOONEY, C. Z. **Monte Carlo simulation**. [S.l.]: Sage, 1997.

72 PIANCÓ, F.; FANZERES, B.; MOREIRA, A. **Case studies for Distribution System Operation Amidst Wildfire-Prone Climate Conditions Under Decision-Dependent Line Availability Uncertainty**. IEEE Dataport, 2023. Disponível em: <https://dx.doi.org/10.21227/96yx-1s93>.

73 DELGADO, G. M. noz; CONTRERAS, J.; ARROYO, J. M. Multistage generation and network expansion planning in distribution systems considering uncertainty and reliability. **IEEE Transactions on Power Systems**, v. 31, n. 5, p. 3715–3728, 2016.

A
Master problem complete formulation

$$\underset{\substack{p_{b,0,r},q_{b,0,r},v^{\dagger}_{b,0,r},f^{p}_{l,0,r},f^{q}_{l,0,r},\\ \Delta D^{p+}_{b,0,r},\Delta D^{p-}_{b,0,r},\Delta D^{q+}_{b,0,r},\Delta D^{q-}_{b,0,r}\\ z_{l,r},y^{sw}_{l,r},y^{sw,in}_{l},y^{in}_{l},y^{ha}_{l,h}\\ \psi_{l,r},\varphi_{r},f^{p+}_{l,0,r},f^{p-}_{l,0,r},\xi_{l,0,r},\\ \delta_{l,0,e,r},\rho_{l,0,r},\rho^{ha}_{l,0,r,h},\chi_{l,0,r}}}{\text{Minimize}}$$

$$\sum_{r\in\mathcal{R}}\Bigg\{\Bigg(\sum_{b\in\mathcal{N}}\Big(C^{p+}\Delta D^{p+}_{b,0,r}+C^{p-}\Delta D^{p-}_{b,0,r}+C^{q+}\Delta D^{q+}_{b,0,r}+C^{q-}\Delta D^{q-}_{b,0,r}\Big)+\sum_{l\in\mathcal{L}}\Big(\gamma_{l,0,r}\psi_{l,r}+\beta_{l,0,r}\chi_{l,0,r}\Big)-\sum_{l\in\mathcal{L}^{ha}}\Big(\beta_{l,0,r}\sum_{h\in\mathcal{H}_l}w^{ha}_{l,h}\rho^{ha}_{l,0,r,h}\Big)+\varphi_r\Bigg)w^{1}_{r}+\Bigg(\sum_{l\in\mathcal{L}^{sw}}C^{sw}_{l}y^{sw}_{l,r}\Bigg)w^{2}_{r}\Bigg\}+\sum_{l\in\mathcal{L}^{sw,c}}C^{sw,in}_{l}y^{sw,in}_{l}+\sum_{l\in\mathcal{L}^{c}}C^{in}_{l}y^{in}_{l}+\sum_{l\in\mathcal{L}^{ha}}\sum_{h\in\mathcal{H}_l}C^{ha}_{l,h}\;y^{ha}_{l,h} \tag{A-1}$$

subject to:

$$p_{b,0,r}+\sum_{l\in\mathcal{L}|to(l)=b}f^{p}_{l,0,r}-\sum_{l\in\mathcal{L}|fr(l)=b}f^{p}_{l,0,r}-D^{p}_{b,0,r}-\Delta D^{p+}_{b,0,r}+\Delta D^{p-}_{b,0,r}=0;\quad\forall b\in\mathcal{N}^{sub},r\in\mathcal{R} \tag{A-2}$$

$$q_{b,0,r}+\sum_{l\in\mathcal{L}|to(l)=b}f^{q}_{l,0,r}-\sum_{l\in\mathcal{L}|fr(l)=b}f^{q}_{l,0,r}-\tan(\arccos(PF_b))D^{p}_{b,0,r}-\Delta D^{q+}_{b,0,r}+\Delta D^{q-}_{b,0,r}=0;\forall b\in\mathcal{N}^{sub},r\in\mathcal{R} \tag{A-3}$$

$$\sum_{l\in\mathcal{L}|to(l)=b}f^{p}_{l,0,r}-\sum_{l\in\mathcal{L}|fr(l)=b}f^{p}_{l,0,r}-D^{p}_{b,0,r}-\Delta D^{p+}_{b,0,r}+\Delta D^{p-}_{b,0,r}=0;\quad\forall b\in\mathcal{N}\setminus\mathcal{N}^{sub},r\in\mathcal{R} \tag{A-4}$$

$$\sum_{l\in\mathcal{L}|to(l)=b}f^{q}_{l,0,r}-\sum_{l\in\mathcal{L}|fr(l)=b}f^{q}_{l,0,r}-\tan(\arccos(PF_b))D^{p}_{b,0,r}-\Delta D^{q+}_{b,0,r}+\Delta D^{q-}_{b,0,r}=0;\forall b\in\mathcal{N}\setminus\mathcal{N}^{sub},r\in\mathcal{R} \tag{A-5}$$

$$v^{\dagger}_{to(l),0,r}-v^{\dagger}_{fr(l),0,r}+2(R_l f^{p}_{l,0,r}+X_l f^{q}_{l,0,r})\le(1-z_{l,r})M;\forall l\in\mathcal{L},r\in\mathcal{R} \tag{A-6}$$

$$v^{\dagger}_{fr(l),0,r}-v^{\dagger}_{to(l),0,r}-2(R_l f^{p}_{l,0,r}+X_l f^{q}_{l,0,r})\le(1-z_{l,r})M;\forall l\in\mathcal{L},r\in\mathcal{R} \tag{A-7}$$

$$f^{q}_{l,0,r}-\cot\Big(\Big(\frac{1}{2}-e\Big)\frac{\pi}{4}\Big)\Big(f^{p}_{l,0,r}-\cos\Big(e\frac{\pi}{4}\Big)\overline{F}_l\Big)-\sin\Big(e\frac{\pi}{4}\Big)\overline{F}_l\le 0;\quad\forall l\in\mathcal{L},e\in\{1,\dots,4\},r\in\mathcal{R} \tag{A-8}$$

$$-f^{q}_{l,0,r}-\cot\Big(\Big(\frac{1}{2}-e\Big)\frac{\pi}{4}\Big)\Big(f^{p}_{l,0,r}-\cos\Big(e\frac{\pi}{4}\Big)\overline{F}_l\Big)-\sin\Big(e\frac{\pi}{4}\Big)\overline{F}_l\le 0;\quad\forall l\in\mathcal{L},e\in\{1,\dots,4\},r\in\mathcal{R} \tag{A-9}$$

$$0 \leq p_{b,0,r} \leq \overline{P}_b; \forall b \in \mathcal{N}^{sub}, r \in \mathcal{R} \tag{A-10}$$

$$\underline{Q}_b \leq q_{b,0,r} \leq \overline{Q}_b; \forall b \in \mathcal{N}^{sub}, r \in \mathcal{R} \tag{A-11}$$

$$\underline{V}_b^2 \leq v_{b,0,r}^{\dagger} \leq \overline{V}_b^2; \forall b \in \mathcal{N} \setminus \mathcal{N}^{sub}, r \in \mathcal{R} \tag{A-12}$$

$$v_{b,0,r}^{\dagger} = V^{ref^2}; \forall b \in \mathcal{N}^{sub}, r \in \mathcal{R} \tag{A-13}$$

$$-z_{l,r}\overline{F}_l \leq f_{l,0,r}^{p} \leq z_{l,r}\overline{F}_l; \forall l \in \mathcal{L}, r \in \mathcal{R} \tag{A-14}$$

$$-z_{l,r}\overline{F}_l \leq f_{l,0,r}^{q} \leq z_{l,r}\overline{F}_l; \forall l \in \mathcal{L}, r \in \mathcal{R} \tag{A-15}$$

$$0 \leq \Delta D_{b,0,r}^{p+} \leq D_{b,0,r}^{p}; \forall b \in \mathcal{N}, r \in \mathcal{R} \tag{A-16}$$

$$0 \leq \Delta D_{b,0,r}^{p-} \leq D_{b,0,r}^{p}; \forall b \in \mathcal{N}, r \in \mathcal{R} \tag{A-17}$$

$$0 \leq \Delta D_{b,0,r}^{q+} \leq \tan(\arccos(PF_b))D_{b,0,r}^{p}; \forall b \in \mathcal{N}, r \in \mathcal{R} \tag{A-18}$$

$$0 \leq \Delta D_{b,0,r}^{q-} \leq \tan(\arccos(PF_b))D_{b,0,r}^{p}; \forall b \in \mathcal{N}, r \in \mathcal{R} \tag{A-19}$$

$$y_{l,r}^{sw} = 0; \forall l \in \mathcal{L} \setminus \mathcal{L}^{sw}, r \in \mathcal{R} \tag{A-20}$$

$$y_{l}^{sw,in} = 0; \forall l \in (\mathcal{L}^{sw,e}) \cup (\mathcal{L} \setminus \mathcal{L}^{sw}) \tag{A-21}$$

$$y_{l}^{in} = 0; \forall l \in \mathcal{L}^{e} \tag{A-22}$$

$$z_{l,r} = 1; \forall l \in \mathcal{L}^{e} \setminus \mathcal{L}^{sw}, r \in \mathcal{R} \tag{A-23}$$

$$y_{l,r}^{sw} \leq y_{l}^{sw,in}; \forall l \in \mathcal{L}^{sw,c}, r \in \mathcal{R} \tag{A-24}$$

$$y_{l}^{sw,in} \leq y_{l}^{in}; \forall l \in (\mathcal{L}^{c}) \cap (\mathcal{L}^{sw,c}) \tag{A-25}$$

$$y_{l,r}^{sw} \geq +z_{l,r} - z_{l,r}^{init}; \forall l \in \mathcal{L}^{e}, r \in \mathcal{R} \tag{A-26}$$

$$y_{l,r}^{sw} \geq -z_{l,r} + z_{l,r}^{init}; \forall l \in \mathcal{L}^{e}, r \in \mathcal{R} \tag{A-27}$$

$$y_{l}^{in} - y_{l}^{sw,in} \leq z_{l,r}; \forall l \in \mathcal{L}^{c} \setminus \mathcal{L}^{sw,e}, r \in \mathcal{R} \tag{A-28}$$

$$z_{l,r} \leq y_{l}^{in}; \forall l \in \mathcal{L}^{c}, r \in \mathcal{R} \tag{A-29}$$

$$\sum_{l \in \mathcal{L}_k^{forb}} z_{l,r} \leq |\mathcal{L}_k^{forb}| - 1; \forall k \in \mathcal{K}^{forb}, r \in \mathcal{R} \tag{A-30}$$

$$z_{l,r}, y_{l,r}^{sw} \in \{0,1\}; \forall l \in \mathcal{L}, r \in \mathcal{R} \tag{A-31}$$

$$y_{l}^{sw,in}, y_{l}^{in} \in \{0,1\}; \forall l \in \mathcal{L} \tag{A-32}$$

$$\sum_{h \in \mathcal{H}_l} y_{l,h}^{ha} \leq 1; \forall l \in \mathcal{L}^{ha} \tag{A-33}$$

$$y_{l,h}^{ha} \in \{0,1\}; \forall h \in \mathcal{H}_l, l \in \mathcal{L}^{ha} \tag{A-34}$$

$$\psi_{l,r} \geq 0; \forall l = \{1, \ldots, 2|\mathcal{L}|\}, r \in \mathcal{R} \tag{A-35}$$

$$\varphi_r \in \mathbb{R}; \forall r \in \mathcal{R} \tag{A-36}$$

$$f_{l,0,r}^{p} = f_{l,0,r}^{p+} - f_{l,0,r}^{p-}; \forall l \in \mathcal{L}, r \in \mathcal{R} \tag{A-37}$$

$$0 \leq f_{l,0,r}^{p+} \leq \overline{F}_l \xi_{l,0,r}; \forall l \in \mathcal{L}, r \in \mathcal{R} \tag{A-38}$$

$$0 \leq f_{l,0,r}^{p-} \leq \overline{F}_l (1 - \xi_{l,0,r}); \forall l \in \mathcal{L}, r \in \mathcal{R} \tag{A-39}$$

$$f_{l,0,r}^{p+} + f_{l,0,r}^{p-} = s \sum_{e=1}^{E_l} \left(2^{e-1} \delta_{l,0,e,r}\right); \forall l \in \mathcal{L}, r \in \mathcal{R} \tag{A-40}$$

$$\chi_{l,0,r} = s\sum_{e=1}^{E_l}\left(2^{e-1}\rho_{l,0,e,r}\right); \forall l \in \mathcal{L}, r \in \mathcal{R} \tag{A-41}$$

$$-(1-\delta_{l,0,e,r})M \leq \psi_{l,r} - \rho_{l,0,e,r} \leq (1-\delta_{l,0,e,r})M; \quad \forall l \in \mathcal{L}, e \in \{1,\cdots,E_l\}, r \in \mathcal{R} \tag{A-42}$$

$$-\delta_{l,0,e,r}M \leq \rho_{l,0,e,r} \leq \delta_{l,0,e,r}M; \forall l \in \mathcal{L}, e \in \{1,\cdots,E_l\}, r \in \mathcal{R} \tag{A-43}$$

$$-(1-y_{l,h}^{ha})M \leq \chi_{l,0,r} - \rho_{l,0,r,h}^{ha} \leq (1-y_{l,h}^{ha})M; \quad \forall l \in \mathcal{L}^{ha}, r \in \mathcal{R}, h \in \mathcal{H}_l \tag{A-44}$$

$$-y_{l,h}^{ha}M \leq \rho_{l,0,r,h}^{ha} \leq y_{l,h}^{ha}M; \forall l \in \mathcal{L}^{ha}, r \in \mathcal{R}, h \in \mathcal{H}_l \tag{A-45}$$

$$\xi_{l,0,r} \in \{0,1\}; \forall l \in \mathcal{L}, r \in \mathcal{R} \tag{A-46}$$

$$\delta_{l,0,e,r} \in \{0,1\}; \forall l \in \mathcal{L}, e \in \{1,\cdots,E_l\}, r \in \mathcal{R} \tag{A-47}$$

$$\chi_{l,0,r} \in \mathbb{R}; \forall l \in \mathcal{L}, r \in \mathcal{R} \tag{A-48}$$

$$\rho_{l,0,e,r} \in \mathbb{R}; \forall l \in \mathcal{L}, e \in \{1,\cdots,E_l\}, r \in \mathcal{R} \tag{A-49}$$

$$\rho_{l,0,r,h}^{ha} \in \mathbb{R}; \forall l \in \mathcal{L}^{ha}, r \in \mathcal{R}, h \in \mathcal{H}_l \tag{A-50}$$

$$\varphi_r \geq \text{Cutting Plane}_r^{(j)}; \forall j \in \mathcal{J}, \forall r \in \mathcal{R} \tag{A-51}$$

$$\sum_{l\in\mathcal{L}}\left(\gamma_{l,0,r}\psi_{l,r} + \beta_{l,0,r}\chi_{l,0,r}\right) - \sum_{l\in\mathcal{L}^{ha}}\left(\beta_{l,0,r}\sum_{h\in\mathcal{H}_l} w_{l,h}^{ha}\rho_{l,0,r,h}^{ha}\right) + \varphi_r \geq 0; \quad \forall r \in \mathcal{R} \tag{A-52}$$

B
Subproblem complete formulation

$$
\begin{aligned}
&\underset{\substack{\eta^1_{b,t,r},\eta^2_{b,t,r},\eta^3_{b,t,r},\eta^4_{b,t,r},\eta^5_{l,t,r},\eta^6_{l,t,r},\eta^7_{l,e,t,r},\\ \eta^8_{l,e,t,r},\eta^9_{b,t,r},\eta^{10}_{b,t,r},\eta^{11}_{b,t,r},\eta^{12}_{b,t,r},\eta^{13}_{b,t,r},\eta^{14}_{b,t,r},\\ \eta^{15}_{b,t,r},\eta^{16}_{l,t,r},\eta^{17}_{l,t,r},\eta^{18}_{l,t,r},\eta^{19}_{l,t,r},\eta^{20}_{b,t,r},\eta^{21}_{b,t,r},\\ \eta^{22}_{b,t,r},\eta^{23}_{b,t,r},\eta^{24}_{b,t,r},\eta^{25}_{b,t,r},\eta^{26}_{b,t,r},\eta^{27}_{b,t,r},a\\ \lambda^5_{l,t,r},\lambda^6_{l,t,r},\lambda^{16}_{l,t,r},\lambda^{17}_{l,t,r},\lambda^{18}_{l,t,r},\lambda^{19}_{l,t,r}}}{\text{Maximize}}\\
&\sum_{t\in\mathcal{T}}\sum_{b\in\mathcal{N}^{sub}}\Big(-D^p_{b,t,r}\eta^1_{b,t,r}-\tan\left(\arccos\left(PF_b\right)\right)D^p_{b,t,r}\eta^2_{b,t,r}\\
&\qquad-\overline{P}_b\eta^{10}_{b,t,r}+\underline{Q}_b\eta^{11}_{b,t,r}-\overline{Q}_b\eta^{12}_{b,t,r}-{V^{ref}}^2\eta^{15}_{b,t,r}\\
&\qquad-D^p_{b,t,r}\eta^{21}_{b,t,r}-D^p_{b,t,r}\eta^{23}_{b,t,r}-\tan(\arccos(PF_b))D^p_{b,t,r}\eta^{25}_{b,t,r}\\
&\qquad-\tan(\arccos(PF_b))D^p_{b,t,r}\eta^{27}_{b,t,r}\Big)\\
&+\sum_{t\in\mathcal{T}}\sum_{b\in\mathcal{N}\setminus\mathcal{N}^{sub}}\Big(-D^p_{b,t,r}\eta^3_{b,t,r}-\tan\left(\arccos\left(PF_b\right)\right)D^p_{b,t,r}\eta^4_{b,t,r}\\
&\qquad+\underline{V}^2_b\eta^{13}_{b,t,r}-\overline{V}^2_b\eta^{14}_{b,t,r}-D^p_{b,t,r}\eta^{21}_{b,t,r}-D^p_{b,t,r}\eta^{23}_{b,t,r}\\
&\qquad-\tan(\arccos(PF_b))D^p_{b,t,r}\eta^{25}_{b,t,r}\\
&\qquad-\tan(\arccos(PF_b))D^p_{b,t,r}\eta^{27}_{b,t,r}\Big)\\
&+\sum_{t\in\mathcal{T}}\sum_{l\in\mathcal{L}}\Bigg(-((1-a_{l,r})M+(1-z_{l,r})M)\eta^5_{l,t,r}\\
&\qquad-((1-a_{l,r})M+(1-z_{l,r})M)\eta^6_{l,t,r}\\
&\qquad+\sum_{e\in\{1,2,3,4\}}\Bigg[\overline{F}_l\Big(\cot\Big((1/2-e)(\pi/4)\Big)\cos\Big(e(\pi/4)\Big)\\
&\qquad\qquad-\sin\Big(e(\pi/4)\Big)\Big)(\eta^7_{l,e,t,r}+\eta^8_{l,e,t,r})\Bigg]\\
&\qquad-z_{l,r}a_{l,r}\overline{F}_l(\eta^{16}_{l,t,r}+\eta^{17}_{l,t,r}+\eta^{18}_{l,t,r}+\eta^{19}_{l,t,r})\Bigg)\\
&-\sum_{l\in\mathcal{L}}\Big((\psi_{l,r}-\psi_{l+|\mathcal{L}|,r})(1-a_{l,r})\Big) \qquad \text{(B-1)}
\end{aligned}
$$

subject to:

$$\sum_{l\in\mathcal{L}}a_{l,r}\geq|\mathcal{L}|-K \qquad \text{(B-2)}$$

$$a_{l,r}\in\{0,1\};\forall l\in\mathcal{L} \qquad \text{(B-3)}$$

$$C^{tr}_b/|\mathcal{T}|+\eta^1_{b,t,r}-\eta^9_{b,t,r}+\eta^{10}_{b,t,r}=0:(p^c_{b,t,r});\forall b\in\mathcal{N}^{sub},t\in\mathcal{T} \qquad \text{(B-4)}$$

$$\eta^{2}_{b,t,r} - \eta^{11}_{b,t,r} + \eta^{12}_{b,t,r} = 0 : (q^{c}_{b,t,r}); \forall b \in \mathcal{N}^{sub}, t \in \mathcal{T} \tag{B-5}$$

$$\sum_{l \in \mathcal{L} | b = fr(l)} \Big(\eta^{6}_{l,t,r} - \eta^{5}_{l,t,r} \Big) + \sum_{l \in \mathcal{L} | b = to(l)} \Big(\eta^{5}_{l,t,r} - \eta^{6}_{l,t,r} \Big) - \eta^{13}_{b,t,r} + \eta^{14}_{b,t,r} = 0 : (v^{\dagger^{c}}_{b,t,r}); \forall b \in \mathcal{N} \setminus \mathcal{N}^{sub}, t \in \mathcal{T} \tag{B-6}$$

$$\sum_{l \in \mathcal{L} | b = fr(l)} \Big(\eta^{6}_{l,t,r} - \eta^{5}_{l,t,r} \Big) + \sum_{l \in \mathcal{L} | b = to(l)} \Big(\eta^{5}_{l,t,r} - \eta^{6}_{l,t,r} \Big) + \eta^{15}_{b,t,r} = 0 : (v^{\dagger^{c}}_{b,t,r}); \forall b \in \mathcal{N}^{sub}, t \in \mathcal{T} \tag{B-7}$$

$$\begin{aligned} &\sum_{b \in \mathcal{N}^{sub} | b = to(l)} \eta^{1}_{b,t,r} - \sum_{b \in \mathcal{N}^{sub} | b = fr(l)} \eta^{1}_{b,t,r} + \sum_{b \in \mathcal{N} \setminus \mathcal{N}^{sub} | b = to(l)} \eta^{3}_{b,t,r} \\ &- \sum_{b \in \mathcal{N} \setminus \mathcal{N}^{sub} | b = fr(l)} \eta^{3}_{b,t,r} + 2R_l \eta^{5}_{l,t,r} - 2R_l \eta^{6}_{l,t,r} \\ &+ \sum_{e \in \{1,2,3,4\}} \Big[- \cot\Big((1/2 - e)(\pi/4) \Big) \Big(\eta^{7}_{l,e,t,r} \Big) \\ &\qquad - \cot\Big((1/2 - e)(\pi/4) \Big) \Big(\eta^{8}_{l,e,t,r} \Big) \Big] - \eta^{16}_{l,t,r} + \eta^{17}_{l,t,r} = 0 : (f^{p^{c}}_{l,t,r}); \forall l \in \mathcal{L}, t \in \mathcal{T} \end{aligned} \tag{B-8}$$

$$\begin{aligned} &\sum_{b \in \mathcal{N}^{sub} | b = to(l)} \eta^{2}_{b,t,r} - \sum_{b \in \mathcal{N}^{sub} | b = fr(l)} \eta^{2}_{b,t,r} + \sum_{b \in \mathcal{N} \setminus \mathcal{N}^{sub} | b = to(l)} \eta^{4}_{b,t,r} \\ &- \sum_{b \in \mathcal{N} \setminus \mathcal{N}^{sub} | b = fr(l)} \eta^{4}_{b,t,r} + 2X_l \eta^{5}_{l,t,r} - 2X_l \eta^{6}_{l,t,r} \\ &+ \sum_{e \in \{1,2,3,4\}} \Big(\eta^{7}_{l,e,t,r} - \eta^{8}_{l,e,t,r} \Big) - \eta^{18}_{l,t,r} + \eta^{19}_{l,t,r} = 0 : (f^{q^{c}}_{l,t,r}); \forall l \in \mathcal{L}, t \in \mathcal{T} \end{aligned} \tag{B-9}$$

$$C^{p+}/|\mathcal{T}| - \eta^{1}_{b,t,r} - \eta^{20}_{b,t,r} + \eta^{21}_{b,t,r} = 0 : (\Delta D^{p+^{c}}_{b,t,r}); \forall b \in \mathcal{N}^{sub}, t \in \mathcal{T} \tag{B-10}$$

$$C^{p+}/|\mathcal{T}| - \eta^{3}_{b,t,r} - \eta^{20}_{b,t,r} + \eta^{21}_{b,t,r} = 0 : (\Delta D^{p+^{c}}_{b,t,r}); \forall b \in \mathcal{N} \setminus \mathcal{N}^{sub}, t \in \mathcal{T} \tag{B-11}$$

$$C^{p-}/|\mathcal{T}| + \eta^{1}_{b,t,r} - \eta^{22}_{b,t,r} + \eta^{23}_{b,t,r} = 0 : (\Delta D^{p-^{c}}_{b,t,r}); \forall b \in \mathcal{N}^{sub}, t \in \mathcal{T} \tag{B-12}$$

$$C^{p-}/|\mathcal{T}| + \eta^{3}_{b,t,r} - \eta^{22}_{b,t,r} + \eta^{23}_{b,t,r} = 0 : (\Delta D^{p-^{c}}_{b,t,r}); \forall b \in \mathcal{N} \setminus \mathcal{N}^{sub}, t \in \mathcal{T} \tag{B-13}$$

$$C^{q+}/|\mathcal{T}| - \eta^{2}_{b,t,r} - \eta^{24}_{b,t,r} + \eta^{25}_{b,t,r} = 0 : (\Delta D^{q+^{c}}_{b,t,r}); \forall b \in \mathcal{N}^{sub}, t \in \mathcal{T} \tag{B-14}$$

$$C^{q+}/|\mathcal{T}| - \eta^{4}_{b,t,r} - \eta^{24}_{b,t,r} + \eta^{25}_{b,t,r} = 0 : (\Delta D^{q+^{c}}_{b,t,r}); \forall b \in \mathcal{N} \setminus \mathcal{N}^{sub}, t \in \mathcal{T} \tag{B-15}$$

$$C^{q-}/|\mathcal{T}| + \eta^{2}_{b,t,r} - \eta^{26}_{b,t,r} + \eta^{27}_{b,t,r} = 0 : (\Delta D^{q-^{c}}_{b,t,r}); \forall b \in \mathcal{N}^{sub}, t \in \mathcal{T} \tag{B-16}$$

$$C^{q-}/|\mathcal{T}| + \eta^{4}_{b,t,r} - \eta^{26}_{b,t,r} + \eta^{27}_{b,t,r} = 0 : (\Delta D^{q-^{c}}_{b,t,r}); \forall b \in \mathcal{N} \setminus \mathcal{N}^{sub}, t \in \mathcal{T} \tag{B-17}$$

$$\eta^{1}_{b,t,r}, \eta^{2}_{b,t,r}, \eta^{15}_{b,t,r} \in \mathbb{R}; \forall b \in \mathcal{N}^{sub}, t \in \mathcal{T} \tag{B-18}$$

$$\eta^{3}_{b,t,r}, \eta^{4}_{b,t,r} \in \mathbb{R}; \forall b \in \mathcal{N} \setminus \mathcal{N}^{sub}, t \in \mathcal{T} \tag{B-19}$$

$$\eta^{20}_{b,t,r}, \eta^{21}_{b,t,r}, \eta^{22}_{b,t,r}, \eta^{23}_{b,t,r}, \eta^{24}_{b,t,r}, \eta^{25}_{b,t,r}, \eta^{26}_{b,t,r}, \eta^{27}_{b,t,r} \geq 0; \forall b \in \mathcal{N}, t \in \mathcal{T} \tag{B-20}$$

$$\eta^{13}_{b,t,r}, \eta^{14}_{b,t,r} \geq 0; \forall b \in \mathcal{N} \setminus \mathcal{N}^{sub}, t \in \mathcal{T} \tag{B-21}$$

$$\eta^{9}_{b,t,r}, \eta^{10}_{b,t,r}, \eta^{11}_{b,t,r}, \eta^{12}_{b,t,r} \geq 0; \forall b \in \mathcal{N}^{sub}, t \in \mathcal{T} \tag{B-22}$$

$$\eta^{5}_{l,t,r}, \eta^{6}_{l,t,r}, \eta^{16}_{l,t,r}, \eta^{17}_{l,t,r}, \eta^{18}_{l,t,r}, \eta^{19}_{l,t,r} \geq 0; \forall l \in \mathcal{L}, t \in \mathcal{T} \tag{B-23}$$

$$\eta^{7}_{l,e,t,r}, \eta^{8}_{l,e,t,r} \geq 0; \forall l \in \mathcal{L}, \forall e \in \{1,2,3,4\}, t \in \mathcal{T} \tag{B-24}$$

$$-(1-a_{l,r})M \leq \eta^{5}_{l,t,r} - \lambda^{5}_{l,t,r} \leq (1-a_{l,r})M; \forall l \in \mathcal{L}, t \in \mathcal{T} \quad \text{(B-25)}$$

$$-a_{l,r}M \leq \lambda^{5}_{l,t,r} \leq a_{l,r}M; \forall l \in \mathcal{L}, t \in \mathcal{T} \quad \text{(B-26)}$$

$$-(1-a_{l,r})M \leq \eta^{6}_{l,t,r} - \lambda^{6}_{l,t,r} \leq (1-a_{l,r})M; \forall l \in \mathcal{L}, t \in \mathcal{T} \quad \text{(B-27)}$$

$$-a_{l,r}M \leq \lambda^{6}_{l,t,r} \leq a_{l,r}M; \forall l \in \mathcal{L}, t \in \mathcal{T} \quad \text{(B-28)}$$

$$-(1-a_{l,r})M \leq \eta^{16}_{l,t,r} - \lambda^{16}_{l,t,r} \leq (1-a_{l,r})M; \forall l \in \mathcal{L}, t \in \mathcal{T} \quad \text{(B-29)}$$

$$-a_{l,r}M \leq \lambda^{16}_{l,t,r} \leq a_{l,r}M; \forall l \in \mathcal{L}, t \in \mathcal{T} \quad \text{(B-30)}$$

$$-(1-a_{l,r})M \leq \eta^{17}_{l,t,r} - \lambda^{17}_{l,t,r} \leq (1-a_{l,r})M; \forall l \in \mathcal{L}, t \in \mathcal{T} \quad \text{(B-31)}$$

$$-a_{l,r}M \leq \lambda^{17}_{l,t,r} \leq a_{l,r}M; \forall l \in \mathcal{L}, t \in \mathcal{T} \quad \text{(B-32)}$$

$$-(1-a_{l,r})M \leq \eta^{18}_{l,t,r} - \lambda^{18}_{l,t,r} \leq (1-a_{l,r})M; \forall l \in \mathcal{L}, t \in \mathcal{T} \quad \text{(B-33)}$$

$$-a_{l,r}M \leq \lambda^{18}_{l,t,r} \leq a_{l,r}M; \forall l \in \mathcal{L}, t \in \mathcal{T} \quad \text{(B-34)}$$

$$-(1-a_{l,r})M \leq \eta^{19}_{l,t,r} - \lambda^{19}_{l,t,r} \leq (1-a_{l,r})M; \forall l \in \mathcal{L}, t \in \mathcal{T} \quad \text{(B-35)}$$

$$-a_{l,r}M \leq \lambda^{19}_{l,t,r} \leq a_{l,r}M; \forall l \in \mathcal{L}, t \in \mathcal{T} \quad \text{(B-36)}$$

$$\lambda^{5}_{l,t,r}, \lambda^{6}_{l,t,r}, \lambda^{16}_{l,t,r}, \lambda^{17}_{l,t,r}, \lambda^{18}_{l,t,r}, \lambda^{19}_{l,t,r} \in \mathbb{R}; \forall l \in \mathcal{L}, t \in \mathcal{T} \quad \text{(B-37)}$$

C
Nomenclature

Table C.1: Sets

Symbol	Description
$\mathcal{H}_l$	Set of hardening investments of line l
$\mathcal{J}$	Set of iterations of the solution algorithm
$\mathcal{K}^{forb}$	Set of rules of topology forbidden patterns
$\mathcal{L}$	Set of lines
$\mathcal{L}^e$	Set of existing lines
$\mathcal{L}^c$	Set of candidate lines
$\mathcal{L}^{sw}$	Set of switchable line segments
$\mathcal{L}^{sw,e}$	Set of existing switchable lines
$\mathcal{L}^{sw,c}$	Set of candidates lines to become switchable
$\mathcal{L}^{ha}$	Set of lines ta have hardening investment options
$\mathcal{L}_k^{forb}$	Set of lines in the forbidden pattern rule k in $\mathcal{K}^{forb}$
$\mathcal{N}$	Set of buses
$\mathcal{N}^{sub}$	Set of buses with substation
$\mathcal{R}$	Set of representative days
$\mathcal{T}$	Set of periods

Table C.2: Indexes

Symbol	Description
b	Bus
h	Line hardening investment option
j	Iteration
l	Line
r	Representative day
t	Time period
0	Prior operating period ($t = 0$)

Table C.3: Parameters

Symbol	**Description**
β	Sensitivity of line failure probability to the active power flow
γ	Estimated upper bound for the nominal line failure probability
C^{p+}	Cost of active power surplus
C^{p-}	Cost of active power loss
C^{q+}	Cost of reactive power surplus
C^{q-}	Cost of reactive power loss
C^{sw}	Cost of line switching action
$C^{sw,in}$	Investment cost of turning a line to be switchable
C^{in}	Investment cost of constructing a line
C^{ha}	Investment cost of line l hardening action h in $\mathcal{H}_l$
C^{tr}	Cost of active power from main transmission grid at the substations
D^p	Active power demand at the buses
E	Number of digits for binary expansion linearization
$\overline{F}$	Maximum power flow at the lines
K	Number of simultaneous lines that can go off for the security criterion
M	Sufficiently large number (Big M)
$\overline{P}$	Maximum active power injection at the buses
PF	Power factor at the buses
$\overline{Q}$	Maximum reactive power injection at the substations
$\underline{Q}$	Minimum reactive power injection at the substations
R	Resistance of the lines
s	Step for binary expansion used in Master problem linearization
S	Auxiliary matrix of second-level problem
$\underline{V}$	Voltage lower bound at the buses
$\overline{V}$	Voltage upper bound at the buses
V^{ref}	Voltage reference at the substations
w^1	Weight parameter of first-level objective function
w^2	Weight parameter of first-level objective function
w^{ha}	Weight of hardening investment decrease of β
X	Reactance of the lines
z^{init}	Initial switching status of the lines

Table C.4: Variables

Symbol	**Description**
ΔD^{p+}	Amount of buses active power surplus
ΔD^{p-}	Amount of buses active power loss
ΔD^{q+}	Amount of buses reactive power surplus
ΔD^{q-}	Amount of buses reactive power loss
δ	Auxiliary binary variable for binary expansion in Master problem
η_{1-21}	Dual variables of the third-level problem
λ_{16-19}	Auxiliary variables for linearization of the Subproblem
ξ	Auxiliary binary variable for linearization of Master problem
ρ	Auxiliary binary variable for linearization of Master problem
ρ^{ha}	Auxiliary binary variable for linearization of Master problem
φ	Dual decision variable of the worst expected value of third-level problem
χ	Auxiliary variable for linearization of Master problem
ψ	Dual variable of the worst expected value of third-level problem
a	Binary variable associated with line availability
f^p	Active power flow at the lines
f^{p-}	Non-negative auxiliary variable for linearization of Master problem
f^{p+}	Non-negative auxiliary variable for linearization of Master problem
f^q	Reactive power flow at the lines
p	Amount of active power injected at the substations
q	Amount of reactive power injected at the substations
$v^\dagger$	Squared voltage at the buses
y^{sw}	Binary variable of line switching action
$y^{sw,in}$	Binary variable of investment action for a line to become switchable
y^{in}	Binary variable of investment action to construct a line
y^{ha}	Binary variable of line hardening investment action
z	Binary variable of a line status

Table C.5: Functions

Symbol	**Description**
μ	Exo/endogenous dependency vector of means at second-level problem
$\hat{a}$	Line unavailability vector
C^d	Cost of prior operating point deficit/surplus at $t = 0$
C^e	Worst expected cost of the multiperiod operation
C^h	Hardening investments costs
C^i	Line investments costs
C^s	Switching action costs
w^β	Weight that reduces β according to hardening investments